Hydrothermal Synthesis and Characterization of Cadmium Selenide Nanocrystals

by

Juandria V. Williams

A dissertation submitted in partial fulfillment
of the requirements for the degree of
Doctor of Philosophy
(Chemical Engineering)
in The University of Michigan
2008

Doctoral Committee:

Professor Phillip E. Savage, Chair
Professor Levi T. Thompson, Jr.
Associate Professor Rachel S. Goldman
Associate Professor Nicholas A. Kotov

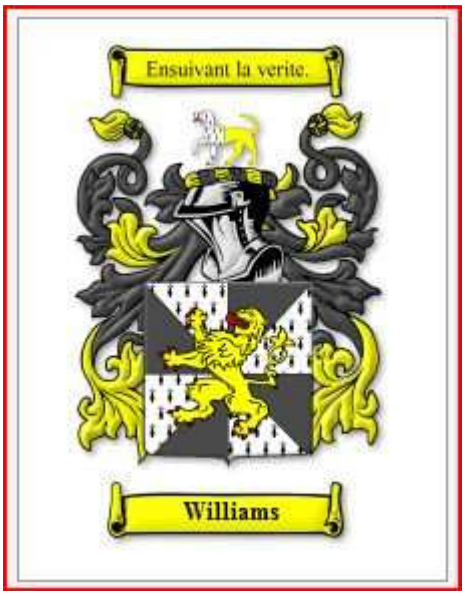
Ensuivant la verite.
Williams

To Grandma
(Bernice E Lee – 1912-2001)

But without faith it is impossible to please Him, for he who comes to God must believe that He is, and that He is a rewarder of those who diligently seek Him.—Hebrews 11:6

Acknowledgements

I would first like to give praise to Jesus Christ for putting up with my doubts and complaining, and for enabling me to persevere through what I perceived, at times, to be impossible. I must also thank my advisor, Professor Phillip E. Savage for his deep technical knowledge, superior writing skills and patience. His door was always open and he never wavered to help me with a technical issue. I also wish to thank my doctoral committee: Professor Nick Kotov, Professor Levi Thompson and Professor Rachel Goldman for sharing their advice to enrich my research and dissertation. I am grateful to the Chemical Engineering department at Michigan for the financial assistance, and especially to Susan Hamlin for her ability to always provide me with any ancillary support when needed.

I must thank Claire Adams for her tireless work in the lab and providing results for our first publication.

William Johnson (PhD ’07) from the Thompson group served as a great friend and sounding board.

Finally, I thank my mother, Bobbie Williams, father, Juan Williams, sister, Lacia Williams and brother, Nathaniel Williams, for their never-ending prayers, love and support.

Table of Contents

List of Figures

List of Tables

Abstract

Hydrothermal Synthesis and Characterization of Cadmium Selenide Nanocrystals

by

Juandria V. Williams

Cadmium Selenide (CdSe), a type of semiconductor nanocrystal, is of interest because its optical properties can be tuned by varying its size, thus yielding a material that has potential application in electronics and biology. Conventional preparations of CdSe primarily use organic solvents. We explored the use of high-temperature liquid water (HTW) as an alternative reaction medium because of its environmental benignity and solvent properties which could potentially mimic the function of the conventional organic-based mediums.

The base case experimental conditions for the feasibility study (non-isothermal conditions) produced nanocrystals that exhibited quantum confinement behavior. The quantum yield (QY) for the base case nanocrystals was 1.5%, but was easily increased to ~7% by adding a cadmium sulfide (CdS) shell. The nanocrystal mean size increased with increasing reaction time, temperature, stabilizer concentration and Cd:Se molar ratio. The mean size decreased with increasing pH.

Under isothermal synthesis conditions, nanocrystals smaller than those produced in the feasibility study were obtained when using the same process parameters. The mean nanocrystal size did not increase with reaction temperature at 2 minutes, but did increase with time and stabilizer concentration. The mean size also decreased with increasing pH and Cd:Se molar ratio. An increase in the Cd:Se molar ratio, pH and Cd:stabilizer molar ratio increased the QY. The reaction temperature and time had no affect on QY.

We used red-shift rates to determine an activation energy Q for the CdSe growth in HTW. We calculated Q = 0.24 ± 0.04 eV/molecule from the red-shift rate method. Compared with organic-based systems, this value is lower, possibly due to the less bulky cadmium-citrate complex used. The kinetics analysis indicates that the synthesis in HTW could be both reaction- and diffusion-controlled.

This work indicates that HTW is a viable alternative reaction medium. Nanocrystals can be grown that exhibit quantum confinement, and certain process parameters have a profound effect on the nanocrystal's quality. Further studies can identify the optimum process conditions to produce the nanocrystal with the highest quality.

Chapter 1

Introduction

Unique physical, optical and electrical phenomena can occur when a macroscopic material decreases in size. At a length scale of 1 x 10^{-9} of a meter, a "nanomaterial" can display properties not exhibited by its macroscopic (bulk) analogue. Carbon black, an amorphous form of carbon, is one of the first nanomaterials ever to be produced commercially, as is fumed silica. Because of their size, carbon black and fumed silica particles, as well as other materials, have greatly benefited society. As the needs and desires of society expand so does the demand for novel materials and devices whose properties are controlled by phenomena that occur in materials structured at the nanoscale.

Conventional bulk manufacturing strategies could be reaching the limit of successfully fabricating and characterizing nano-structured materials [1]. Many of these "top-down" methods – the building of objects by incorporating small pieces of bulk material – cannot effectively allow a scientist or engineer to control the structure at the nanoscale, thereby influencing the resulting properties. The ability to design materials with desired properties has been achieved through a "bottom-up" method – incorporating atomic and molecular building blocks into a material or device. Even though the "top-down" method can yield nanoscale material, it lacks atomic control, and, thus, is not very reproducible.

Nanotechnology is boundless in its research, but more limited in its successful application to date. This does not mean that knowledge has not impacted a number of industries. According to the National Nanotechnology Initiative [2], some of the products that benefit from unique properties of nanomaterials include sunscreens and cosmetics, metal-cutting tools, protective paints and coatings and, of course, semiconductors. Bulk semiconductors have had a monumental impact on society, but researchers are finding even greater promise with semiconductors on the nanoscale.

Semiconductor nanocrystals, a type of nanoparticle sometimes termed "quantum dots", exhibit size and shape dependent electronic and optical properties that make them attractive. Types of commonly fabricated semiconductor nanocrystals include cadmium sulfide (CdS), lead sulfide and selenide (PbS and PbSe), cadmium telluride (CdTe) and cadmium selenide (CdSe). These nanocrystals possess characteristics that make them attractive for opto-electronic applications such as light-emitting diodes (LEDs) [3, 4, 5], solar cells [6, 7] and biological markers [8, 9, 10, 11]. Their properties are currently being exploited in the field of energy conservation, most notably as alternatives to conventional phosphors in solid-state lighting (SSL). According to researchers at Sandia National Laboratories in Albuquerque, New Mexico, conventional phosphors used in fluorescent lighting are not ideal in SSL due to their poor energy absorption properties [5]. They also account for a 50% reduction in package efficiency due to light scattering and associated optical losses. The small size of a quantum dot eliminates the light scattering, reducing optical losses. Furthermore, ensembles of quantum dots have nearly continuous absorption spectra from their band gap wavelength (near infra-red) into ultraviolet, allowing for multi-color emission by simultaneous excitation of different

sized quantum dots, according to Lee et al [4]. Their narrow emission spectra almost guarantee pure color emission. These specific advantages are reasons for implementing them as active agents in SSL.

Photovoltaics is another application where quantum dots have demonstrated promise. Current solar cells carry, at best, a 31% efficiency, meaning only 31% of the sun's energy (rays) are converted into electricity as the remaining energy is wasted as heat [12]. The current technology is limited due to absorption and emission dynamics above the semiconductor band gap. Nozik asserts that these dynamics can be markedly affected by the quantization effects in quantum dots, potentially realizing an increase in solar energy conversion to 66% [12]. A group led by Nozik demonstrated multiple exciton generation (MEG) in colloidal PbSe and PbS quantum dots, an important mechanism that may increase the conversion efficiency of solar cell devices [6]. Schaller et al. demonstrated a 10% reduction in energy loss by generating seven excitons from one photon as opposed to only one exciton produced by a single photon which accounts for the traditional high energy loss [7].

Biological applications for imaging require materials and devices with intrinsic optical integrity – good photostability and emission efficiency. Conventional dyes and fluorophores, used by researchers to visualize cellular matter, are limited by their narrow absorption range, broad emission spectra and short fluorescent lifetime [8]. Quantum dots can especially overcome these limitations by providing narrow emission spectra, a broad absorption range and an excellent photostability and resistance to photobleaching [8, 13]. ZnS/CdSe core/shell quantum dots covalently coupled to biomolecules have been demonstrated in use for ultra-sensitive biological detection [9, 10, 11, 13].

Nanoparticle synthesis can be achieved myriad ways. Four generic routes exist to make nanoparticles [14]: gas phase synthesis, mechanical methods, form-in-place and wet chemistry. Each results in a material with significantly different properties depending on the synthetic route. Additionally, some routes are more amenable to a certain class of raw materials than others. Of the routes listed, wet chemical processes have the advantage of producing a large variety of inorganic and organic compounds and some metals in significant quantities using inexpensive equipment (as opposed to costly furnaces, vacuum deposition equipment, ball mills). Furthermore, the ability to control particle size and achieve high monodispersity is another attractive factor. One drawback, though, is that for bulk production, a large infrastructure for bulk chemical processing may be required, rendering it expensive.

Conventional growth techniques such as molecular beam epitaxy and chemical vapor deposition have been used to fabricate CdSe. However, these techniques may limit the practical application of the nanocrystal because it is attached to a substrate or embedded in a matrix [15]. Organic solvent-based colloidal methods have realized high quality semiconductor nanocrystals for over 15 years [16, 17, 18, 19, 20]. Key chemicals used in this synthetic route are often hazardous and the experiments can lack sufficient control, making the results difficult to reproduce [21, 22]. This has inspired researchers to develop greener chemistries such as alternative precursors [22, 23, 24, 25].

Researchers have demonstrated aqueous-based synthetic routes at relatively low temperatures (<100 °C) with various cadmium and selenium precursors and stabilizing ligands [26, 27, 28, 29]. Each of these routes, although successfully producing physical samples, has yet to be optimized to obtain highly luminescent, photostable, crystalline

structures. In general, the quality of nanocrystals resulting from aqueous-based synthetic methods is not as good as those obtained from the organic-based methods. The literature provides supporting evidence that the high temperature processes (250-350 °C), common in organic-based methods, yield higher quality product [16, 30, 31].

A reaction medium that has not been previously used for the synthesis of CdSe is high- temperature liquid water (> 200 ˚C). This medium is of interest because high temperature processes (250 °C-350 °C) such as those in organic-based methods, generally yield higher quality product. By varying temperature, the properties of water could be tuned to obtain a medium that can, i) mimic polar solvents commonly used in nanoparticle synthesis, ii) provide low surface tension (for excellent wetting of surfaces), and, iii) provide high diffusion coefficients. Numerous studies have demonstrated the successful fabrication of metallic and ceramic nanomaterials using high-temperature water [32, 33, 34, 35, 36, 37, 38].

1.1 Semiconductor Nanocrystals

The most remarkable characteristic of a semiconductor nanocrystal is the ability to tune its optical and electronic properties by controlling its size. As the size of a bulk semiconductor is reduced, the surface area/volume ratio increases and the optical and electronic properties become strongly influenced by its surface structure. Moreover, the electronic structure at the nanoscale ceases to resemble the bulk. This phenomenon is a result of quantum confinement effects: the behavior of electrons in a particle due to spatial limitations. “Quantum dots” are those particles that exhibit the behavior.

When a semiconductor absorbs light, an electron moves from the nearly-full valence band to the nearly-empty conduction band. The minimum energy required to excite an electron is dictated by the energy band gap. The loss of the electron creates a "hole" (the absence of a negative charge). The electron-hole pair, characterized by a preferred distance known as the Bohr radius, becomes electrostatically bound, forming an exciton. As the free electron loses any excess energy in the conduction band, it will drop to the lower energy state (valence band) and recombine with the hole. This energy loss occurs in the form of light.

When an exciton is created within a spatially confined box smaller than the Bohr radius, the semiconductor's (now a quantum dot) band gap widens since it takes much more energy to confine the exciton. The energy loss associated with this electron-hole recombination manifests itself through shorter wavelength light emission (higher energy), also known as a "blue shift". In essence, as the nanocrystal's size decreases, the absorption and emission wavelengths decrease and the light emitted transforms to a bluer color. This behavior is one reason why quantum dots are being explored for many different applications.

The minimum energy required for creating an exciton can be attributed to the bulk band gap energy, E_g, and the confinement energy for the charge carriers in a potential well. The overall confinement energy for the exciton can then be described as the ground state energy for the familiar "particle in a box" system:

$$E_{well} = \frac{h^2}{2m^* d^2} \tag{1.1}$$

where h is Planck's constant, d is the diameter and m^* is the reduced mass of the exciton:

$$\frac{1}{m^*} = \frac{1}{m_e} + \frac{1}{m_h} \tag{1.2}$$

Here, m_e and m_h are the effective masses for the electrons and holes, respectively. Another contribution to the exciton energy is the Coulombic interaction between the electron and the hole. This can be written as:

$$E_{Coul} = \frac{-1.8e^2}{2\pi\varepsilon\varepsilon_0 d} \tag{1.3}$$

where e = electron charge (C), ε = dielectric constant and ε_0= permittivity constant. Combining Equations 1.1, 1.2 and 1.3 gives an estimate of the size-dependent energy gap for a quantum dot:

$$E(\text{dot}) = E_g(\text{bulk}) + E_{well} + E_{Coul} \tag{1.4}$$

$$E = E_g + \frac{h^2}{2m^* d^2} - \frac{1.8e^2}{2\pi\varepsilon\varepsilon_0 d} \tag{1.5}$$

This is known as the effective mass approximation [31, 39, 40, 41] and is only a first approximation. Other contributions can be included that describe a more precise interaction, but doing so requires a more sophisticated calculation. The approximation contains size dependence in both the confinement ($1/d^2$) and Coulombic ($1/d$) terms. For very small quantum dot sizes, the confinement term becomes the dominant term. Although this approximation is not valid for all semiconductors, for practical purposes, it is useful in estimating the size of a nanocrystal given a peak wavelength in the emission spectrum. It also provides a useful qualitative understanding of quantum confinement effects on semiconductor nanocrystals.

1.2 Characterization

Because the purpose for fabricating semiconductor nanocrystals has been to exploit their size-tunable optical characteristics, the control of the photoluminescence properties has been a major goal for developing tailored synthetic chemistries. These properties, which comprise absorption and emission, arise from interactions between electrons, holes and their local environments.

Photoluminescence spectra serve as an optical fingerprint by which the effect of process parameters on the size and overall intensity of quantum dots can be analyzed. Semiconductor nanocrystal emissions are collected in a fluorimeter and displayed as a peak that may be Gaussian. The peak of the curve corresponds to the emission wavelength from the mean size of the nanoparticle. The width of the peak, typically reported as the full-width-at-half-maximum (fwhm), is one common method used to evaluate the particle size distribution. An ensemble of quantum dots is comprised of individual dots with slightly different electronic properties and energy levels based on the size [42]. This leads to inhomogeneous broadening and displays what is reasonable to assume as a Gaussian function [42]. Thus, the emission spectra represent size distributions of individual emissions. The fwhm serves as a statistic that can accurately represent the size distribution.

The excitation of an electron in a semiconductor nanocrystal by a photon eventually results in a loss of energy as the electron returns to the ground state from an excited state. This loss of energy (deactivation) can either manifest as fluorescence (emission of light), non-radiative heat to the surroundings, or some other deactivation process. As the size of the energy band gap increases, the fluorescence process can be

interrupted since the electron has to lose more energy to reach the ground state. The ability for a nanocrystal to emit the photons it has absorbed is described as quantum efficiency. Quantitatively, the ratio of photons emitted to photons absorbed is the quantum yield. It can be determined experimentally as:

$$QY_{sample} = QY_{std}\left[\left(I_{sample}/I_{std}\right)\left(OD_{std}/OD_{sample}\right)\right] \quad (1.6)$$

where QY_{sample} is the quantum yield for the nanocrystal sample; QY_{std} is the quantum yield for a known organic fluorophore such as Rhodamine B; I_{sample} and I_{std} are the integrated intensities of the photoluminescence emission spectra for the nanocrystal sample and organic standard, respectively; OD_{std} and OD_{sample} are the optical densities of the organic standard and nanocrystal sample, respectively.

Since the emissive properties and quantum efficiencies are affected by the particle size, it would stand to reason that the absorption is size-dependent as well. This means that absorption depends on the energy band gap. For a direct band gap semiconductor, the optical absorption near the band edge follows the equation [43]:

$$\alpha h\upsilon = A(h\upsilon - E_g)^{1/2} \quad (1.7)$$

where α is the absorption coefficient, $h\upsilon$ is the photon energy (h is Planck's constant; υ = photon frequency (Hz)), A is a constant, and E_g is the energy band gap (eV). This equation clearly shows the dependence of the band gap on the absorption properties.

UV-vis absorption is a useful tool for determining nanocrystal size, however, for our studies, we primarily focused on photoluminescence emission spectra to analyze size evolution.

The physical determination of size and approximate morphology of the nanocrystals can be obtained by high-resolution transmission electron microscopy (HRTEM). TEM uses a beam of electrons to pass through the crystalline sample. A detector collects the electrons and an image is formed, magnified and viewed on a phosphor screen which is coupled to a digital camera for viewing.

1.3 High-temperature Water

One property of liquid water is that as the temperature increases, the static dielectric constant decreases. Under high-temperature (T > 200 °C) conditions, water behaves more like a polar organic solvent than water at room temperature. By varying temperature, some of the properties of high temperature water can be tuned to mimic those of common organic solvents which are often used as reaction mediums, as well for storage, and to exchange capping groups on nanocrystals. Ambient liquid water also possesses a high surface tension because of the hydrogen bonding. But, as water temperature increases, hydrogen bonding and surface tension become less pronounced. A lower surface tension increases wettability, and, when coupled with the high-temperature water, could effectively anneal the surface of the nanocrystal and reduce the number of surface defects. These attributes, coupled with its environmental benignity, make high-temperature water an intriguing reaction medium for the synthesis and processing of nanomaterials.

High-temperature water has attracted a growing interest due to its applications in destroying toxic waste and its uses as a medium for chemical synthesis. Hydrothermal synthesis methods have also been established for a variety of particulate chemistries to produce materials such as ceramics and catalysts. In particular, the synthesis of nanocrystalline metal oxides, using high-temperature water, has been demonstrated in groups led by Adschiri [33, 34, 38, 44] and Arai [32, 37, 45, 46], among others. Particle morphology, size and crystal structure were controlled by varying the reaction time, temperature and pressure [33, 34]. High temperatures also promote crystallization which eliminates the need for post-process annealing [47]. The results of these studies indicate the potential for these methods to affect the quantum behavior of semiconductor nanocrystals because of the controllable thermodynamic and transport properties of this high-temperature medium.

1.4 Cadmium Selenide Nanocrystals

1.4.1 Properties

Much attention has been paid to semiconductor nanocrystals such as cadmium selenide (CdSe), a II-VI metal chalcogenide semiconductor. The CdSe nanocrystal has an interior structure and bonding identical to that of bulk CdSe. Bulk CdSe has a band gap energy of about 1.74 eV at room temperature. Its Bohr radius (size of the exciton) is approximately 6 nm. A CdSe particle smaller than this will exhibit quantum confinement.

1.4.2 Synthesis

A number of methods that have been developed for the preparation of CdSe nanocrystals include photochemical [48], γ-irradiation [49], sonochemical [50] and solvothermal [51] methods. While these strategies yield particulates with properties unique to their fabrication strategy, the best preparation technique that exhibits strong confinement effects comes from colloidal chemistry using molecular precursors [52].

The traditional synthesis of semiconductor nanocrystals based on the pyrolysis of an organometallic cadmium reagent in a hot coordinating solvent serves as a powerful means of achieving a high quality product. The pioneers of CdSe and other nanocrystal synthesis are Murray et al. [18] who, in 1993, developed a robust method by injecting an organic cadmium reagent, with an inorganic selenium reagent, into a hot (300 C) coordinating solvent – tri-n-octylphosphine oxide (TOPO). TOPO, also acting as an organic ligand, served two purposes – to stabilize the growth and, to some degree, eliminate surface defects by binding to cadmium surface sites. Hines and Guyo-Sionnest [53] progressed the research more by developing a method to encapsulate a CdSe nanocrystal with an inorganic shell (ZnS). This enhanced the fluorescence, thereby increasing the nanocrystal's utility. Alivisatos' labs at the University of California, Berkeley, and Lawrence Berkeley National laboratory demonstrated, through numerous studies, that the conventional method, with some modifications, could produce high-quality anisotropic shapes of CdSe nanocrystals [19, 20, 54, 55]. Hundreds of publications dealing with the various aspects of CdSe nanocrystal preparations exist, but the highlights of the research will be briefly described in the Literature Review section.

This thesis is the culmination of investigative studies of the synthesis of CdSe nanocrystals in high-temperature water. The objective of our studies were to i) demonstrate the one-pot synthesis of CdSe nanocrystals and examine the effects of process variables on the size and quality, ii) modify the injection method and examine the effect of the method on the nanocrystal size and quality, iii) explore and quantitatively model the growth evolution of CdSe nanocrystals in an aqueous medium. The thesis is organized as follows:

1. Chapter 2 presents the motivation for our work;
2. Chapter 3 describes past and present work of CdSe nanocrystal synthesis;
3. Chapter 4 describes the experimental and analytical methods used to prepare and characterize our samples;
4. Chapter 5 examines the feasibility of using high-temperature water as an alternative reaction medium;
5. Chapter 6 examines the effects of process variables on the nanocrystals using rapid hot-injection;
6. Chapter 7 discusses the evolution of growth of CdSe nanocrystals and provides some preliminary analytical framework for a kinetics study;
7. Chapter 8 provides a summary of the investigative findings and concludes with thoughts on implementing future studies that can build and enhance present work

1.5 Bibliography

1. National Institute of Standards and Technology Nanomanufacturing. (accessed November 20, 2007).

2. NNI National Nanotechnology Initiative. *http://www.nano.gov/html/facts/appsprod.html* (accessed November 15, 2007).

3. Steckel, J. S.; Zimmer, J. P.; Coe-Sullivan, S.; Stott, N. E.; Bulovic, V.; Bawendi, M. G. Blue Luminescence from (CdS)ZnS Core–Shell Nanocrystals. *Angew. Chem. Int. Ed.* **2004***, 43*, 2154-2158.

4. Lee, J. W.; Sundar, V. C.; Heine, J. R.; Bawendi, M. G.; Jensen, K. F. Full Color Emission from II±VI Semiconductor Quantum Dot-Polymer Composites. *Adv. Mater.* **2000***, 12*, 1102-1105.

5. Sandia National Laboratories Sandia researchers use quantum dots as a new approach to solid-state lighting. *http://www.sandia.gov/news-center/news-releases/2003/elect-semi-sensors/quantum.html* (accessed December 07, 2007).

6. Ellingson, R. J.; Beard, M. C.; Johnson, J. C.; Yu, P. R.; Micic, O. I.; Nozik, A. J.; Shabaev, A.; Efros, A. L. Highly Efficient Multiple Exciton Generation in Colloidal PbSe and PbS Quantum Dots. *Nano Lett.* **2005***, 5*, 865-871.

7. Schaller, R. D.; Sykora, M.; Pietryga, J. M.; Klimov, V. I. Seven Excitons at a Cost of One: Redefining the Limits for Conversion Efficiency of Photons into Charge Carriers. *Nano Lett.* **2006***, 6*, 424-429.

8. Bruchez, M.; Moronne, M.; Gin, P.; Weiss, S.; Alivisatos, A. P. Semiconductor Nanocrystals as Fluorescent Biological Labels. *Science* **1998***, 281*, 2013-2016.

9. Chan, W. C. W.; Nie, S. Quantum Dot Bioconjugates for Ultrasensitive Noniostopic Detection. *Science* **1998***, 281*, 2016.

10. Gao, X. H.; Chan, W. C. W.; Nie, S. M. Quantum-Dot Nanocrystals for Ultrasensitive Biological Labeling and Multicolor Optical Encoding. *J. Biomed. Opt.* **2002***, 7*, 532-537.

11. Mattoussi, H.; Mauro, J. M.; Goldman, E. R.; Anderson, G. P.; Sundar, V. C.; Mikulec, F. V.; Bawendi, M. G. Self-Assembly of CdSe-ZnS Quantum Dot Bioconjugates using an Engineered Recombinant Protein . *J. Am. Chem. Soc.* **2000***, 122*, 12142-12150.

12. Nozik, A. J. Quantum Dot Solar Cells. *Physica E* **2002***, 14*, 115-120.

13. Gerion, D.; Pinaud, F.; Williams, S. C.; Parak, W. J.; Zanchet, D.; Weiss, S.; Alivisatos, A. P. Synthesis and Properties of Biocompatible Water-Soluble Silica-Coated CdSe/ZnS Semiconductor Quantum Dots. *J. Phys. Chem. B* **2001***, 105*, 8861-8871.

14. Pitkethly, M. J. Nanoparticles as Building Blocks? *Mat. Today* **2003***, 6*, 36.

15. Gaponenko, S. V. In *Optical Properties of Semiconductor Nanocrystals;* Cambridge University Press: Cambridge, U.K., 1998; .

16. Murray, C. B.; Sun, S. H.; Gaschler, W.; Doyle, H.; Betley, T. A.; Kagan, C. R. Colloidal Synthesis of Nanocrystals and Nanocrystal Superlattices. *J. Res. Dev.* **2001***, 45*, 47-56.

17. Murray, C. B.; Nirmal, M.; Norris, D. J.; Bawendi, M. G. Synthesis and Structural Characterization of Ii-Vi Semiconductor Nanocrystallites (Quantum Dots). *Zeits. Fur Phys. D* **1993***, 26*, S231-S233.

18. Murray, C. B.; Norris, D. J.; Bawendi, M. G. Synthesis and Characterization of nearly Monodisperse Cde (E = S, Se, Te) Semiconductor Nanocrystallites. *J. Am. Chem. Soc.* **1993***, 115*, 8706-8715.

19. Peng, X. G.; Manna, L.; Yang, W. D.; Wickham, J.; Scher, E.; Kadavanich, A.; Alivisatos, A. P. Shape Control of CdSe Nanocrystals. *Nature* **2000***, 404*, 59-61.

20. Peng, X. G.; Wickham, J.; Alivsatos, A. P. Kinetics of II-VI and III-V Colloidal Semiconductor Nanocrystal Growth: "Focusing" of Size Distributions. *J. Am. Chem. Soc.* **1998***, 120*, 5343-5344.

21. Gaponik, N.; Talapin, D. V.; Rogach, A. L.; Eychmuller, A.; Weller, H. Efficient Phase Transfer of Luminescent Thiol-Capped Nanocrystals: From Water to Nonpolar Organic Solvents. *Nano Lett.* **2002***, 2*, 803-806.

22. Peng, X. G. Green Chemical Approaches Toward High-Quality Semiconductor Nanocrystals. *Chem. Eur. J.* **2002***, 8*, 335-339.

23. Peng, Z. A.; Peng, X. G. Nearly Monodisperse and Shape-Controlled CdSe Nanocrystals Via Alternative Routes: Nucleation and Growth. *J. Am. Chem. Soc.* **2002***, 124*, 3343-3353.

24. Qu, L. H.; Peng, Z. A.; Peng, X. G. Alternative Routes Toward High Quality CdSe Nanocrystals. *Nano Lett.* **2001***, 1*, 333-337.

25. Bunge, S. D.; Krueger, K. M.; Boyle, T. J.; Rodriguez, M. A.; Headley, T. J.; Colvin, V. L. Growth and Morphology of Cadmium Chalcogenides: The Synthesis of Nanorods, Tetrapods, and Spheres from CdO and $Cd(O_2CCH_3)_2$. *J. Mater. Chem.* **2003***, 13*, 1705-1709.

26. Rogach, A. L.; Kornowski, A.; Gao, M. Y.; Eychmuller, A.; Weller, H. Synthesis and Characterization of a Size Series of Extremely Small Thiol-Stabilized CdSe Nanocrystals. *J Phys Chem B* **1999***, 103*, 3065-3069.

27. Pellegrino, T.; Manna, L.; Kudera, S.; Liedl, T.; Koktysh, D.; Rogach, A. L.; Keller, S.; Radler, J.; Natile, G.; Parak, W. J. Hydrophobic Nanocrystals Coated with an Amphiphilic Polymer Shell: A General Route to Water Soluble Nanocrystals. *Nano Lett.* **2004***, 4*, 703-707.

28. Liang, J. G.; Ai, X. P.; He, Z. K.; Pang, D. W. Functionalized CdSe Quantum Dots as Selective Silver Ion Chemodosimeter. *Analyst* **2004***, 129*, 619-622.

29. Skaff, H.; Emrick, T. The use of 4-Substituted Pyridines to Afford Amphiphilic, Pegylated Cadmium Selenide Nanoparticles. *Chem. Comm.* **2003**, 52-53.

30. Qu, L. H.; Peng, X. G. Control of Photoluminescence Properties of CdSe Nanocrystals in Growth. *J. Am. Chem. Soc.* **2002***, 124*, 2049-2055.

31. Steigerwald, M. L.; Brus, L. E. Semiconductor Crystallites - a Class of Large Molecules. *Acc. Chem. Res.* **1990***, 23*, 183-188.

32. Sue, K.; Murata, K.; Kimura, K.; Arai, K. Continuous Synthesis of Zinc Oxide Nanoparticles in Supercritical Water. *Green Chem.* **2003***, 5*, 659-662.

33. Adschiri, T.; Hakuta, Y.; Sue, K.; Arai, K. Hydrothermal Synthesis of Metal Oxide Nanoparticles at Supercritical Conditions. *J. Nano. Res.* **2001***, 3*, 227-235.

34. Adschiri, T.; Hakuta, Y.; Arai, K. Hydrothermal Synthesis of Metal Oxide Fine Particles at Supercritical Conditions. *Ind Eng Chem Res* **2000***, 39*, 4901-4907.

35. Holmes, J. D.; Lyons, D. M.; Ziegler, K. J. Supercritical Fluid Synthesis of Metal and Semiconductor Nanomaterials. *Chem. A Euro. J.* **2003***, 9*, 2144-2150.

36. Hakuta, Y.; Onai, S.; Terayama, H.; Adschiri, T.; Arai, K. Production of Ultra-Fine Ceria Particles by Hydrothermal Synthesis Under Supercritical Conditions. *J. Mater. Sci. Lett.* **1998***, 17*, 1211-1213.

37. Hakuta, Y.; Haganuma, T.; Sue, K.; Adschiri, T.; Arai, K. Continuous Production of Phosphor YAG : Tb Nanoparticles by Hydrothermal Synthesis in Supercritical Water. *Mater. Res. Bull.* **2003***, 38*, 1257-1265.

38. Hakuta, Y.; Seino, K.; Ura, H.; Adschiri, T.; Takizawa, H.; Arai, K. Production of Phosphor (YAG : Tb) Fine Particles by Hydrothermal Synthesis in Supercritical Water. *J. Mater. Chem.* **1999***, 9*, 2671-2674.

39. Brus, L. E. Electron Electron and Electron-Hole Interactions in Small Semiconductor Crystallites - the Size Dependence of the Lowest Excited Electronic State. *J. Chem. Phys.* **1984***, 80*, 4403-4409.

40. Schmid, G., Ed.; In *Nanoparticles: From Theory to Application;* WILEY-VCH Verlag GmbH &Co.: Germany, 2004; , pp 434.

41. Brus, L. E. A Simple-Model for the Ionization-Potential, Electron-Affinity, and Aqueous Redox Potentials of Small Semiconductor Crystallites. *J. Chem. Phys.* **1983***, 79*, 5566-5571.

42. Bimberg, D.; Grundmann, M.; Ledentsov, N. N. In *Quantum Dot Heterostructures;* John Wiley and Sons: 1999; , pp 338.

43. Butler, M. A. Photoelectrolysis and Physical Properties of the Semiconducting Electrode WO_3. *J. Appl. Phys.* **1977***, 48*, 1914-1920.

44. Hakuta, Y.; Adschiri, T.; Hirakoso, H.; Arai, K. Chemical Equilibria and Particle Morphology of Boehmite (AlOOH) in Sub and Supercritical Water. *Fluid Phase Equilib.* **1999***, 160*, 733-742.

45. Li, G.; Smith, R. L.; Inomata, H.; Arai, K. Synthesis and Thermal Decomposition of Nitrate-Free Boehmite Nanocrystals by Supercritical Hydrothermal Conditions. *Mater Lett* **2002***, 53*, 175-179.

46. Li, G. S.; Smith, R. L.; Inomata, H.; Arai, K. Preparation and Magnetization of Hematite Nanocrystals with Amorphous Iron Oxide Layers by Hydrothermal Conditions. *Mater. Res. Bull.* **2002***, 37*, 949-955.

47. Darr, J. A.; Poliakoff, M. New Directions in Inorganic and Metal-Organic Coordination Chemistry in Supercritical Fluids. *Chem. Rev.* **1999***, 99*, 495.

48. Yan, Y. L.; Li, Y.; Qian, X. F.; Yin, J.; Zhu, Z. K. Preparation and Characterization of CdSe Nanocrystals Via Na2SO3-Assisted Photochemical Route. *Mat. Sci. Eng.* **2003***, 103*, 202-206.

49. Yang, Q.; Tang, K. B.; Wang, F.; Wang, C. R.; Qian, Y. T. A Gamma-Irradiation Reduction Route to Nanocrystalline CdE (E = Se, Te) at Room Temperature. *Mater. Lett.* **2003***, 57*, 3508-3512.

50. Ge, J. P.; Li, Y. D.; Yang, G. Q. Mechanism of Aqueous Ultrasonic Reaction: Controlled Synthesis, Luminescence Properties of Amorphous Cluster and Nanocrystalline CdSe. *Chem. Comm.* **2002**, 1826-1827.

51. Gautam, U. K.; Rajamathi, M.; Meldrum, F.; Morgan, P.; Seshadri, R. A Solvothermal Route to Capped CdSe Nanoparticles. *Chem. Comm.* **2001**, 629-630.

52. Weller, H. Quantized Semiconductor Particles - a Novel State of Matter for Materials Science. *Adv Mater* **1993***, 5*, 88-95.

53. Hines, M. A.; Guyot-Sionnest, P. Synthesis and Characterization of Strongly Luminescing ZnS-Capped CdSe Nanocrystals. *J. Phys. Chem.* **1996***, 100*, 468-471.

54. Manna, L.; Scher, E. C.; Alivisatos, A. P. Shape Control of Colloidal Semiconductor Nanocrystals. *Journal of Cluster Science* **2002***, 13*, 521-532.

55. Manna, L.; Scher, E. C.; Alivisatos, A. P. Synthesis of Soluble and Processable Rod-, Arrow-, Teardrop-, and Tetrapod-Shaped CdSe Nanocrystals. *J. Am. Chem. Soc.* **2000***, 122*, 12700-12706.

Chapter 2

Motivation

A prerequisite for the synthesis of high-quality CdSe nanocrystals is a high-temperature reaction medium to promote growth. Another requirement is an organic or inorganic capping agent to chemically passivate the surface and mediate growth. The judicious control of the competition between the temperature and capping agent will yield a nanocrystal with a size leading to quantum confinement as exhibited by emission spectra within the visible light region. The synthetic process must also facilitate surface reconstruction to eliminate surface defects due to energy traps which can suppress emission and lower quantum yields. These achievements have been demonstrated, with varying degrees of success, through the conventional organic-based synthetic routes, but many limitations and hindrances do exist.

The workhorse for the benchmark organic route consists of the organic solvent TOPO. It coordinates the surface of the nanocrystal, permitting slow steady growth. The ligands are quite bulky and present a significant barrier to bulk cadmium and selenium monomer as they add to the nanocrystal surface. Additionally, the solvent electronically passivates the surface as the ligands terminate dangling cadmium bonds, reducing energy traps. While a seemingly perfect solvent, one of TOPO's shortcomings is its flammability. The temperatures needed to produce the nanocrystals in TOPO often

exceed its flashpoint (180-200 °C). Talapin et al.[1] and Gaponik [2] cite another problem with the TOPO method being the irreproducibility of the growth dynamics and the shape of the CdSe nanocrystals because of the grade of chemical provided. The impurities in technical grade TOPO have offered benefits over the pure grade [1, 3], but only serendipitously. Researchers have sought to use pure TOPO and add other solvents in order to mimic the presence of the tech-grade impurities [3]. This method can lack control as the type of impurities and amounts are often not known since they are not deliberately added.

Another limitation present in the original TOPO method is the use of hazardous precursors, in particular, dimethyl cadmium. The range of compatible cadmium precursors is limited when using TOPO, thus the reason for the use of dimethyl cadmium. It is highly toxic and can be unstable at the high temperature required for the reactions [4].

Fatty acids, an alternative to TOPO, are the most versatile solvent/ligand [5]. A wider range of greener precursors are compatible with fatty acids. Stearic acid, for example, promotes faster reactions, and, thus, larger nanoparticles than what are produced from TOPO [5]. But, the fear here may be that the nanoparticles produced by fatty acids will not exhibit quantum behavior [6]. Other solvents have been used to act as a co-solvent to TOPO or to replace it altogether with the goal of reducing hazards and extra processing steps [5, 7]. In spite of this "green" effort, the usage of hazardous chemicals continues. And while these are used in a laboratory setting, it is hoped that these methods can be parlayed into high-volume process technologies. With the goal of

industry cutting down on materials that burden the environment, these methods will simply not be feasible in the long run.

Semiconductor nanocrystals that are synthesized in and remain in organic solvents are limited to opto-electronic applications. A water-soluble nanocrystal is required to function in biological entities. Many complex methods have been developed for making nanocrystals water-soluble that were originally synthesized in organic solvents. Water as the reaction medium, at temperatures below ambient conditions (<100 °C), has been used with little success, resulting in very low quantum yields [8, 9].

While the methods outlined above represent a step forward in the right direction, there remains a need to find a solvent and precursors that are at least as good as in the traditional organometallic approach, but are safe, inexpensive and environmentally friendly. An ideal synthetic route to high-quality nanocrystals would (i) reduce environmental and safety risks, (ii) operate with relatively small quantities of reagents, (iii) incorporate a single-step and scalable process, (iv) promote solubility in organic and aqueous matrices, and (v) facilitate a successful technology transfer.

We propose that high-temperature water could be a medium that will offer tremendous opportunities as an alternative to conventional methods, which are often chemically complex, experimentally tedious and hazardous. First and foremost, it is a benign solvent, at any temperature. Secondly, its properties can be tuned continuously, and adapted to a desired process technology. More interestingly, though, at high temperatures, it behaves more like a polar organic solvent, possibly enabling the use of a wide variety of precursors that are deemed safe. It is the most versatile solvent abundantly available and could offer more process benefits than a traditional organic

solvent. To date, no one has elucidated the effects of high-temperature water on the physical, surface and optical properties of CdSe nanocrystals synthesized therein.

2.1 Bibliography

1. Talapin, D. V.; Rogach, A. L.; Kornowski, A.; Haase, M.; Weller, H. Highly Luminescent Monodisperse CdSe and CdSe/ZnS Nanocrystals Synthesized in a Hexadecylamine-Trioctylphosphine Oxide-Trioctylphospine Mixture. *Nano Lett.* **2001***, 1*, 207-211.

2. Gaponik, N.; Talapin, D. V.; Rogach, A. L.; Hoppe, K.; Shevchenko, E. V.; Kornowski, A.; Eychmuller, A.; Weller, H. Thiol-Capping of CdTe Nanocrystals: An Alternative to Organometallic Synthetic Routes. *J Phys Chem B* **2002***, 106*, 7177-7185.

3. Hollingsworth, J. A. In *Semiconductor Nanocrystal Quantum Dots;* Encyclopedia of Inorganic Chemistry; John Wiley and Sons: 2007; .

4. Peng, X. G. Green Chemical Approaches Toward High-Quality Semiconductor Nanocrystals. *Chem. Eur. J.* **2002***, 8*, 335-339.

5. Qu, L. H.; Peng, Z. A.; Peng, X. G. Alternative Routes Toward High Quality CdSe Nanocrystals. *Nano Lett.* **2001***, 1*, 333-337.

6. Alivisatos, A. P. Semiconductor Clusters, Nanocrystals, and Quantum Dots. *Science* **1996***, 271*, 933-937.

7. Qu, L. H.; Peng, X. G. Control of Photoluminescence Properties of CdSe Nanocrystals in Growth. *J. Am. Chem. Soc.* **2002***, 124*, 2049-2055.

8. Deng, D. W.; Y, J. S.; Pan, Y. Water-Soluble CdSe and CdSe/CdS Nanocrystals: A Greener Synthetic Route. *J. Coll. Int. Sci.* **2006***, 299*, 225-232.

9. Rogach, A. L.; Nagesha, D.; Ostrander, J. W.; Giersig, M.; Kotov, N. A. "Raisin Bun"-Type Composite Spheres of Silica and Semiconductor Nanocrystals. *Chem. Mater.* **2000***, 12*, 2676-2685.

Chapter 3

Literature Review

The synthesis of II-VI semiconductor nanoparticles has experienced an enormous development in the past two decades. CdSe, in particular, has been the subject of much basic research into the electronic and optical properties of quantum dots. The amount of literature dealing with this topic is too voluminous to review within the context of this dissertation. As such, we will initially discuss the type of reaction mediums used to prepare the nanocrystals and the results of the effects of experimental parameters on the nanocrystals. We will then focus on the works performed by researchers in their attempts to understand and eventually model the growth kinetics of CdSe nanocrystals. This narrower focus is justified because these are the central topics of this dissertation.

3.1 Reaction Solvent

3.1.1 Organic-based Systems

The most successful preparations that realize high quality nanocrystals with narrow size distributions entail the pyrolysis of organometallic precursors in hot coordinating solvents. Murray et al. [1] pioneered this strategy by injecting cadmium and selenium precursors into a hot (300 °C) solution of tri-n-octylphosphine oxide (TOPO) and maintaining growth at 230-260 °C. The TOPO served multiple crucial roles by acting as the reaction medium, controlling the growth process, stabilizing the colloidal

dispersion, and passivating the nanocrystal's surface. This strategy produced TOPO-capped CdSe nanocrystals with a tunable size range from 1.2 – 11.5 nm. The average size and the size distribution were dependent on the growth temperature, and growth appeared consistent with Ostwald ripening. They assert that as the size distribution sharpens, the reaction temperature must increase to maintain steady growth. Conversely, they add, if the size distribution broadens, the necessary temperature for slow steady growth decreases. Crude estimates of the size distribution yielded an fwhm = 50 nm, but modulation of the reaction temperature allowed the maintenance of a narrow size distribution as the sample grew. A size distribution with a standard deviation of 10% for one sample with a mean particle diameter of 3.5nm was reduced to ~5% for particles with a mean diameter of 3.7 nm using size-selective precipitation procedures They calculated a QY of 9.6% for CdSe samples with an average size of 3.5 nm. Their work formed the basis of the organometallic preparative routes and they cite several advantages. For instance, nucleation does not continue during the growth stage; this helps establish the narrow size distribution. The higher temperatures allowed by this method enable faster reactions and more crystalline product due to the annealing process during the nanocrystal's growth. This can often translate to higher quantum yields. But the quantum yields achieved in this strategy do not exceed 5-15% for as-prepared particles. The luminescent properties can be enhanced by growing a shell with a wide-band gap semiconductor around the bare particles. The TOPO method, again, yields just a small amount of nanoparticles. Another problem with the TOPO method is the irreproducibility of the growth dynamics.

Adding a solvent, such as a primary amine, to TOPO has allowed researchers to overcome some of the disadvantages inherent in TOPO alone. Primary amines have been found to provide superior passivation to bare nanocrystals, such as ZnSe [2], as they may provide higher capping density and boost the quantum efficiency. Furthermore, they allow for a higher reaction rate than TOPO, and monodispersity can be achieved quickly and maintained throughout the reaction. Knowing this, Talapin et al. [3] tried to improve upon the original TOPO synthesis by introducing HDA (hexadecylamine). Exceptionally monodisperse samples (fwhm = 27-31 nm) were obtained, thus, the need for post-preparative size-selective precipitation was eliminated. The alkylamines effectively passivated the bare CdSe nanocrystals allowing them to reproducibly reach quantum yields of 40-50%.

Qu and Peng [4] examined the QY of nanocrystals under various conditions in a solvent mixture of TOPO and HDA, as well as TOPO mixed with other amines, such as dodecylamine (DDA) and octadecylamine (ODA). They performed a systematic study on the relationship between the optical properties of as-prepared CdSe nanocrystals and a variety of growth conditions. They looked at higher wavelength (red emitting) nanocrystals, in particular, those that fluoresced between 600 and 650 nm. In general, their results showed that the fwhm and QY were strongly affected by the initial Cd:Se molar ratio. They demonstrated that an excess of either cadmium or selenium promoted the formation of CdSe nanoparticles with high QY. In excess selenium the reaction started out focused, or with a very narrow size-distribution as determined by the small fwhm. But, as the system became more cadmium-rich, the size-distribution, over time, began to broaden; concurrently, the quantum yield gradually increased, came to a

maximum, and then gradually decreased. At a Cd:Se molar ratio of 1:1, the size-distribution was initially broad, but quickly narrowed over time. The QY, under these conditions, over time, quickly increased then decreased. A reaction in excess cadmium (Cd:Se = 2:1) did not greatly affect the size-distribution. The QY, however, sharply increased, then decreased and stabilized over time.

The nature of the amines was found to be an important parameter in their system for growing nanocrystals with high quantum efficiency. However, among the amines, DDA was the worst due to the limited reaction temperature range (<230 °C). The reactions that took place in TOPO/ODA yielded nanocrystals with maximum quantum yields of 50-60% over a given time, albeit in a large excess of selenium. HDA was the best amine to produce a high quantum yield at any one point in time. A secondary amine, dioctylamine (DOA), had no appreciable effect on the emission properties of the nanocrystals produced.

Alternatives to TOPO have been used due to TOPO's inherent hazards. For example, Qu et al. [5] used a one-pot approach to produce CdSe nanocrystals in a fatty acid solvent, namely, stearic acid at a growth temperature set between 200 and 320 °C. Fatty acids are much less expensive and more environmentally friendly. This solvent system yielded nanocrystals in a broad size range (2 to >25 nm). They observed extremely fast reaction rates, compared with the traditional TOPO method, and stated that this solvent was ideal for synthesizing larger nanoparticles (>4 nm). The system did luminesce well with a QY = 20-30%. The QY did tend to decrease with an increase in particle size.

Dickerson et al. [6] also noticed rapid growth of CdSe nanoparticles in a reaction mixture comprised of 95% stearic acid, achieving a maximum QY of about 26% at a temperature of 255 °C. Nanoparticles synthesized in dodecylamine obtained a maximum QY of 28% at a reaction temperature of 195 °C. In general, the evolution of the QY and emission peak width (fwhm) correlated more consistently with the emission wavelength than with temperature. Furthermore, the nanoparticle radius was virtually unaffected by the initial Cd:Se ratio. They also observed that higher selenium levels led to the formation of more initial nuclei.

Bullen et al. [7] used a non-coordinating solvent, octadecene (ODE), as their reaction medium and cadmium oleate as their capping agent. Their as-prepared CdSe nanoparticles, grown at a reaction temperature of 265 °C, initially exhibited an fwhm of 43 nm, but quickly narrowed to 30 nm after the first 200 seconds. The main focus of their work was toward the growth kinetics of the nanoparticles and it will be referenced further in this chapter.

Asokan et al. [8] demonstrated the formation of CdSe nanocrystals using heat transfer fluids DTA and T66 as reaction media. At a growth temperature of 280 °C, nanocrystals formed in T66 were smaller than those formed in ODE. After 1h of growth at 220 °C, synthesis in DTA and T66 yielded particles with an average diameter of 2.9 and 3.1 nm, respectively. These sizes were slightly less than those prepared in ODE (3.1 nm) and TOPO (4.0 nm). The size distributions for those nanocrystals prepared in DTA and T66 were reported as 18% and 17%, respectively. These are higher than those reported for ODE (15%) and TOPO (13%). Although these are rather broad, they cite the reason for this as an artifact of TEM analysis. An ensemble of 2.7 nm CdSe

nanocrystals yielded quantum yields of 3.3% and 8.4% for DTE and T66, respectively, lower than those for the nanocrystals prepared in ODE (11.7%) and TOPO (15.9%). The fwhms for the same ensemble were estimated to be 24 and 27nm for DTE and T66, respectively, compared with 33 and 34 nm for ODE and TOPO, respectively. Reasons for this, they cite, include differences in surface structure and no exclusion of oxygen and moisture during their synthesis and characterization processes.

The advancement of TOPO-based preparations has served as the benchmark for the widespread success of producing CdSe nanocrystals. Early applications of CdSe are based on this strategy, such as the fabrication of a light-emitting diode and a single electron transistor. But the success has, in the recent years, been tempered by the need to maintain environmental benignity. As such, researchers have been motivated to develop alternative synthetic methods for the well-studied model system. Peng [9], in particular, discussed the drawbacks to using the organometallic synthetic approach in a hot coordinating solvent such as TOPO, citing toxic and hazardous conditions, expensive chemicals and sophisticated equipment. Additionally, this approach is not easily controllable or reproducible, and only preparation of cadmium chalcogenides has been successfully developed.

3.1.2 Aqueous-based Systems

Another method commonly used to prepare nanocrystals uses an aqueous medium. Aqueous synthetic approaches are in general, simpler, less expensive, more reproducible, and scalable. Moreover, water-soluble materials are required for biological applications. Attempts have been made to initially prepare the nanocrystals in organic

media, and then manipulate the surface through ligand exchange [1, 3, 5, 10, 11] or application of a polymer shell [12, 13] to make it water-soluble. But these methods require more chemical processing. Researchers have investigated various types of precursors, stabilizers, heating technologies and other experimental parameters in attempts to further develop the aqueous-based method.

Zhang and company [14] produced cubic-structured nanocrystalline CdSe, with an average size of 5 nm, in an aqueous solution at room temperature. The reaction took place in an excess volume of alkaline selenium solution. This was done to prevent dilution of the selenium source so that selenium ion would not precipitate. A cadmium complex rather than cadmium ion served as the cadmium source; the complex proved to be more stable, greatly reducing the byproduct of cadmium hydroxide. A TEM image showed spherical but slightly agglomerated particles.

Xu et al. [15] produced CdSe quantum dots in an aqueous solution using a gelatin stabilizer at room temperature. They observed quenched photoluminescence, suggesting inadequate passivation or overall low crystallinity.

Li et al. [16] realized highly photoluminescent CdSe nanocrystals from room-temperature aqueous synthesis, followed by a low temperature chemical etching process. Prior to etching, the nanoparticles showed no photoluminescence. The etching process served to eliminate surface defects, thereby increasing the quantum efficiency to as high as 50%. Furthermore, they observed narrower size-distributions post-etching, with fwhm values as low as 30 nm, in addition to smaller size nanoparticles.

Sondi et al. [17] synthesized CdSe nanoparticles in the presence of aminodextran (Amdex) in an aqueous solution at room temperature. The Amdex served as a growth

stabilizer and capping agent. They produced CdSe nanocrystals with quantum yields of 15-16%. They observed wider particle distribution in the presence of Amdex compared with CdSe prepared in the conventional TOPO method. They attribute this to the wide molecular weight distribution of the polymer itself.

Water alone cannot provide a ligand suitable for stabilizing and/or passivating the nanocrystal surface. Therefore, judicious effort must be taken to provide a ligand or capping agent that is soluble and can withstand the reaction conditions. The above examples describe a variety of capping agents that served the researcher's purpose. The use of thiols in aqueous solutions, however, was made prominent by researchers in their effort for producing cadmium telluride [18], and CdS-core clusters [19].

Rogach et al. [20] extended the use of thiols to CdSe nanocrystal synthesis. They prepared CdSe in higher temperature aqueous-solutions using various thiols as a stabilizer. One preparation involved refluxing the solution for different lengths of times, resulting in larger nanoparticles at longer times. They noticed that, during the heating of the solution, particle growth proceeded about 5 times faster in the presence of thioacid-stabilized CdSe compared with thioalcohol-stabilized CdSe. As a result, thioacid-stabilized CdSe nanocrystals were larger (2.1-3.2 nm) than thioalcohol-stabilized samples (1.4-2.2 nm). The CdSe samples prepared showed a quantum yield of less than 0.1%.

Rogach [21] later demonstrated the presence of citrate-stabilized CdSe nanocrystals in 70 °C water. The QY was quite weak at 0.1-0.15%, but the size-distribution was relatively narrow (fwhm = 30-50 nm).

Deng et al. [22] also synthesized citrate-stabilized CdSe nanoparticles in water at 75 C. They incorporated a photoactivation procedure by exposing the nanoparticles to

ambient light for a few days, hypothesizing that this would eliminate topological surface defects. They noticed a trend of increased QY with prolonged exposure to ambient light, reporting a final QY of 4%. They also reported a decrease in the nanoparticle size with an increase in the pH, further noticing that nanoparticles prepared in a pH = 9.1 displayed stronger luminescence properties than those prepared at pH = 8 and 10. They investigated the effects of the initial Cd:Se molar ratio on the nanoparticle properties, and found that the photoluminescence intensity increased as the ratio increased from 2 to 10. Also, the fwhm narrowed to 37 nm as the molar ratio increased.

Most recently, Gao et al. [23] prepared CdSe nanocrystals in water, and then fabricated an LED by redispersing the as-prepared nanocrystals in a surfactant to transfer them to an organic solvent. They noticed that by changing the molar ratio of cadmium and selenium and the reflux time, different size nanocrystals were obtained. The average size obtained was just under 10 nm. Of interest were two characteristics of the integrity of the nanocrystal. The photoluminescence spectra showed weak emission, but electroluminescence spectra displayed strong emission. Basically, the electron transport inside the crystal was quite good as it served to act as an electron carrier while a polymer acted as an electron hole. By applying a voltage between the two entities, an exciton was formed. These results provide more substantive proof that the promise of CdSe can be realized as a device component when fabricated in an aqueous medium.

The articles above report on CdSe synthesis in water, but always at temperatures at or below the normal boiling point. Quantum yields for as-prepared particles tend to be low, and the processes tend to involve several steps. It is apparent that high-temperature synthetic strategies are an important gateway to obtaining ideal CdSe nanocrystals. Past

and present day methods incorporating aqueous reaction mediums have not provided the high temperature required for a true crystalline product. Nonetheless, traditional organic strategies are not desirable in the long run because of safety, cost, processing and environmental issues. More desirable is a fully developed route that is safe, simple, inexpensive, and versatile. High-temperature water has the qualities that can provide tremendous advantages over conventional methods.

Aqueous-based reactions above the boiling point (130 - 180 °C) have been reported for synthesis of various semiconductor nanocrystals such as CdTe [24] and CdS [25]. As-prepared CdTe nanocrystals prepared by Zhang et al. evolved from 2 to 4 nm within 2 hours of growth. They exhibited a QY of 30% without any post-preparative treatment. Liu et al. [25] prepared polymer-capped CdS nanoparticles with an average diameter of 8 nm and an fwhm of ~42 nm. Qian et al. [26] prepared alloyed CdSe-CdS nanocrystals at a reaction temperature of 140 °C for 1 hour. Because of the CdS shell, the QY measured at 25%. They found that after a short heating time (less than 1 hour) the QY measured <0.1%. The prolonging of the heating time allowed the CdS shell to mature on the CdSe surface. The fwhm was about 28 nm. They note that their method of heating, microwave irradiation, greatly accelerated the growth compared with conventional aqueous synthesis. Other hydrothermal methods have produced semiconductor nanocrystals as reported by Rajamathi et al.[27]

3.2 Growth Kinetics

One important aspect of Murray's work with TOPO involved a temporally discrete nucleation event followed by relatively rapid growth from the monomers in the

solution. This permits a controlled growth of the nanocrystals. The challenge then is to understand the mechanisms behind the nucleation and growth. Researchers have just recently begun to study and understand the kinetic behavior of CdSe growth under a variety of reaction conditions.

Bullen et al. [7] investigated the effects of temperature and an oleic acid stabilizer on the growth kinetics of CdSe nanocrystals in octadecene, a non-coordinating solvent. They observed increasing oleic acid concentrations led to lower nuclei concentrations, smaller nuclei size and larger final particle size. They also observed that at higher temperatures, particles nucleated with smaller radii than those present at lower temperatures. This, according to them, indicated that the nucleation is faster as temperature increases and that growth kinetics are less strongly dependent on temperature. Consequently, higher temperatures produced more nuclei.

Peng et al. [28] discussed the focusing of size distributions and its effect on nanocrystal growth. After growing CdSe nanocrystals in TOPO at 200 °C, they observed an initial large size distribution (~20%) for particles with an average diameter of 2.1 nm, and two distinct kinetic regimes. During the first 22 minutes, the size increased rapidly and the initial size distribution of particles began to narrow to ~7.7% (average diameter of 3.3 nm). The nanocrystals then grew more slowly and the size distribution broadened to about 10.6% (average diameter of 3.9 nm). The reason for this broadening was the occurrence of Ostwald ripening. Upon a second injection of precursor, the size-distribution began to narrow and decreased to 8.7%. They later emphasized the importance of maintaining a high enough precursor concentration so that the system does not experience Ostwald ripening which could lead to broader size distributions.

Qu et al. [29] introduced an in situ method for the study of the nucleation and growth kinetics of CdSe nanocrystals. Their observations suggest that the growth process can be divided into four stages. The first stage is the nucleation where the total number of particles increases as a result of nuclei forming. The second stage shows a significant drop in the concentration of the particles, and a narrowing of the size distribution. They contend that the decrease of the particle concentration could not be seen ex situ. A third stage, the stable stage, exhibited an equilibrium between the monomers and the particles in solution. The monomer concentration was close to the solubility of the particles in solution, so little to no growth was occurring. The fourth stage is Ostwald ripening, and thus a broadening of the size distribution occurs.

It is apparent that Ostwald ripening, although regarded as the primary means of growth in earlier research, is not easily controllable, and, because of recent insights in kinetic behavior, can possibly be avoided. Peng, [28] above, provides one example of a solution to prevent Ostwald ripening from occurring. More important, however, is determining where, in the kinetic regime, growth is at its optimum. This understanding is crucial for the control of the growth process. It can also serve as a conceptual framework for developing large-scale systems that can produce uniform particles under optimum conditions.

Dushkin et al. [30] supplied a comprehensive study of the kinetics of CdSe nanocrystal growth in a hot amphiphile (TOPO) matrix. They solved kinetic equations, based on classical theory, to derive analytical expressions for the mean radius and variance of the size distribution. They considered the growth to be a two-stage process in order to describe the time variation of nanoparticle size. During the first stage, called

reaction-limited growth, they noticed the size of the initial nuclei rapidly increased and caused an exhaustion of reactants at the nanoparticle surface. The growth also favored a size focusing or narrowing of the size distribution. Further development of the nanocrystal followed classic diffusion-limited growth. The size distribution began to broaden at this time, however, increasing in proportion to the average particle size. Their theoretical model was in good agreement with their experimental observations. They conclude that the reaction-limited growth is important to obtain well-defined nanocrystals of high quality. Good, precise control of the nucleation process is key to reproducible uniform nanoparticles, but, unfortunately, how to control this process is still unknown.

Dickerson et al. [6, 31] saw the need for developing analytical expressions that would yield the activation energy for CdSe growth in a given reaction solvent. Citing the need for eventual commercialization as a reason for measuring activation energies, they developed expressions based on synthesis time, temperature and reactant concentration. Their model yielded activation energies for nanocrystals prepared in TOPO and stearic acid. Chapter 7 describes, in detail, the model provided by Dickerson and how we adapted it for our aqueous system.

3.3 Bibliography

1. Murray, C. B.; Norris, D. J.; Bawendi, M. G. Synthesis and Characterization of nearly Monodisperse Cde (E = S, Se, Te) Semiconductor Nanocrystallites. *J. Am. Chem. Soc.* **1993***, 115*, 8706-8715.

2. Hines, M. A.; Guyot-Sionnest, P. Bright UV-Blue Luminescent Colloidal ZnSe Nanocrystals. *J. Phys. Chem. B* **1998***, 102*, 3655-3657.

3. Talapin, D. V.; Rogach, A. L.; Kornowski, A.; Haase, M.; Weller, H. Highly Luminescent Monodisperse CdSe and CdSe/ZnS Nanocrystals Synthesized in a Hexadecylamine-Trioctylphosphine Oxide-Trioctylphospine Mixture. *Nano Lett.* **2001***, 1*, 207-211.

4. Qu, L. H.; Peng, X. G. Control of Photoluminescence Properties of CdSe Nanocrystals in Growth. *J. Am. Chem. Soc.* **2002***, 124*, 2049-2055.

5. Qu, L. H.; Peng, Z. A.; Peng, X. G. Alternative Routes Toward High Quality CdSe Nanocrystals. *Nano Lett.* **2001***, 1*, 333-337.

6. Dickerson, B. D. Organometallic Synthesis Kinetics Of CdSe Quantum Dots, Virginia Polytechnic Institute and State University, 2005.

7. Bullen, C. R.; Mulvaey, P. Nucleation and Growth Kinetics of CdSe Nanocrystals in Octadecene. *Nano Lett.* **2004***, 4*, 2303-2307.

8. Asokan, S.; Krueger, K., M; Alhkawaldeh, A.; Carreon, A., R; Mu, Z.; Colvin, V., L; Mantzaris, N., V; Wong Michael, S. The use of Heat Transfer Fluids in the Synthesis of High-Quality CdSe Quantum Dots, core/shell Quantum Dots, and Quantum Rods. *Nanotechnology* **2005***, 16*, 2000.

9. Peng, X. G. Green Chemical Approaches Toward High-Quality Semiconductor Nanocrystals. *Chem. Eur. J.* **2002***, 8*, 335-339.

10. Mattoussi, H.; Mauro, J. M.; Goldman, E. R.; Anderson, G. P.; Sundar, V. C.; Mikulec, F. V.; Bawendi, M. G. Self-Assembly of CdSe-ZnS Quantum Dot Bioconjugates using an Engineered Recombinant Protein . *J. Am. Chem. Soc.* **2000***, 122*, 12142-12150.

11. Chan, W. C. W.; Nie, S. Quantum Dot Bioconjugates for Ultrasensitive Noniostopic Detection. *Science* **1998***, 281*, 2016.

12. Pellegrino, T.; Manna, L.; Kudera, S.; Liedl, T.; Koktysh, D.; Rogach, A. L.; Keller, S.; Radler, J.; Natile, G.; Parak, W. J. Hydrophobic Nanocrystals Coated with an Amphiphilic Polymer Shell: A General Route to Water Soluble Nanocrystals. *Nano Lett.* **2004***, 4*, 703-707.

13. Wu, X. Y.; Liu, H. J.; Liu, J. Q.; Haley, K. N.; Treadway, J. A.; Larson, J. P.; Ge, N. F.; Peale, F.; Bruchez, M. P. Immunofluorescent Labeling of Cancer Marker Her2 and Other Cellular Targets with Semiconductor Quantum Dots. *Nature Biotechnology* **2002***, 21*, 41-46.

14. Zhang, W. X.; Wang, C.; Zhang, L.; Zhang, X. M.; Liu, X. M.; Tang, K. B.; Qian, Y. T. Room-Temperature Synthesis of Cubic Nanocrystalline CdSe in Aqueous Solution. *Journal of Solid State Chemistry* **2000***, 151*, 241-244.

15. Xu, L.; Chen, K.; El-Khair, H. M.; Li, M. H.; Huang, X. F. Enhancement of Band-Edge Luminescence and Photo-Stability in Colloidal CdSe Quantum Dots by various Surface Passivation Technologies. *Applied Surface Science* **2001***, 172*, 84-88.

16. Li, R.; Lee, J. H.; Kang, D.; Luo, Z. T.; Aindow, M.; Papadimitrakopoulos, F. Band-Edge Photoluminescence Recovery from Zinc-Blende CdSe Nanocrystals Synthesized at Room Temperature. *Advanced Functional Materials* **2005***, 16*, 345-350.

17. Sondi, I.; Siiman, A.; Matijevic, E. Synthesis of CdSe Nanoparticles in the Presence of Aminodextran as Stabilizing and Capping Agent. *J. Coll. Inter. Sci.* **2004***, 275*, 503-507.

18. Gaponik, N.; Talapin, D. V.; Rogach, A. L.; Hoppe, K.; Shevchenko, E. V.; Kornowski, A.; Eychmuller, A.; Weller, H. Thiol-Capping of CdTe Nanocrystals: An Alternative to Organometallic Synthetic Routes. *J Phys Chem B* **2002***, 106*, 7177-7185.

19. Herron, N.; Calabrese, J. C.; Farneth, W. E.; Wang, Y. Crystal Structure and Optical Properties of Cd_{32} S_{14} (SC_6H_5) $_{36}$ DMF_4, a Cluster with a 15 Angstrom CdS Core. *Science* **1993***, 259*, 1426-1428.

20. Rogach, A. L.; Kornowski, A.; Gao, M. Y.; Eychmuller, A.; Weller, H. Synthesis and Characterization of a Size Series of Extremely Small Thiol-Stabilized CdSe Nanocrystals. *J Phys Chem B* **1999***, 103*, 3065-3069.

21. Rogach, A. L.; Nagesha, D.; Ostrander, J. W.; Giersig, M.; Kotov, N. A. "Raisin Bun"-Type Composite Spheres of Silica and Semiconductor Nanocrystals. *Chem. Mater.* **2000***, 12*, 2676-2685.

22. Deng, D. W.; Y, J. S.; Pan, Y. Water-Soluble CdSe and CdSe/CdS Nanocrystals: A Greener Synthetic Route. *J. Coll. Int. Sci.* **2006***, 299*, 225-232.

23. Gao, Y. H.; Liang, C. J.; Tang, A.; Teng, F.; Li, D.; Deng, Z.; Huang, S. H. Electroluminescence of Cadmium Selenium Nanocrystals Synthesized in Aqueous Solution. *Journal of Luminescence* **2007***, 122-123*, 648.

24. Zhang, H.; Wang, L. P.; Xiong, H. M.; Hu, L. H.; Yang, B.; Li, W. Hydrothermal Synthesis for High-Quality CdTe Nanocrystals. *Adv Mater* **2003***, 15*, 1712-1715.

25. Liu, S. H.; Qian, X. F.; Yin, J.; Ma, X. D.; Yuan, J. Y.; Zhu, Z. K. Preparation and Characterization of Polymer-Capped CdS Nanocrystals. *J. Phys. Chem. Solids* **2003***, 64*, 455-458.

26. Qian, H. F.; Li, L.; Ren, J. One-Step and Rapid Synthesis of High Quality Alloyed Quantum Dots (CdSe–CdS) in Aqueous Phase by Microwave Irradiation with Controllable Temperature. *Mater. Res. Bull.* **2005***, 40*, 1726-1736.

27. Rajamathia, M.; Seshadrib, R. Oxide and Chalcogenide Nanoparticles from Hydrothermal/ Solvothermal Reactions. *Curr. Opin. Solid State Mat. Sci.* **2002***, 6*, 337-345.

28. Peng, X. G.; Wickham, J.; Alivsatos, A. P. Kinetics of II-VI and III-V Colloidal Semiconductor Nanocrystal Growth: "Focusing" of Size Distributions. *J. Am. Chem. Soc.* **1998***, 120*, 5343-5344.

29. Qu, L. H.; Yu, W. W.; Peng, X. P. In Situ Observation of the Nucleation and Growth of CdSe Nanocrystals. *Nano Lett.* **2004***, 4*, 465-469.

30. Dushkin, C. D.; Saita, S.; Yoshie, K.; Yamaguchi, Y. The Kinetics of Growth of Semiconductor Nanocrystals in a Hot Amphiphile Matrix. *Adv. Coll. Inter. Sci.* **2000***, 88*, 37-78.

31. Dickerson, B. D.; Irving, D. M.; Herz, E.; Claus, R. O.; Spillman, W. B.; Meissner, K. E. Synthesis Kinetics of CdSe Quantum Dots in Trioctylphosphine Oxide and in Stearic Acid. *Applied Physics Letters* **2005***, 86*, 171915-1-171915-3.

Chapter 4

Experimental Methods

Batch reactor studies of the effects of experimental parameters such as time, temperature, pH and reagent concentrations on the optical and physical properties of CdSe nanocrystals were performed. Three studies were performed – a feasibility study, rapid hot-injection study and a kinetic study. Analyses were performed using spectroscopy and electron microscopy techniques.

4.1 Materials

The reagents used were a cadmium and selenium precursor, sodium hydroxide for pH adjustment, sodium citrate as a capping agent, thioacetamide as a sulfur source, and deionized water as the reaction medium. These reagents were used because they were successfully employed to produce CdSe nanocrystals in experiments by Rogach et al.[1] Cadmium perchlorate (Aldrich , 99%), N,N-dimethylselenourea (Sigma-Aldrich, 97%), sodium citrate tribasic dihydrate (Sigma-Aldrich, 99%), sodium hydroxide (Fisher, 0.1N) and thioacetamide (Sigma-Aldrich, 99+%) were used as received.

The batch reactors comprised 3/8” stainless steel Swagelok® fittings (port connectors and end caps) that, when assembled, created a reactor volume of approximately 1.54 ml (Figure 4.1a-b). An additional high-temperature rated bellows valve, attached to one end of a batch reactor, was used for the rapid hot-injection and

kinetics studies (Figure 4.1c). Our heat source consisted of a fluidized sand bath (Techne SBL-2) fitted with a Techne temperature controller.

Figure 4.1a-c. Graphic of the materials for the batch reactor system used for the syntheses. The batch reactor consisted of 3/8" stainless steel **(A)** port connectors and **(B)** end caps. A bellows valve **(C)** was fitted to a batch reactor for the rapid hot-injection study.

4.2 Method

The batch reactors were assembled and conditioned in the following manner. Two 3/8" inch stainless steel Swagelok caps were attached to the two ends of a 3/8" port connector using a vice and a wrench. This was done so that one end would be permanently capped and the other end would be fitted with the compression ferrule and ready to receive the cap when needed. Conditioning consisted of triple rinsing each reactor with acetone, followed by a rinse with deionized water. The empty reactors were then capped on both ends and placed in the preheated sand bath for 1 hour at 300 °C. The conditioned reactors were taken out of the sand bath, cooled and rinsed prior to starting the experiments.

We examined the following process variables for the feasibility and rapid hot-injection studies: reaction temperature, reaction time, pH, initial Cd:Se molar ratio and stabilizer loading. For the kinetics study, we varied only time and temperature. Table 4.1 shows the range of the process variables.

	Feasibility Study	**Rapid Hot-injection Study**	**Kinetics Study**
Temperature, C	200 – 215	200 – 240	200 – 240
Time, min	1.5 – 2.5	1 – 10	1 – 45
pH	8 – 11	8 – 11	9
Stabilizer Loading, g	2.80×10^{-3} – 1.40×10^{-2}	2.80×10^{-3} – 1.40×10^{-2}	2.80×10^{-3}
Cd:Se Molar Ratio	4 – 16	4 – 40	8

Table 4.1. Range of process parameters used for the feasibility, rapid hot-injection and kinetics experiments. All values are on a per reactor basis.

4.2.1 Feasibility Study

Citrate-stabilized nanocrystals were prepared in the following manner (based on a procedure by others): using a pipette, 5 ml of $8x10^{-2}$ M cadmium perchlorate dihydrate solution was added to 45 ml of deionized water containing 0.1 g sodium citrate. Different Cd:stabilizer molar ratios were obtained by adding different amounts of sodium citrate. Enough 0.1 M NaOH was added to increase the pH to 9.0. Then, 5 mL of this mixture was added to a glass vial. Immediately prior to running an experiment, a carefully measured amount of $1x10^{-2}$ M N,N-dimethylselenourea solution was added to the cadmium/sodium citrate solution in the vial. 1.5 ml of this resulting solution was then transferred to the reactor which was tightly sealed. The selenium reagent was added immediately before the reaction to minimize the fast oxidative loss of the selenourea. Adding 0.5 ml of the selenourea solution yielded a Cd:Se molar ratio of 8:1. Different Cd:Se molar ratios were obtained by adding different volumes of the N,N-dimethylselenourea. We chose to run experiments with excess cadmium, primarily due to successes with a similar CdSe synthesis by Rogach et al. The sealed reactor was immersed in the preheated sand bath. After the appointed time, the reactors were withdrawn from the sand bath, immediately placed in a water bath at room-temperature, and allowed to cool for about 1 minute. They were then opened and their contents were retained in glass vials and stored in a dark, cool cabinet.

It is important to note that the temperature inside the reactor was not the same as the sand bath temperature in the feasibility experiments. The synthesis took place under non-isothermal conditions as the batch holding times we explored (<3 min) coincided with the reactor heat up time. This mode of operation was not problematic because the

method of heat-up yielded reproducible results. Moreover, our goals in this work are to assess the feasibility of hydrothermal syntheses and to determine the effects of different process variables. Non-isothermal reaction conditions do not hinder the accomplishment of these goals. Figure 4.2 shows the measured temperature inside the reactor as a function of the time elapsed since being placed in the sand bath.

Core-shell CdSe/CdS nanocrystals were prepared as follows (based on a procedure by others [1]): 15 μL of a $4x10^{-2}$ M solution of thioacetamide was added to an already-prepared solution (~1.5 mL) of CdSe nanocrystals synthesized under the base case conditions. The solution was transferred to a reactor and tightly sealed. Subsequent steps were identical to those for synthesizing the bare CdSe nanocrystals.

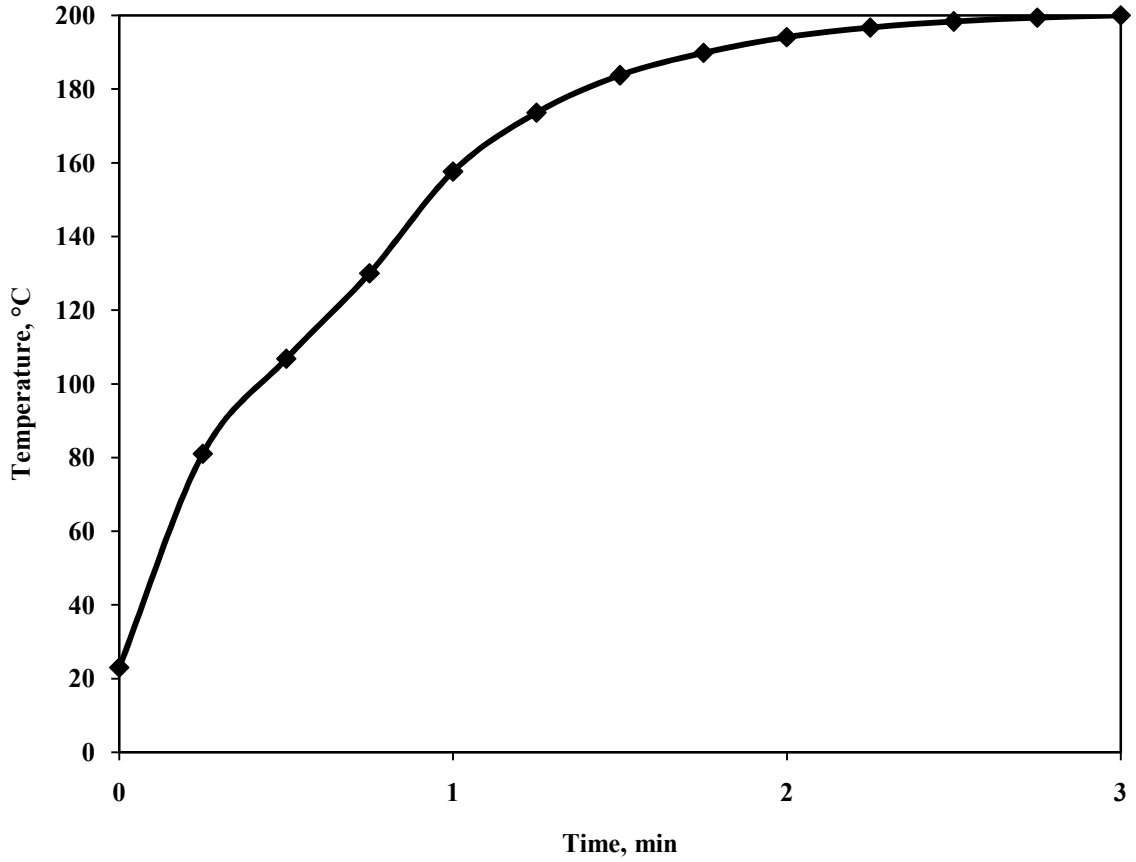

Figure 4.2. Reactor heat-up profile for a batch reactor in a sand bath at 200 C for 3 minutes. A Type-K thermocouple was inserted through a bored Swagelok reducing union at one end of the reactor.

4.2.2 Rapid Hot-injection and Kinetics Studies

The procedure to prepare the reagents for this study was identical to that for the feasibility study up to the point of pH adjustment. After the sodium hydroxide was added to the cadmium/sodium citrate solution, the reactor assembly, comprising a batch reactor fitted with the bellows valve, was placed in the preheated sand bath and allowed to heat for at least 3 minutes. The selenourea solution, described in the feasibility section, was made at the last possible moment minimize reaction with the oxygen in the atmosphere. Once the reagents were mixed thoroughly in the glass vial, a syringe was used to withdraw approximately 2 ml of solution. The contents in the syringe were immediately injected into the open port of the valve. The valve was quickly closed, and the reaction was allowed to take place. At the appointed time, the reactor assembly was then quickly withdrawn from the sand bath and submerged into an ice water bath where the reactor contents were allowed to cool. The reactors were then opened and their contents were retained in glass vials and stored in a dark, cool cabinet to await analysis.

Table 4.2 summarizes the quantities of materials used in the stock solutions, vials and batch reactors.

	Cadmium	Selenium	Sodium Citrate	Water
Molecular Weight	311.30 g	151.07 g	294.10 g	18.00 g
Amount in stock solution	0.1245 g	------	0.1000 g	50 ml
# of moles in stock solution	$4.0x10^{-4}$	------	$3.4x10^{-4}$	-----
Amount in vial	$4.0x10^{-5}$ moles	$5.0x10^{-6}$ moles	$3.4x10^{-5}$ moles	5 ml
Amount in a reactor	$1.12x10^{-5}$ moles	$1.40x10^{-6}$ moles	$9.52x10^{-6}$ moles	1.54 ml

Table 4.2. Amounts and concentrations of the cadmium and selenium precursors and the capping agent (sodium citrate) used for the base case synthesis for one batch reactor. Each was modified accordingly as process variables changed for each investigation.

4.3 Analysis

4.3.1 Photoluminescence Emission

Spectroscopic analysis was performed on as-prepared aqueous solutions of nanocrystals. Photoluminescence spectra were acquired for each sample by using a modular Fluorolog 3 SPEX spectrofluorimeter. Using a pipette, the stored sample was placed in a rinsed 1-cm quartz cuvette. The cuvette was placed into the sample holder. For all cases, the excitation wavelength was programmed to 380 nm and emission was monitored from 400 to 750 nm. After the scan was completed, the fwhm of the spectrum was obtained by using the fluorimeter's Datamax software built-in statistical analysis.

4.3.2 Absorption

Absorption spectra were acquired on a HP8453 diode array Hewlett-Packard spectrophotometer with a cell temperature of 25 °C. Using a pipette, the stored sample was placed in a clean 1-cm quartz cuvette. The instrument software was programmed to run in manual mode at fixed wavelength. This allowed us to readily examine the absorbance at desired wavelengths. Prior to data acquisition, a blank was used to calibrate. The cuvette full of sample was loaded into the sample holder and the data acquisition proceeded.

4.3.3 Quantum Yield

Determining absolute quantum yields (QY) are difficult, but one can find the relative quantum yield of a sample in reference to a standard. In order to calculate an accurate quantum yield, it is necessary to avoid high concentrations of sample solution

which can give rise to multiple scattering processes. The standard and sample solutions, therefore, need to be diluted. For our samples, a Rhodamine B standard was used as our organic standard. The diluents used were ethylene glycol and deionized water for Rhodamine B and the CdSe samples, respectively. Our goal was to obtain an absorption of .08 at an excitation wavelength of 380. We began by diluting Rhodamine B with ethylene glycol and loading into a 1-cm quartz cuvette. We selected a fixed wavelength of 380 nm then followed the procedure described for the UV-vis absorption analysis. We repeatedly diluted each analyzed solution until the absorption was .08, or slightly less, for a wavelength of 380 nm. We then proceeded to collect fluorescence data for the diluted standard by following the procedure described for acquiring photoluminescence emission spectra. Once the data for the Rhodamine B was collected, we proceeded to collect the data for the CdSe sample by following the procedure used for Rhodamine B. Our only difference was the use of a different diluent which was deionized water rather than ethylene glycol.

After the data was collected, we used Equation (1.6) to determine QY. We obtained the integrated intensities of the photoluminescence spectra from the fluorimeter's Datamax software built-in statistical analysis.

4.3.4 TEM

High-resolution transmission electron microscopy was performed on a JEOL 3011 HRTEM microscope operating at 300 kV. Samples were prepared by drying a drop on a 300 mesh copper grid pre-coated with thin hole-y carbon film. Images were recorded on a Gatan 794 slow scan CCD TV system.

4.4 Bibliography

1. Rogach, A. L.; Nagesha, D.; Ostrander, J. W.; Giersig, M.; Kotov, N. A. "Raisin Bun"-Type Composite Spheres of Silica and Semiconductor Nanocrystals. *Chem. Mater.* **2000***, 12*, 2676-2685.

Chapter 5

Feasibility Study

In this chapter, we test the hypothesis that the synthesis of CdSe nanocrystals in high-temperature water will yield nanocrystals that exhibit quantum behavior. This will be defined by a blue shift of the photoluminescence emission. We will also verify the presence of nanocrystals through TEM. We will test the quality of the CdSe nanocrystals by calculating a quantum yield.

5.1 Introduction

The purpose of the feasibility study was to conduct exploratory research on the viability of high-temperature water as a possible reaction medium for the preparation of CdSe nanocrystals. A previous aqueous-base synthesis method [1] which we adapted used a conventional microwave oven as a heat source which provided, on average, a temperature of 70 °C. As noted in a previous chapter, higher temperatures tend to provide higher quality nanoparticles. Therefore, the goal of this chapter is to provide the results of a baseline study of CdSe preparation as an extension of previous work to higher temperature realms not yet studied.

5.2 Experimental Methods

We conducted experiments in stainless steel batch reactors as described in Chapter 4. All analytical methods used for this study include spectroscopy and TEM, descriptions of which are in Chapter 4. All emission data is displayed as normalized curves to show only the effect of the experimental conditions on the peak wavelength.

5.3 Results and Discussion

5.3.1 Base Case Synthesis

We chose T = 200 °C, t = 1.5 minutes, a Cd:Se ratio of 8:1, a Cd:stabilizer ratio of 1.04 and a pH of 9 as the base case conditions for our experiments. Figure 5.1, which shows the emission spectrum from particles synthesized at these conditions, reveals a blue shift from the bulk band gap (~700 nm). This shift indicates the existence of quantum confinement in the nanoparticles. The presence of a strong, single peak indicates that CdSe is the only nanoparticle being synthesized. If any by-products are formed, they are irrelevant, and are most likely not in the form of a nanocrystal.

The wavelength at which the peak maximum occurs (λ_{max}) is related to the mean size of the nanoparticles. Smaller particles emit at shorter wavelengths. Thus, one can use λ_{max} as an indicator of the mean particle size. Our λ_{max} of 579 nm represents a mean particle size of approximately 5 nm, as confirmed by HRTEM. Rogach et al. demonstrate CdSe particles synthesized at 3 and 5 nm, corresponding to approximate peak wavelengths of 560 and 580 nm, respectively [1].

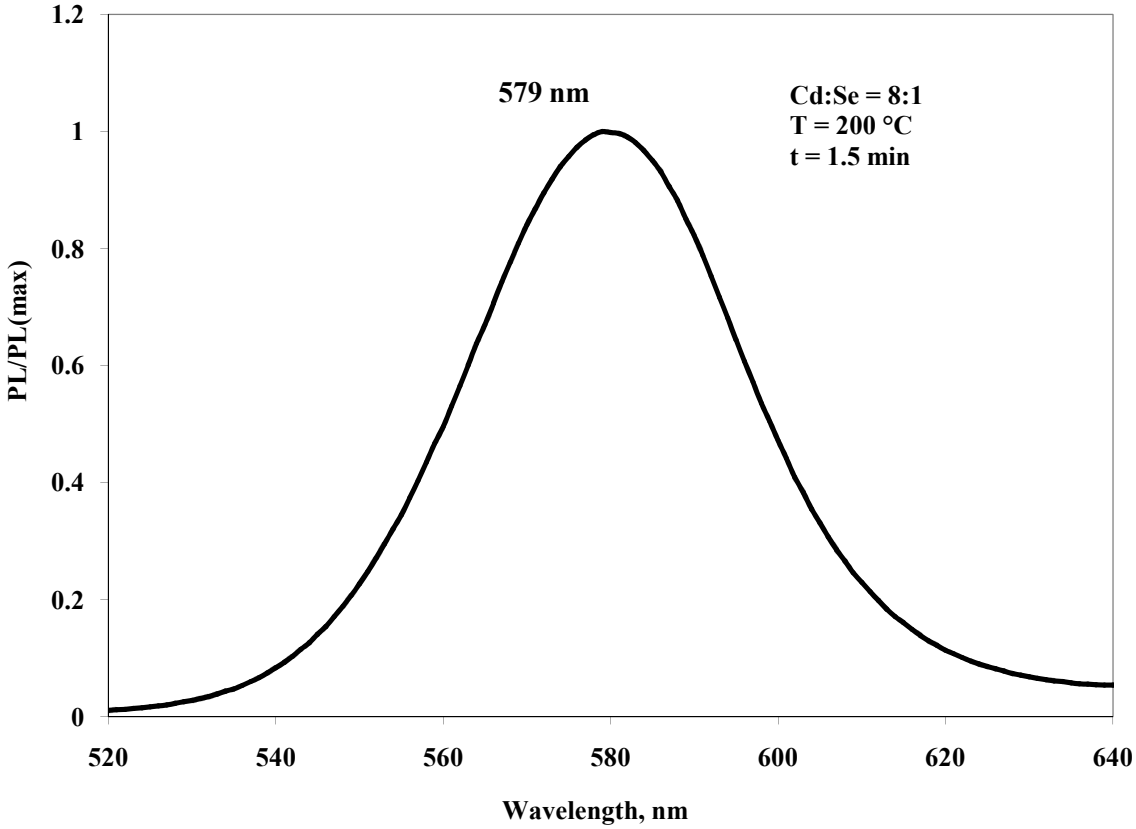

Figure 5.1. Normalized PL emission spectra for CdSe nanocrystals synthesized in high-temperature water under base case conditions.

The full-width-at-half-maximum (fwhm), which is related to the particle size distribution, was calculated from the emission spectrum. The fwhm values provide information about the sample's monodispersity. An fwhm value of ≤40 nm represents a narrow size distribution [2, 3]. The fwhm for the base case product was 36 nm.

To verify the reproducibility of the synthesis, we performed additional independent experiments at the base case conditions. The mean value determined for λ_{max} is 579 ± 5 nm. The mean value for fwhm is 37 ± 0.5 nm. The uncertainties are the standard deviations. Given these results, we conclude that the method is reproducible.

Figure 5.2, an HRTEM image of particles obtained at these base case conditions, further supports the presence of CdSe quantum dots. These images show particles on the order of about 5 nm diameter.

The quantum yield of the particles produced in this base case was 1.5%, which is lower than quantum yields of 10-30% for particles synthesized in organic media [4, 5, 6]. The yield is lower in our experiment, possibly due to weak passivation by sodium citrate and potential CdSe corrosion due to active oxygen species. As we will report in a later section, the quantum yield can easily be improved by capping the particles with a CdS shell in a subsequent hydrothermal treatment. It is also very likely that CdSe with a higher quantum yield can be synthesized hydrothermally by heating the aqueous reaction medium before adding the inorganic reactants. This approach would more closely mimic that used with organic media, and it would allow the particle growth to occur entirely at a high temperature.

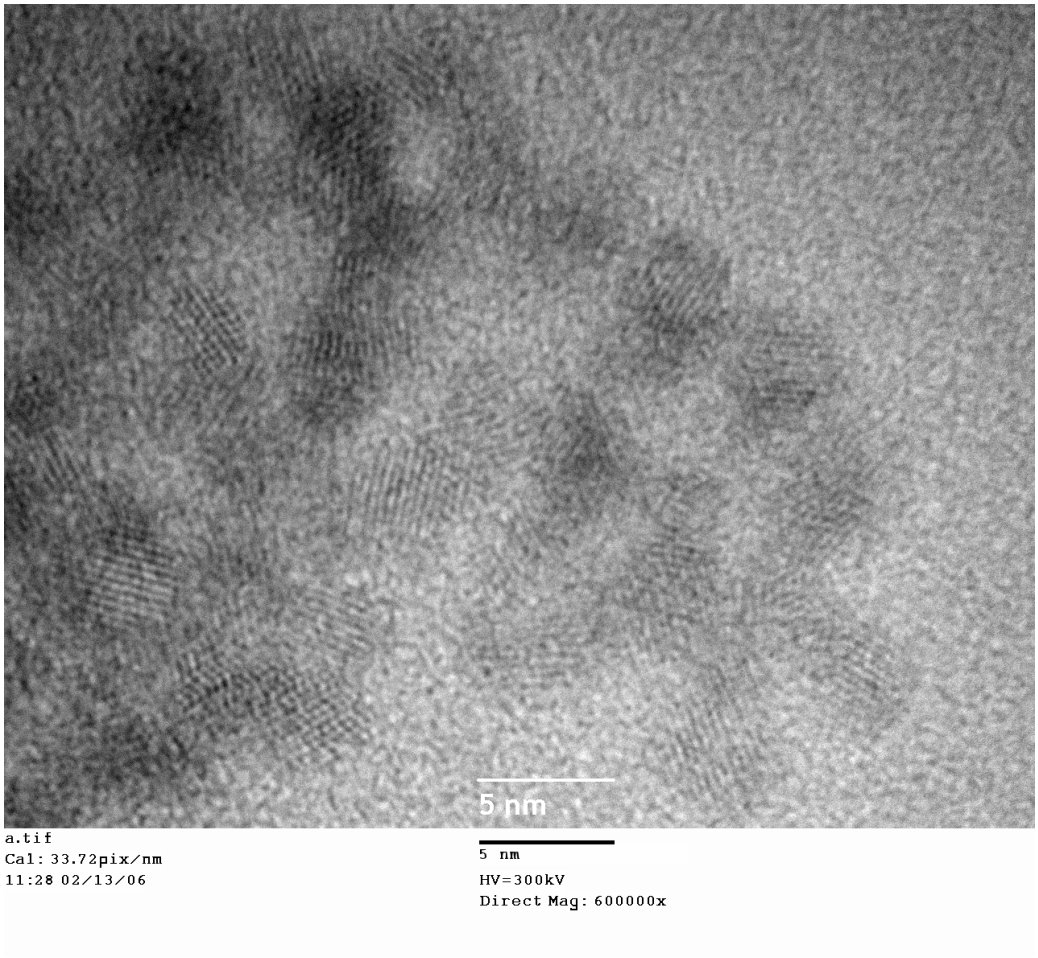

Figure 5.2. HRTEM image of CdSe nanocrystals synthesized in high-temperature water under base case conditions.

5.3.2 Effect of Temperature

We explored the effect of temperature within a range of 200 – 215 °C. All other variables remained at their base case values. Figure 5.3 shows normalized emission spectra for CdSe crystals synthesized at different temperatures. Table 5.1 provides a summary of the effect of reaction temperature on λ_{max} and fwhm. The graphic indicates that as the temperature increases, the nanocrystal size increases. At the higher temperatures, a cloudy, brownish product was observed, suggesting the presence of larger CdSe particles with bulk properties.

The fwhm is 36, 37, 39 and 39 nm for the particles synthesized at 200, 205, 210 and 215 °C, respectively. There is a very modest upward trend in these values, but the increase may be within the bounds of experimental error. Though we cannot completely rule out the existence of a relationship between temperature and particle size distribution, the relationship is a weak one if it indeed exists.

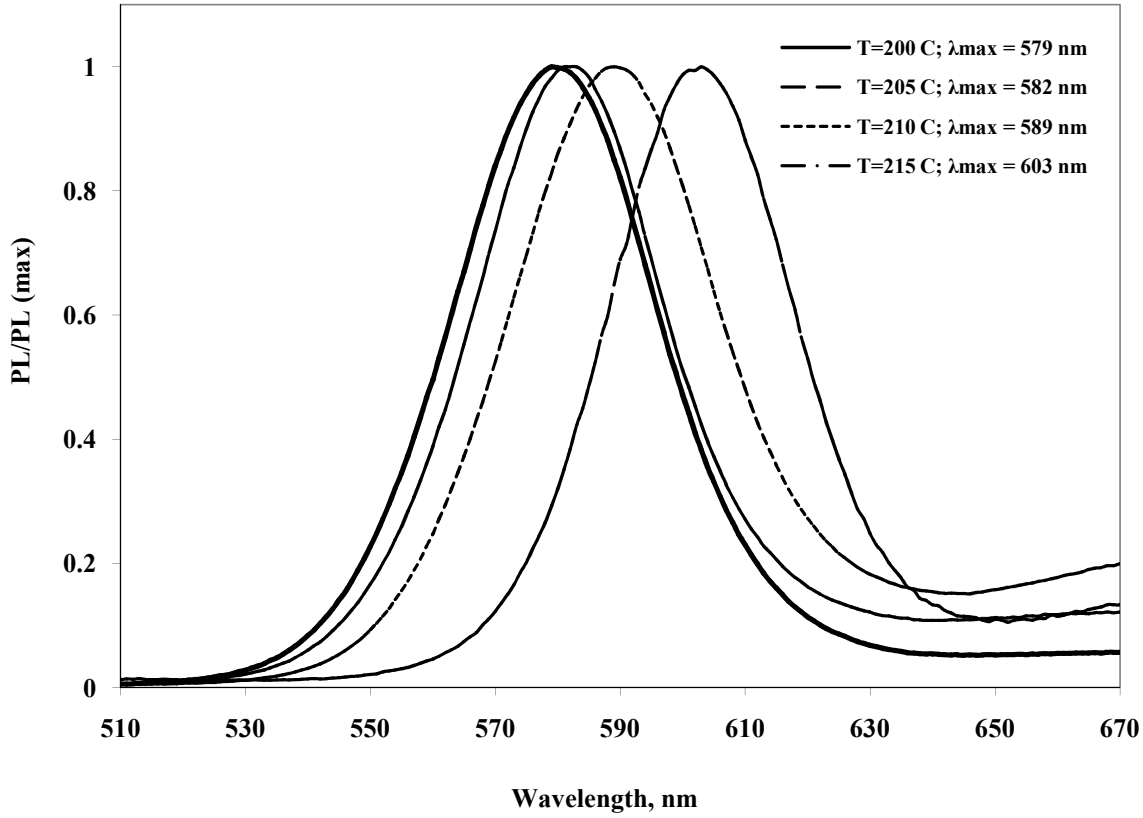

Figure 5.3. Normalized PL emission spectra for CdSe nanocrystals synthesized in high-temperature water at different sand bath temperatures.

T, °C	λ_{max}, nm	fwhm, nm
200	579	36
205	582	37
210	589	39
215	603	39

Table 5.1. A summary of the effect of temperature on the PL emission peak (λ_{max}) and size distribution (fwhm).

5.3.3 Effect of Batch Holding Time

We next focused on the batch holding time. In general, one expects the size of the nanocrystal to increase with increasing reaction time as more material adds to its surface. Figure 5.4 shows emission curves for particles synthesized at the same temperature and Cd:Se ratios, but batch holding times increasing in 30 second increments. Table 5.2 shows the relationship between the batch holding time and the nanocrystal's properties, λ_{max} and fwhm. As expected, the nanocrystal's size (as inferred from λ_{max}) increases as reaction time increases. The increase in λ_{max} with each additional 30 sec of reaction is about the same for all peaks except for those from the runs at 1.5 to 2.0 minutes. There is a larger gap between these two curves. A replicate set of experiments exhibited the same gap. The precise reason for this gap is not clear, but it seems there may exist a nucleation and/or growth process that is sensitive to the higher average reactor temperature in the two-minute experiment.

The fwhm values (34, 34, 36, 36 and 36) are all about the same for the different synthesis times. These experiments suggest that the size distribution is not affected much by the reaction time.

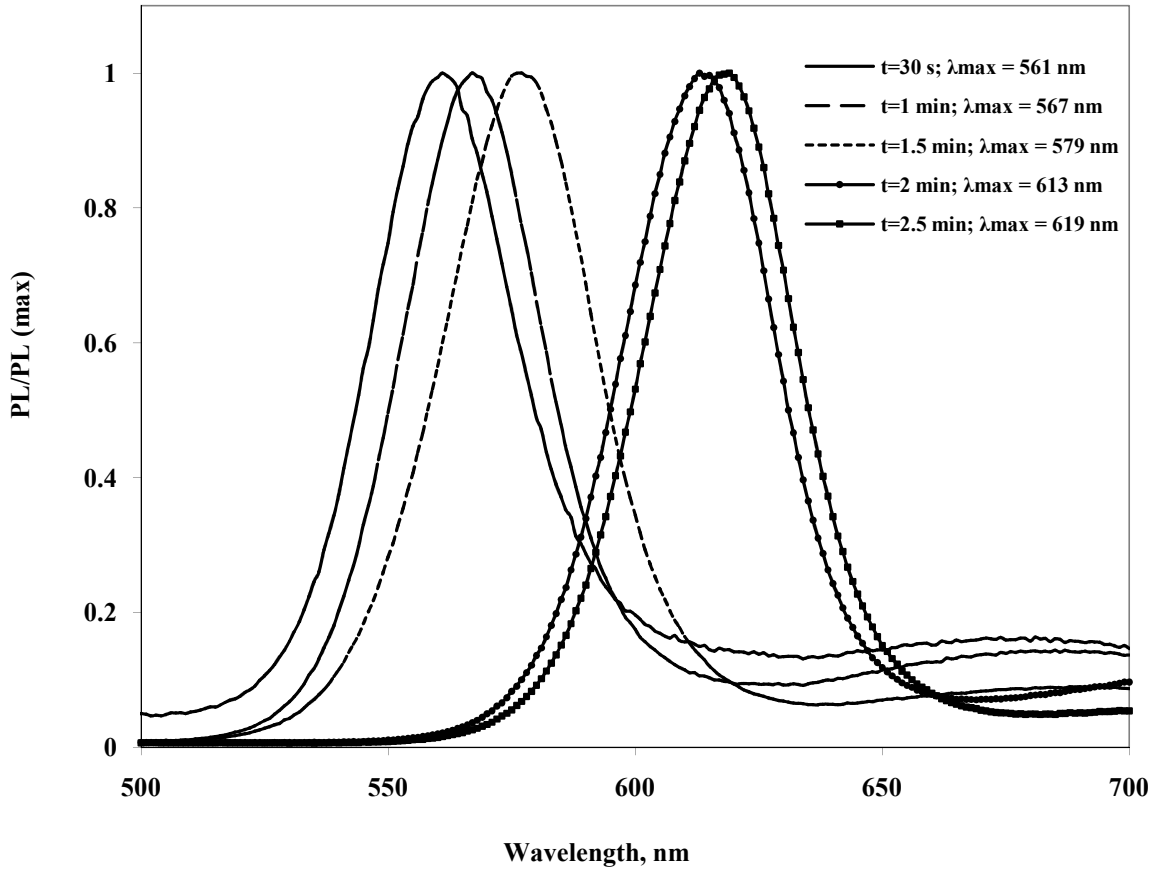

Figure 5.4. Normalized PL emission spectra for CdSe nanocrystals synthesized in high-temperature water at different batch holding times.

t, min	λ_{max}, nm	fwhm, nm
0.5	561	34
1.0	567	34
1.5	579	36
2.0	613	36
2.5	619	36

Table 5.2. A summary of the effect of reaction time on the PL emission peak (λ_{max}) and size distribution (fwhm).

5.3.4 Effect of Cd:Se Molar Ratio

A few previous studies showed that the precursor ratios can dramatically influence the behavior of CdSe synthesis [7, 8, 9]. Donega et al. [8] and Peng [7] both concluded that an excess of Se, in addition to the judicious choices of other parameters, yields highly luminescent and nearly monodisperse nanocrystals without any postpreparative treatment. It must be noted, however, that these two studies involved organic-based systems. No studies exist on the influence of Cd:Se ratio during hydrothermal synthesis of the nanocrystals.

Figure 5.5 shows that λ_{max} increases as the Cd:Se ratio increases. Table 5.3 provides a summary of the effect of Cd:Se molar ratio on the λ_{max} and fwhm trends. This trend indicates that the mean particle size likewise increases. The fwhm of the spectra decreases from 39 to 36 to 32 nm as the Cd:Se ratio increases from 4:1 to 8:1 to 16:1. This trend suggests that the size-distribution narrows as the Cd:Se ratio increases, under the base case conditions for temperature and time, similar to the data previously obtained for microwave synthesis of CdS [10].

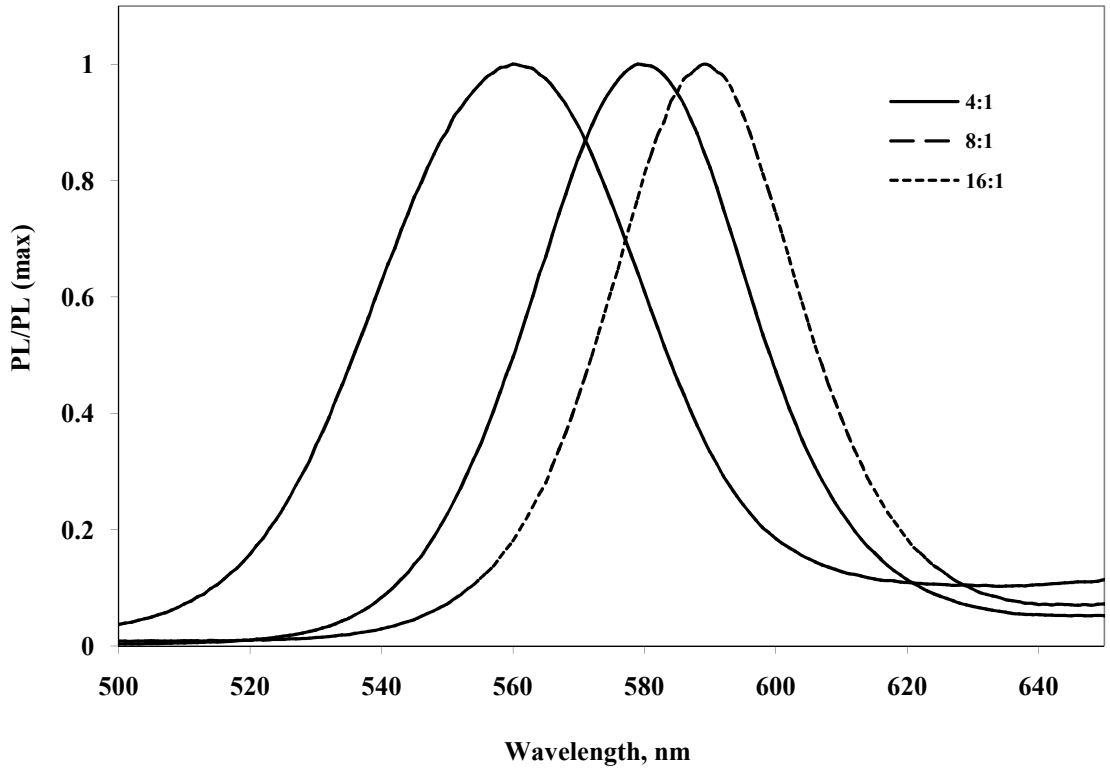

Figure 5.5 Normalized PL emission spectra for CdSe nanocrystals synthesized in high-temperature water at different Cd:Se molar ratios.

Cd:Se	λ_{max}, nm	fwhm, nm
4	560	39
8	579	36
16	589	32

Table 5.3. A summary of the effect of the Cd:Se molar ratio on the PL emission peak (λ_{max}) and size distribution (fwhm).

5.3.5 Effect of pH

Basic conditions facilitate the coordination of the sodium citrate stabilizer to the cadmium ion. We wanted to learn the effect of pH on the average particle size during hydrothermal synthesis. Figure 5.6 shows that the more basic the environment, the smaller the nanocrystal. Table 5.4 summarizes the effect of pH on λ_{max} and fwhm. This result is reasonable because as the coordination between the citrate and cadmium ion strengthens, the particles will become more stabilized and less likely to add more material. The fwhm steadily increases with pH. The values were 34, 36, 37 and 43 nm at a pH of 8, 9, 10 and 11, respectively. These results indicate that the particle size distribution broadened as the pH increased.

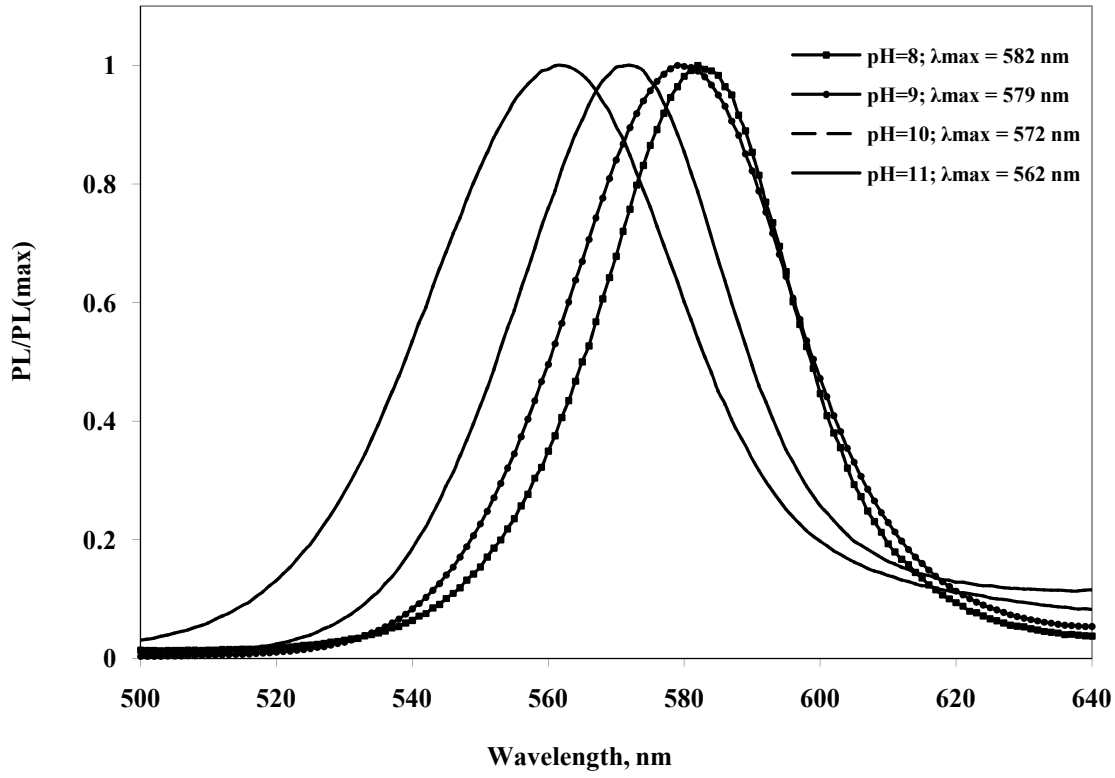

Figure 5.6. Normalized PL emission spectra for CdSe nanocrystals synthesized in high-temperature water at different pHs.

pH	λ_{max}, nm	fwhm, nm
8	582	34
9	579	36
10	572	37
11	562	43

Table 5.4. A summary of the effect of pH on the PL emission peak (λ_{max}) and size distribution (fwhm).

5.3.6 Effect of Stabilizer Loading

The sodium citrate stabilizer helps to control the size of the nanocrystal. The literature suggests that using larger amounts of stabilizer would yield smaller nanocrystals [11]. We observed an opposite trend. Figure 5.7 shows that λ_{max} decreases (smaller particles) as the amount of stabilizer decreases (increasing Cd:stabilizer ratio). Being surprised by this result, we repeated the experiments. Precisely the same trend was observed in the replicate runs. Therefore, we believe the effect in Figure 5.7 is real and cannot be attributed to random error. This unexpected result may indicate that the nucleation and growth processes in this system somehow differ from those in other systems previously explored. Clearly, further research is warranted to understand the effects of the sodium citrate stabilizer on the nanocrystal growth rate. Unlike the mean particle size, the range of the size distribution is virtually unaffected by the increase in stabilizer loadings. The fwhm values were 36, 35, 35 and 36 at the four different Cd:stabilizer ratios. Table 5.5 shows the summary of the effect of stabilizer loading on λ_{max} and fwhm.

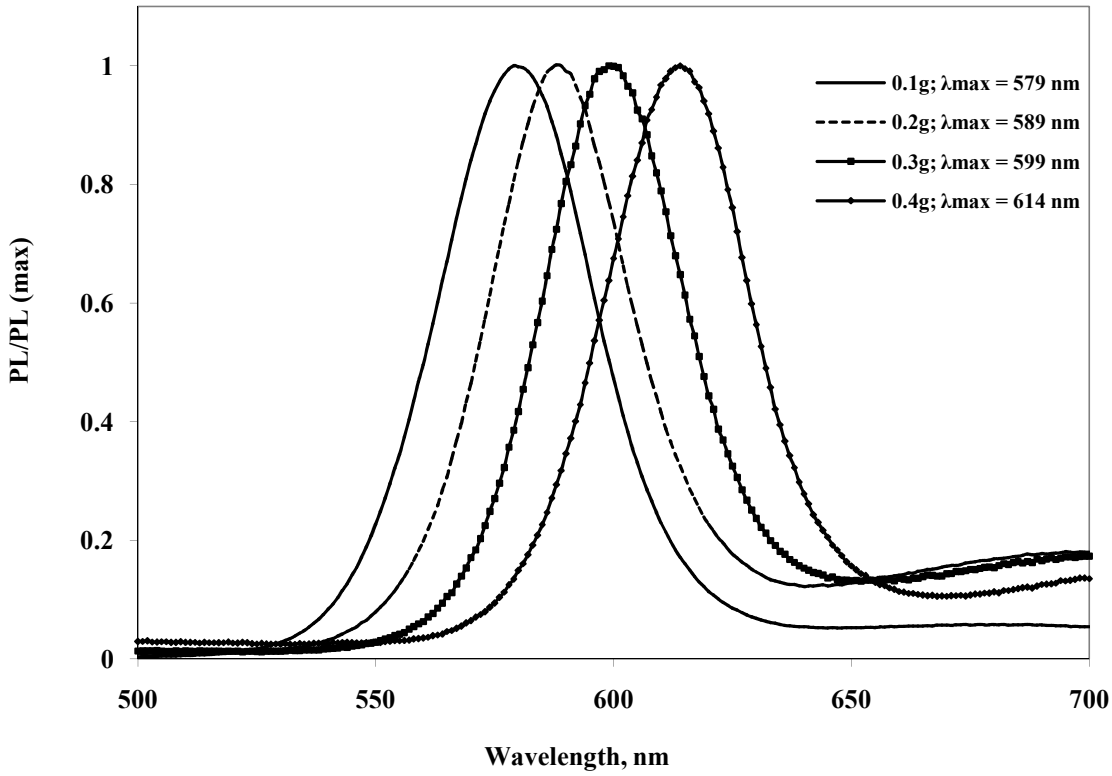

Figure 5.7. Normalized PL emission spectra for CdSe nanocrystals synthesized in high-temperature water at different stabilizer loadings.

Cd: stabilizer ratio	Stabilizer amount, g	λ_{max}, nm	fwhm, nm
1.18	0.1	579	36
.59	0.2	589	35
.39	0.3	599	35
.27	0.4	614	36

Table 5.5. A summary of the effect of the Cd:stabilizer molar ratio on the PL emission peak (λ_{max}) and size distribution (fwhm).

5.3.7 Improving Quantum Yield

The addition of an outer shell layer to CdSe nanocrystals is known to improve the quantum yield. For example, the methods of Rogach et al. for low-temperature aqueous phase synthesis increased the quantum yield from 0.15 to 4.2% by adding a layer of CdS [1]. The shell serves to passivate the crystal's surface, decreasing the number of defects that a bare crystal tends to possess. The quantum yield in the present experiments increased from 1.5% (base case) to approximately 7% by adding a CdS shell. This result shows that CdSe nanoparticles with quantum yields of at least 7% can be prepared from the one-pot hydrothermal synthetic methods we described herein.

5.4 Summary

The one-pot synthesis of CdSe nanoparticles in high temperature water has been demonstrated for the first time. Hydrothermal synthesis at T=200 °C, Cd:Se=8:1, t=1.5 minutes produced CdSe nanocrystals that exhibit quantum confinement behavior as characterized by the blue shift of a strong emission peak and the ability to fluoresce. The nanoparticle size and overall size distribution depended on the reaction temperature, batch holding time, Cd:Se molar ratio, pH and Cd:stabilizer ratio. The size increased with an increase in reaction temperature, time, stabilizer concentration and Cd:Se ratio and, a with a decrease in pH. This trend with the stabilizer loading was unexpected. It suggests that this hydrothermal synthesis method may provide new opportunities to engineer nanoparticle production systems. It also suggests that the chemistry of CdSe nanoparticle synthesis in HTW might differ from that in coordinating organic solvents.

The quantum yield proved to be low for the base-case CdSe crystals. The addition of a CdS shell, which can be done easily in HTW, increased the quantum yield to approximately 7%. The low quantum yield for the bare particle (1.5%) could be a result of allowing both nucleation and growth to occur together in the reactor system. One potential remedy is to develop a method of injecting the molecular precursors into preheated high temperature water.

5.5 Bibliography

1. Rogach, A. L.; Nagesha, D.; Ostrander, J. W.; Giersig, M.; Kotov, N. A. "Raisin Bun"-Type Composite Spheres of Silica and Semiconductor Nanocrystals. *Chem. Mater.* **2000***, 12*, 2676-2685.

2. Murray, C. B.; Norris, D. J.; Bawendi, M. G. Synthesis and Characterization of nearly Monodisperse Cde (E = S, Se, Te) Semiconductor Nanocrystallites. *J. Am. Chem. Soc.* **1993***, 115*, 8706-8715.

3. Michalet, X.; Pinaud, F.; Lacoste, T. D.; Dahan, M.; Bruchez, M. P.; Alivisatos, A. P.; Weiss, S. Properties of Fluorescent Semiconductor Nanocrystals and their Application to Biological Labeling. *Single Mol.* **2001***, 2*, 261.

4. Murray, C. B.; Nirmal, M.; Norris, D. J.; Bawendi, M. G. Synthesis and Structural Characterization of Ii-Vi Semiconductor Nanocrystallites (Quantum Dots). *Zeits. Fur Phys. D* **1993***, 26*, S231-S233.

5. Asokan, S.; Krueger, K., M; Alhkawaldeh, A.; Carreon, A., R; Mu, Z.; Colvin, V., L; Mantzaris, N., V; Wong Michael, S. The use of Heat Transfer Fluids in the Synthesis of High-Quality CdSe Quantum Dots, core/shell Quantum Dots, and Quantum Rods. *Nanotechnology* **2005***, 16*, 2000.

6. Qu, L. H.; Peng, Z. A.; Peng, X. G. Alternative Routes Toward High Quality CdSe Nanocrystals. *Nano Lett.* **2001***, 1*, 333-337.

7. Peng, Z. A.; Peng, X. Formation of High-Quality CdTe, CdSe and CdS Nanocrystals using CdO as a Precursor. *J. Am. Chem. Soc.* **2001***, 123*, 183.

8. Donega, C. D.; Hickey, S. G.; Wuister, S. F.; Vanmaekelbergh, D.; Meijerink, A. Single-Step Synthesis to Control the Photoluminescence Quantum Yield and Size Dispersion of CdSe Nanocrystals. *J Phys Chem B* **2003***, 107*, 489-496.

9. Peng, X. G.; Wickham, J.; Alivisatos, A. P. Kinetics of II-VI and III-V Colloidal Semiconductor Nanocrystal Growth: "Focusing" of Size Distributions. *J. Am. Chem. Soc.* **1998***, 120*, 5343-5344.

10. Ni, T.; Nagesha, D. K.; Robles, J.; Materer, N. F.; Mussig, S.; Kotov, N. A. CdS Nanoparticles Modified to Chalcogen Sites: New Supramolecular Complexes, Butterfly Bridging, and Related Optical Effects. *J. Am. Chem. Soc.* **2002***, 124*, 3980-3992.

11. Sun, S.; Murray, C. B.; Doyle, H. Controlled Assembly of Monodisperse ε-Cobalt-Based Nanocrystals. *Mater. Res. Soc. Symp. Proc.* **1999**, 385-398.

Chapter 6

Rapid Hot-injection Method

In the previous chapter, we demonstrated the formation of CdSe nanocrystals using high-temperature water as a reaction solvent. But, we speculated that the nucleation and growth dynamics were not conducive to creating high-quality nanocrystals. In this chapter, we test the hypothesis that by using a rapid hot-injection method similar to convention, we will be able to affect nucleation and growth dynamics, possibly separating the two more than what the previous method allowed.

6.1 Introduction

The upsurge in the study of CdSe nanocrystals began with the trailblazing work performed by Murray et al. where high quality nanocrystals were obtained, not only due to reaction conditions, but, in part because of the synthetic route. Their synthesis began with the injection of a cold precursor solution into a hot reaction solvent, causing the formation of nuclei. Because the solvent temperature dropped, the formation of new nuclei ceased, and the system contained relatively monodisperse nuclei and enough free cadmium and selenium ions to establish a slow growth at a temperature lower than the injection temperature. Researchers [1, 2, 3, 4, 5, 6, 7] later adapted the Murray method, producing nanocrystals with various physical attributes. Murray et al. set the precedent

for a requisite strategy for obtaining high-quality, uniform nanocrystals: the separation of nucleation and growth. The adoption of separate nucleation and growth events as an important concept in nanocrystal synthesis was made possible from the work performed by LaMer and Dinegar [8]. They showed that a monodisperse preparation of colloids was best achieved by producing just one "brief outburst" of nuclei, leaving enough free monomer to then produce growth by diffusion. This outburst was consistent with classical nucleation theory which states that under a condition of supersaturation and thus high free energy, clusters of monomer can form as a means of relieving the energy. Murray et al. [9] believed that the temperature of the solution was sufficient to decompose the reagents and, upon injection, form a supersaturated solution. The resulting high free energy was relieved by nucleation of nanocrystals wherein the concentration of the monomer dropped below a critical concentration required for nucleation. Growth was then allowed on existing nuclei, the rate of which depended on the temperature.

Donega et al. [10] evaluated the phenomenology of nucleation within the framework of the rapid hot-injection method. They concluded that while it is doubtful that the classical theory can be quantitatively applied to the formation of nuclei in the hot-injection method, it can provide a qualitative basis for it. Their explanation is in agreement with Murray's.

Our hot-injection method is different from convention in that we do not inject a cold fluid into a hot fluid, but, rather, into a hot metal chamber. The cold fluid comes into immediate contact with a metal surface, much like pouring cold water into a hot pan on the stove. When this occurs, there is an instantaneous formation of bubbles. It could stand to reason that similar bubbles form when injecting the cold precursor solution into the hot reactor, and the bubbles themselves serve as nucleation sites. So, while we do not affect the saturation limit of the precursor solution, we may provide an opportunity to induce nucleation due to the temperature differential.

6.2 Experimental Methods

We conducted experiments in stainless steel batch reactors fitted with a high-temperature rated bellows valve as described in Chapter 4. All analytical methods used for this study include spectroscopy and TEM, descriptions of which are in Chapter 4. All emission data is displayed as normalized curves to show only the effect of the experimental conditions on the peak wavelength.

6.3 Results and Discussion

6.3.1 Base Case Synthesis

The following conditions were chosen as a base case: T = 200 °C, t = 2 minutes, pH = 9, Cd:stabilizer molar ratio = 1.18, Cd:Se molar ratio = 8:1. Similar to what was observed in the feasibility study, the emission spectrum does undergo a blue shift from the bulk band gap (~700 nm), indicating the existence of quantum confinement.

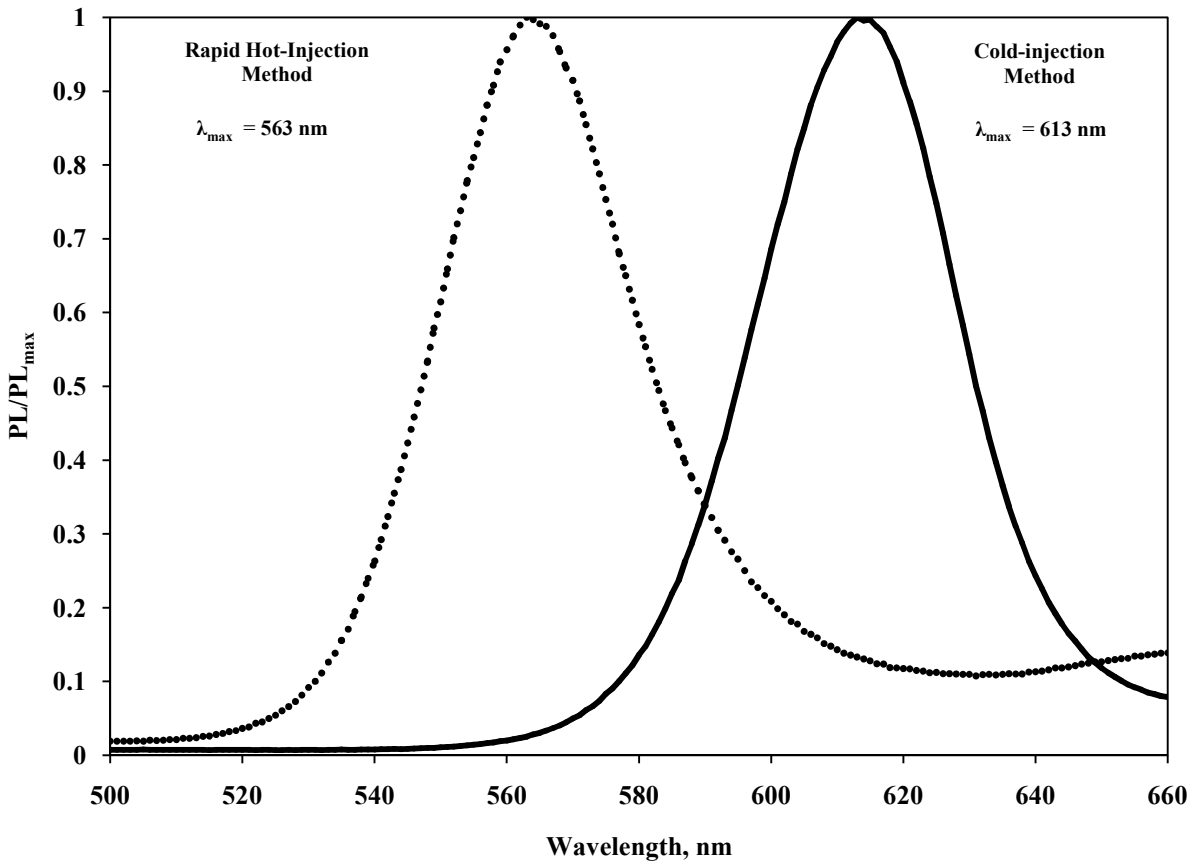

Figure 6.1. Normalized PL peak spectra for CdSe nanocrystals synthesized in high-temperature water using the rapid hot-injection (base case conditions) and cold injection (conditions identical to those for rapid hot-injection) methods.

The mean size of the nanocrystals formed by the rapid hot-injection method is smaller (λ_{max} = 563 nm) than that formed by the method conducted in the feasibility study under the same conditions (λ_{max} = 613 nm) (Figure 6.1). An analysis by HRTEM (Figure 6.2) confirms that the mean particle size (about 3.5 nm) is indeed smaller. The cold-injection method yielded a mean particle size of approximately 5 nm based on HRTEM. The sizes were also determined by using the effective mass approximation and were calculated to be 4.9 nm for the rapid hot-injection study and 5.2 nm for the feasibility study. The effective mass approximation, although not precise for small nanocrystals, does confirm the effects of quantum confinement and the rapid hot-injection method producing smaller particles.

For the base case, repeat experiments resulted in an average λ_{max} of 557 $\pm$ 6.5 nm, where the uncertainty is the standard deviation. We did not repeat experiments for all conditions, but the standard deviation observed at the base case likely applies to the other experiments that were conducted.

The fluorescence intensity of the nanocrystals formed under the rapid hot-injection conditions is a little more than half of that formed under the cold-injection method (Figure 6.3). Nakamura prepared CdSe in a microflow reactor and observed weak intensities by the smaller particles [11].

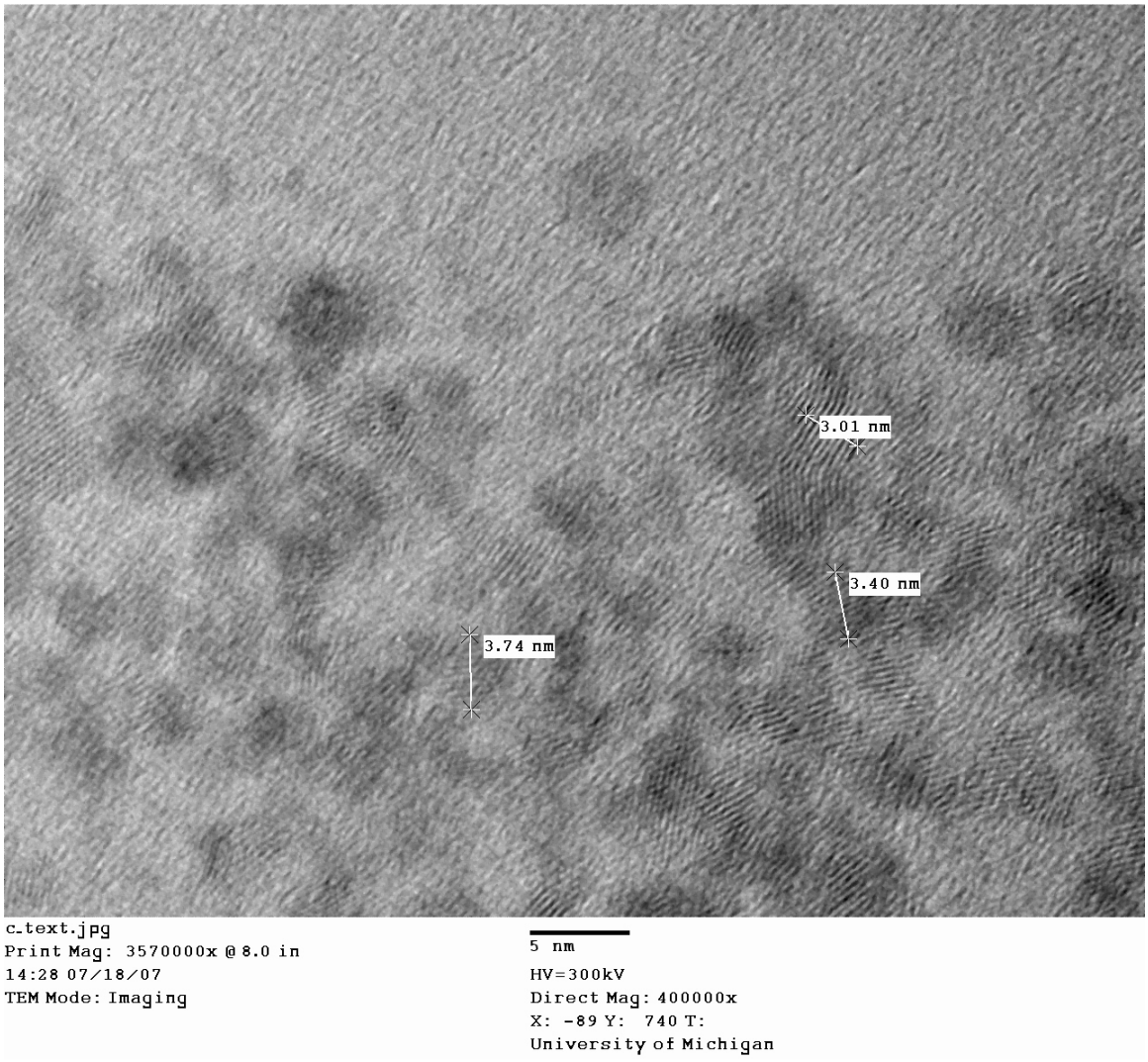

Figure 6.2 HRTEM image of CdSe nanocrystals produced by rapid hot-injection under base case conditions.

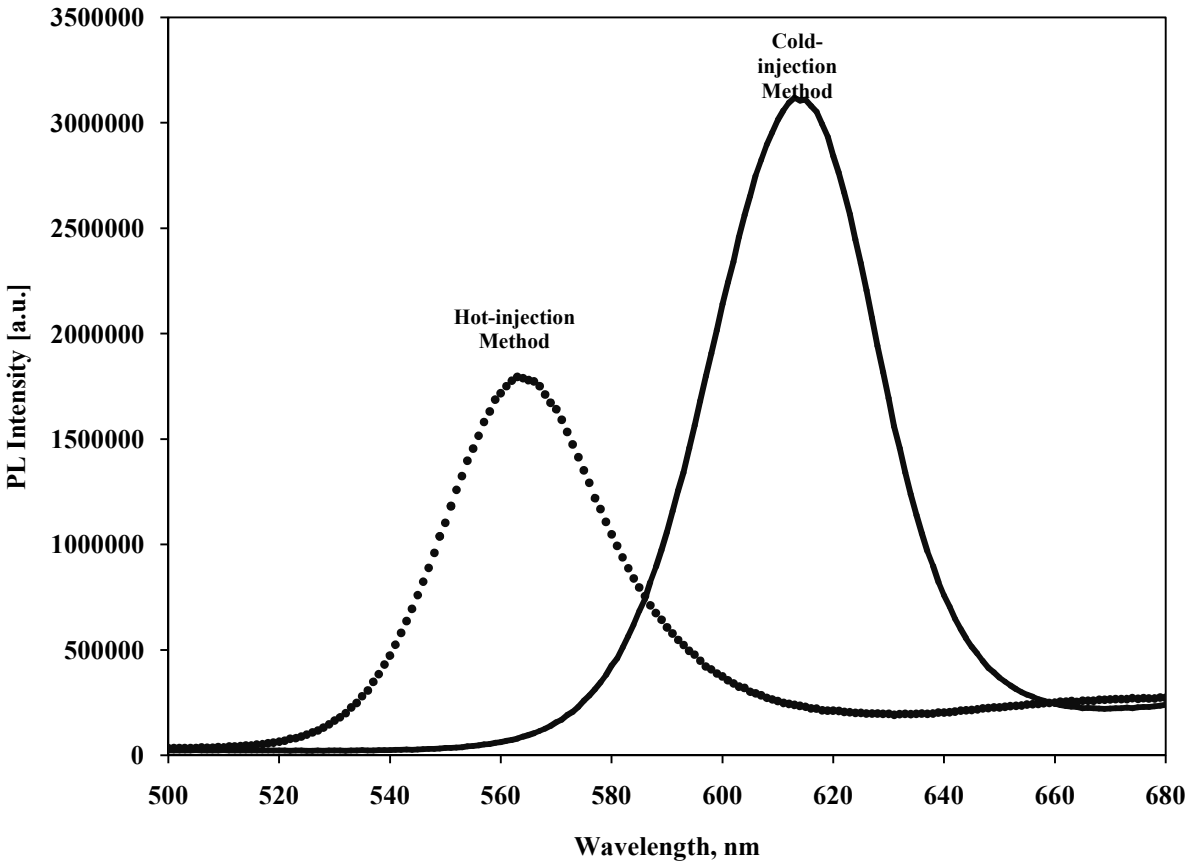

Figure 6.3. Fluorescence intensities for CdSe nanoparticles synthesized in high-temperature water using the rapid hot-injection and cold injection methods. The spectra represent base case conditions.

The full-width-at-half-max (fwhm) was determined from the emission spectrum to be 35 nm. The fwhm for the nanocrystals formed under the cold-injection method with the same conditions is 36 nm. There does not seem to be any difference in the degree of monodispersity for the two methods. For the base case, repeat experiments resulted in an average fwhm of 35.7 $\pm$ 1.1 nm. Again, this measure of the random error is likely applicable to all other experiments that were conducted. Since a narrow size distribution can be defined as fwhm $\leq$ 40 nm [9], we can conclude that the base case for rapid hot-injection has a rather narrow size distribution.

The quantum yield for the base case was calculated to be 0.99 %. This is not much different from the quantum yield calculated for the base case under the cold-injection method (1.5%), even though the batch holding times are different (2 minutes for rapid hot-injection vs. 1.5 minutes for cold-injection). The presence of the weaker emission also supports the lower quantum efficiency, which may arise from either inadequate surface passivation or deep trapped emission due to surface defects. It is easier to tune the particle properties by modifying the surface via passivation, something we investigated and will discuss later.

6.3.2 Effect of Temperature

The temperature dependence of nanoparticle size and quality was investigated for a range of 200 – 240 °C. All other variables remained at their base case values. Normalized PL emission profiles are displayed in Figures 6.4 and 6.5. Table 6.1 shows the fwhm and quantum yield for the particles obtained at each temperature.

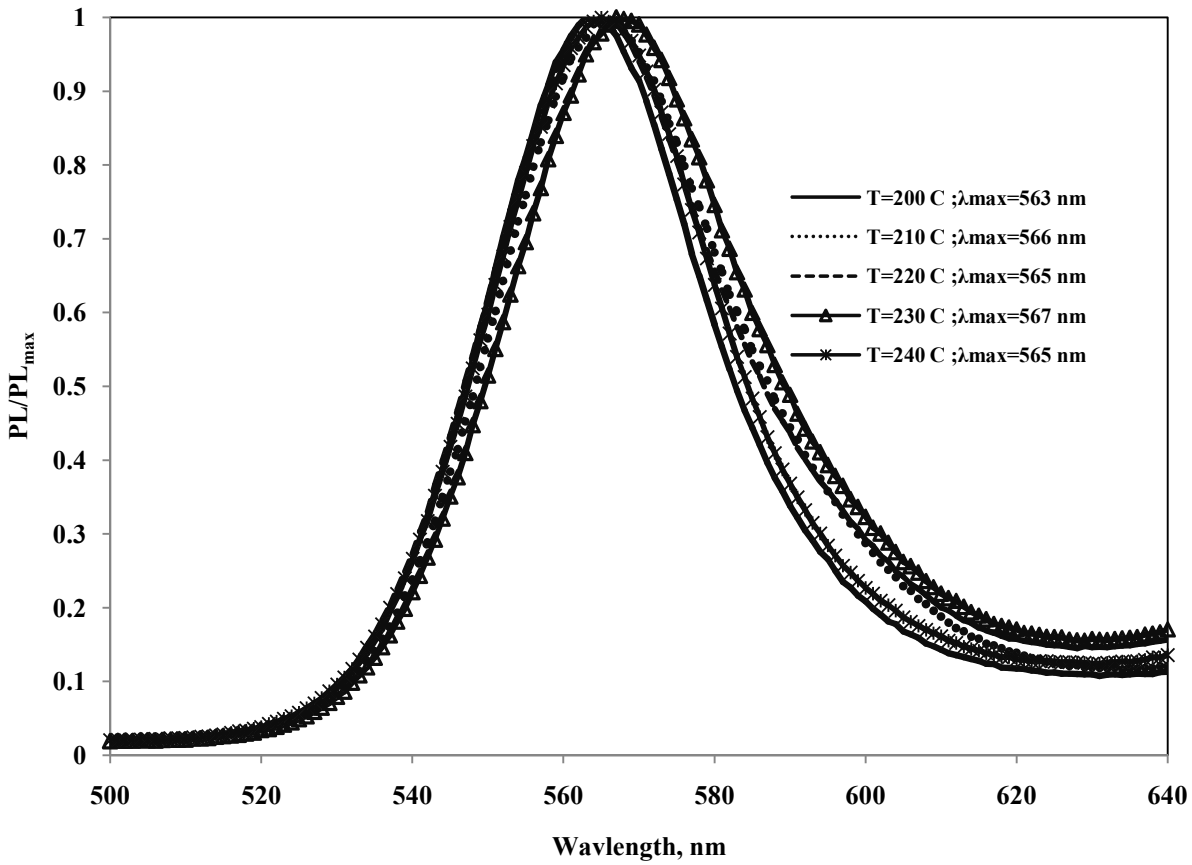

Figure 6.4. Normalized PL emission spectra for CdSe nanocrystals synthesized in high-temperature water at different sand bath temperatures.

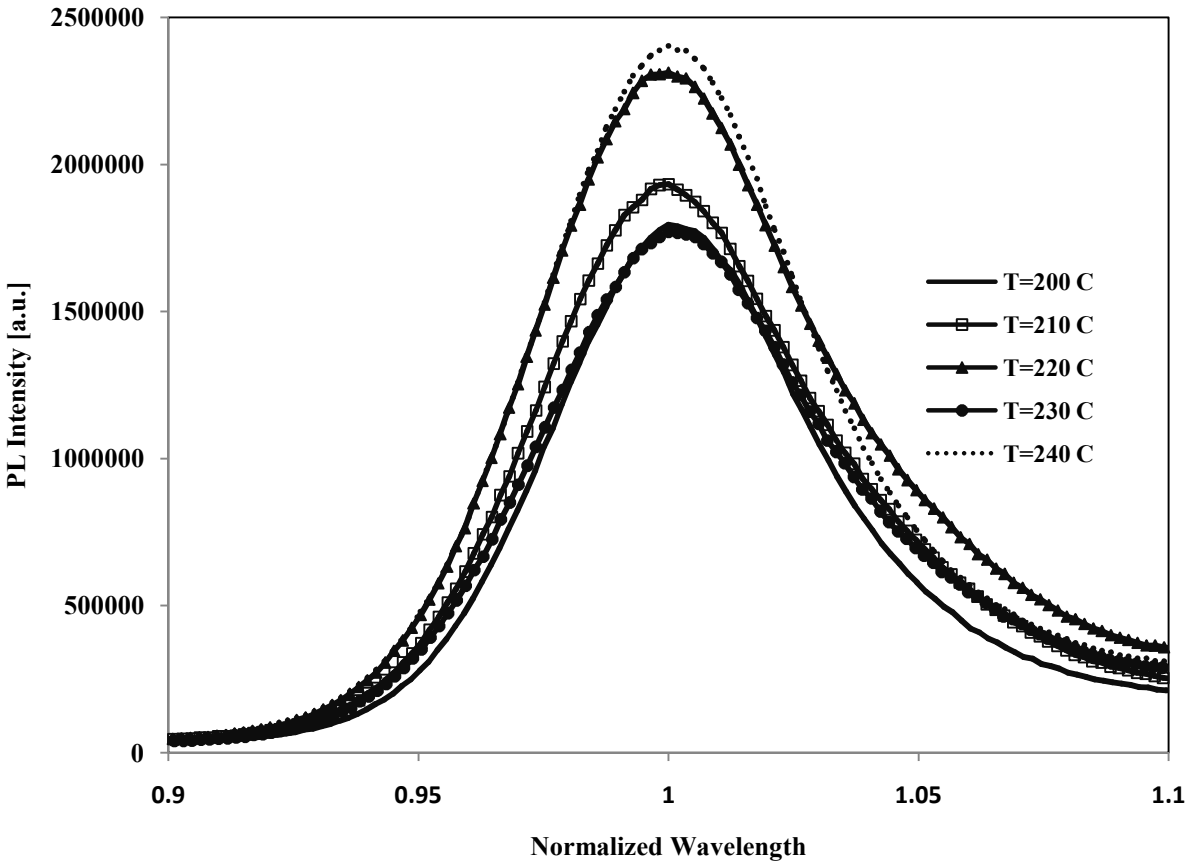

Figure 6.5. Profile of peak intensities for CdSe nanocrystals synthesized in high-temperature water at different sand bath temperatures.

T, °C	λ_{max}, nm	fwhm, nm	QY, %
200	563	35	.99
210	566	38	5.7
220	565	37	5.5
230	567	37	5.3
240	565	37	4.9

Table 6.1. A summary of the effect of temperature on the PL emission peak (λ_{max}), size distribution (fwhm) and quantum yield (QY).

The temperature seems to have very little effect on the particle's mean size, as indicated by the small differences in the λ_{max} values. A temperature range of 40 °C resulted in a λ_{max} range of only 4 nm, which is definitely within the experimental uncertainty of ±6.5 nm. It should be noted that we were able to explore a much wider range of temperatures with the rapid hot-injection method, as the final product did not convert to bulk cadmium selenide. The highest temperature for the cold-injection method was 215 °C as this was a temperature that would still yield cadmium selenide nanocrystals in the time scale we could investigate experimentally. With a temperature range of 15 °C, we observed a 20 nm range in λ_{max}.

Though the temperature does not affect the nanocrystal's size for the rapid hot-injection method, we recognize that the reaction time was only two minutes. It is possible that this reaction time may be too short to exhibit any significant growth. It is also possible that the rapid-injection method may have contributed to this phenomenon because of the nucleation. Dushkin et al. [12] assert that the nucleation event can, and does, define the subsequent growth behavior. Bullen et al. [4] studied nucleation and growth of CdSe nanocrystals in a non-coordinating solvent, observing effects of temperature, among other variables. They observed smaller nuclei and final particle sizes as the temperature increased. They suggest that at higher temperatures, nucleation events are faster, nuclei concentration increases and growth kinetics are less strongly dependent on temperature. This scenario may help explain the results we obtained. As the concentration of CdSe nuclei increases with an increase in temperature, the availability of monomer decreases. With a lack of material to add to existing nuclei, further growth is slowed tremendously.

Table 6.1 shows that the temperature has very little effect on the size distribution within the experimental temperature range, or, on the quantum yield. The quantum yield for T = 200 °C is considerably lower than those for the remaining temperatures. It is important to note that this rapid injection method did achieve quantum yields much higher than those obtained for the base case from the previous method (QY = 1.5%). Although we did not calculate quantum yields for all cases in the cold-injection method, it is likely that the yields would not have increased with an increase in temperature since the nanoparticle size increased dramatically.

It has long been recognized [9, 13] that the growth stage following a nucleation event, if controlled, can increase the quantum yield due to thermal annealing. It is believed that the growth of the nanoparticle allows the surface to restructure through the addition of material. The surface can reorganize by adding ligands needed to passivate dangling cadmium ions and eliminating trapped surface charges to allow for proper electron-hole recombination. Because we observed no appreciable increase in the mean size of the nanocrystal at higher temperatures, we would not expect the quantum yield to change very much with temperature. The temperature increase may have only served to create additional nuclei, thereby influencing the physical properties of the system, rather than the nanoparticle's surface properties. This scenario is consistent with the quantum yields at 210 – 240 °C in Table 6.1 being essentially independent of temperature. This does not explain the sudden increase in quantum yield from T=200 °C to the higher temperatures.

The general trend observed in relation to temperature and nanocrystal intensity was that the highest reaction temperature yielded the brightest nanocrystal (Figure 6.5). We believe that this is due to thermal annealing of the surface.

The temperature of the system is crucial in the overall growth and final size of CdSe nanoparticles, especially under the rapid injection method. Murray et al. pioneered this method, which involved injection of a cold fluid into a hot solvent. The injection led to the instantaneous formation of CdSe nuclei. The subsequent drop in temperature, due to injection of the cold precursor solution, helped to prevent formation of new nuclei. Consequently, a manual increase in the temperature led to a slow growth of the nanoparticles. One difference in our system is that we did not inject the cold precursor solution into a hot solvent, but rather into a hot empty metal reactor. We speculate that a nucleation event was induced simply because of the temperature. The reactor temperature probably decreased upon injection which limited nucleation. As for the growth, it occurred at roughly the same temperature as the injection. Based on the success of others' hot-injection synthetic routes, we hypothesize that nucleation and growth were more discrete events in this hot-injection method than in the injection method discussed in the previous chapter.

6.3.3 Effect of Reaction Time

Time, as a synthesis condition, has been studied to assess its effects on nanoparticle size and overall quality. With all other parameters remaining constant, we should expect the size of the nanocrystals to increase with an increase in reaction time. This is because more material is allowed to add to existing nanoparticles. Figures 6.6 and

6.7 show the temporal evolutions of nanoparticle size (as inferred from λ_{max}) and intensity in a time range of 10 minutes from synthesis at 200 °C. As indicated by the increase in λ_{max}, appreciable growth occurs within the entire 10 minute time span.

We observed no consistent trend in the peak intensity. The base case time of 2 min exhibits the largest intensity. There seems to be an alternating increase/decrease in intensity as the time increases.

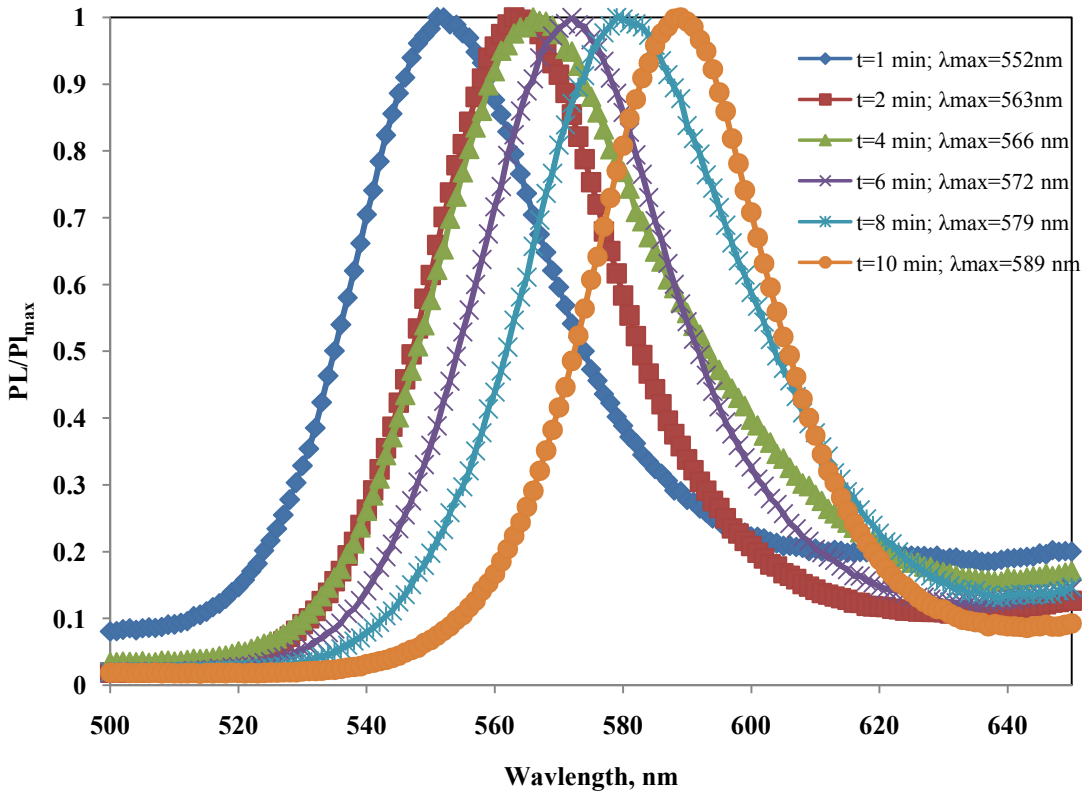

Figure 6.6. Normalized PL emission spectra for CdSe nanocrystals synthesized in high-temperature water at different reaction times.

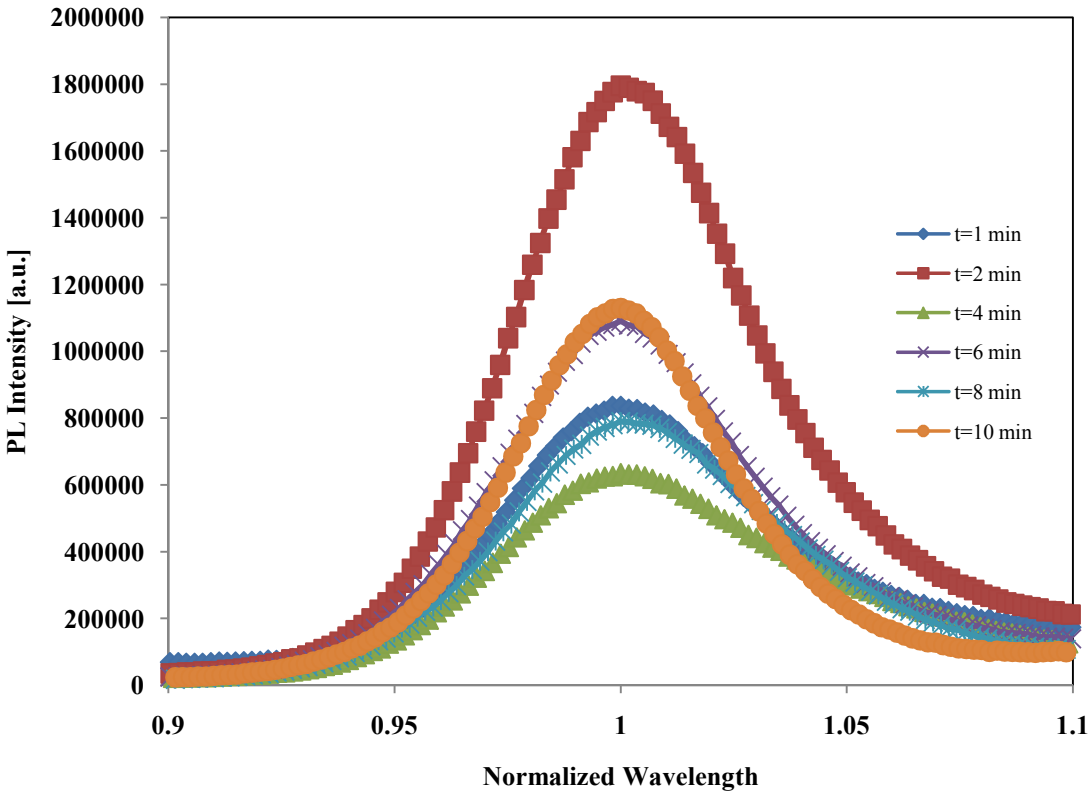

Figure 6.7. Profile of PL peak intensities for CdSe synthesized in high-temperature water at different reaction times.

Table 6.2 shows the effect of reaction time on λ_{max} , the fwhm, and the quantum yield. The fwhm values show a modest change, with the largest value at 4 minutes and at 8 minutes. It is unclear whether there is a true increase in fwhm from t = 1 to 4 minutes and then a decrease from t = 4 to 10 minutes. It does appear that the smaller fwhm values correlate with the lower quantum yields.

t, min	**λ_{max}, nm**	**fwhm, nm**	**QY, %**
1	555	35	1.1
2	563	35	0.99
4	566	40	1.7
6	572	36	1.1
8	579	40	1.3
10	589	33	0.71

Table 6.2. A summary of the effect of reaction time on the PL emission peak (λ_{max}), size distribution (fwhm) and quantum yield (QY).

The feasibility study and this study did reveal similar trends (increase in time yielded an increase in size), but we did find that this study produced smaller nanoparticles. For the feasibility study, a 2.5 min reaction time span produced nanoparticles with λ_{max} = 619 nm. An increase in time ($t \geq 3$ min) resulted in brownish-red precipitate forming, indicating larger bulk CdSe particles. For the rapid hot-injection study, we were able to react for 10 minutes and produce nanoparticles with a λ_{max} = 589 nm. This outcome may be a function of the synthesis method as we allowed contact of the cold precursor solution with a hot metal surface. Small bubbles may have formed on the surface of the reactor, acting as the sites for nuclei on which the bulk material would grow.

We did not observe any effect of time on the fwhm for the feasibility study and we are reluctant to declare the existence of any trend under the rapid hot-injection method. Even when we have assumed, from the base case, that a 95% confidence interval of ± 1.1 nm can be applied for all of our experiments, we still cannot conclude that the initial increase in the fwhm followed by the decrease may in fact be real.

An increase in the reaction time will increase the size of a nanoparticle since there is more time for material to move from the bulk to the nanoparticle's surface. This observation was also apparent in the feasibility study and is not a new concept. Since nanoparticle size is the most important physical attribute, the application of time, in the context of nanoparticle synthesis, is useful when analytical expressions can be derived and used to describe the evolution of nanocrystal growth. We will discuss, in more detail, the aspect of time in regards to the growth kinetics in Chapter 7.

6.3.4 Effect of Cd:Se Molar Ratio

Since the surface of the nanocrystal plays such a crucial role in affecting the overall quality of the nanocrystal, a systematic control of the ratio of metal precursors could in turn control and improve the photoluminescence qualities [13]. Figures 6.8 and 6.9 show normalized emission spectra and a profile of peak intensities for CdSe nanocrystals synthesized at 200 °C and different Cd:Se molar ratios. Table 6.3 further shows the effect of the different molar ratios on the fwhm and the quantum yield.

Our results reveal that the initial Cd:Se molar ratio is a determining factor for the emission properties of the synthesized nanocrystals. The size and quantum yield trends were strongly correlated with the increase in the Cd:Se molar ratio. Figure 6.8 reveals a decrease in nanoparticle size as the Cd:Se molar ratio increases. This is expected with our system since we did not change the number of cadmium ions for each experiment. Thus, the Cd:stabilizer molar ratio remained constant. We did vary, however, the selenium concentration. With less selenium monomer available for particle growth, the size of the nanoparticle should decrease.

Table 6.3 shows that while the fwhm is virtually unaffected by the initial Cd:Se ratio, the quantum yield increases. It is possible that with fewer dangling Se bonds, fewer trapped emission sites exist, thereby increasing the quantum yield [6, 14].

Our results are in stark contrast to those produced from the cold-injection method, where a more cadmium-rich environment yielded larger nanocrystals. The cold-injection method most likely promoted Ostwald ripening. With decreasing amounts of selenium monomer, the critical particle size required to maintain equilibrium increased so any particles that remained in solution were at least slightly larger than the critical size. Peng

et al. [3] even discuss the importance of injecting additional monomer in order to shift the critical particle size of the nanoparticle back to a smaller value.

The rapid hot-injection method may have allowed for instantaneous formation of nuclei, but subsequent growth may have been hindered, possibly due to cadmium-citrate complexes slowing the rate of additional selenium monomer. At a molar ratio of 40:1, selenium monomer may have been virtually unavailable for further growth.

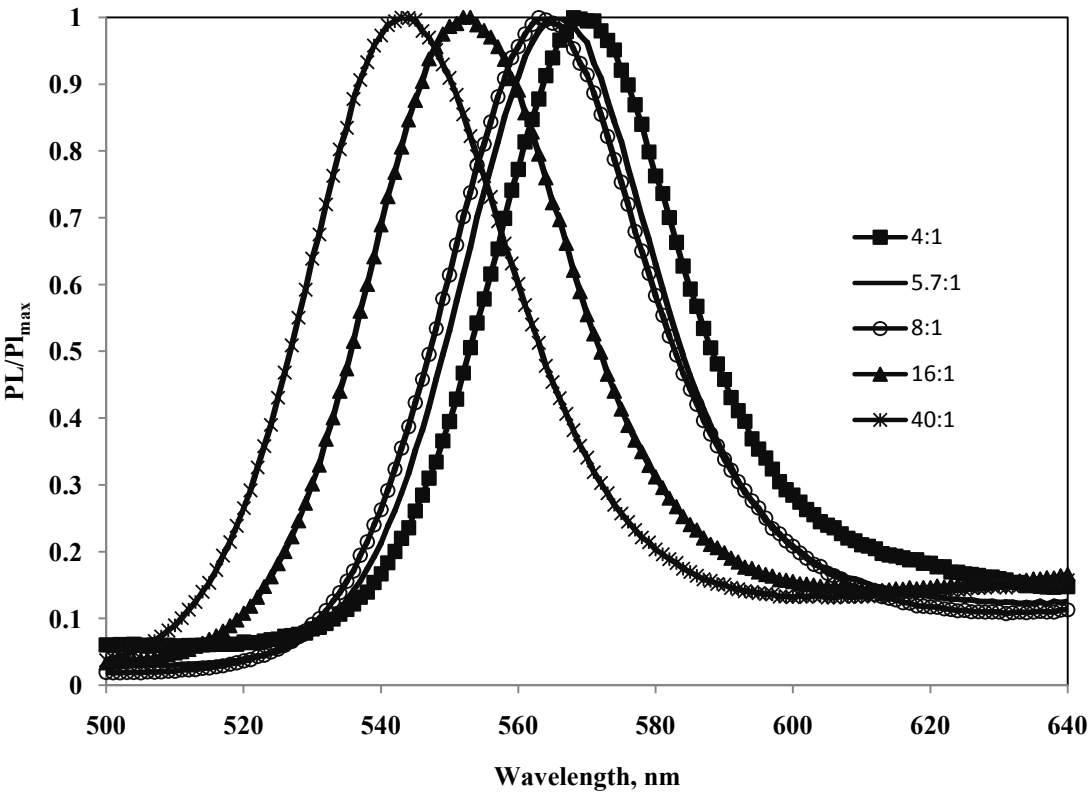

Figure 6.8. Normalized PL emission spectra for CdSe nanocrystals synthesized in high-temperature water at different Cd:Se molar ratios.

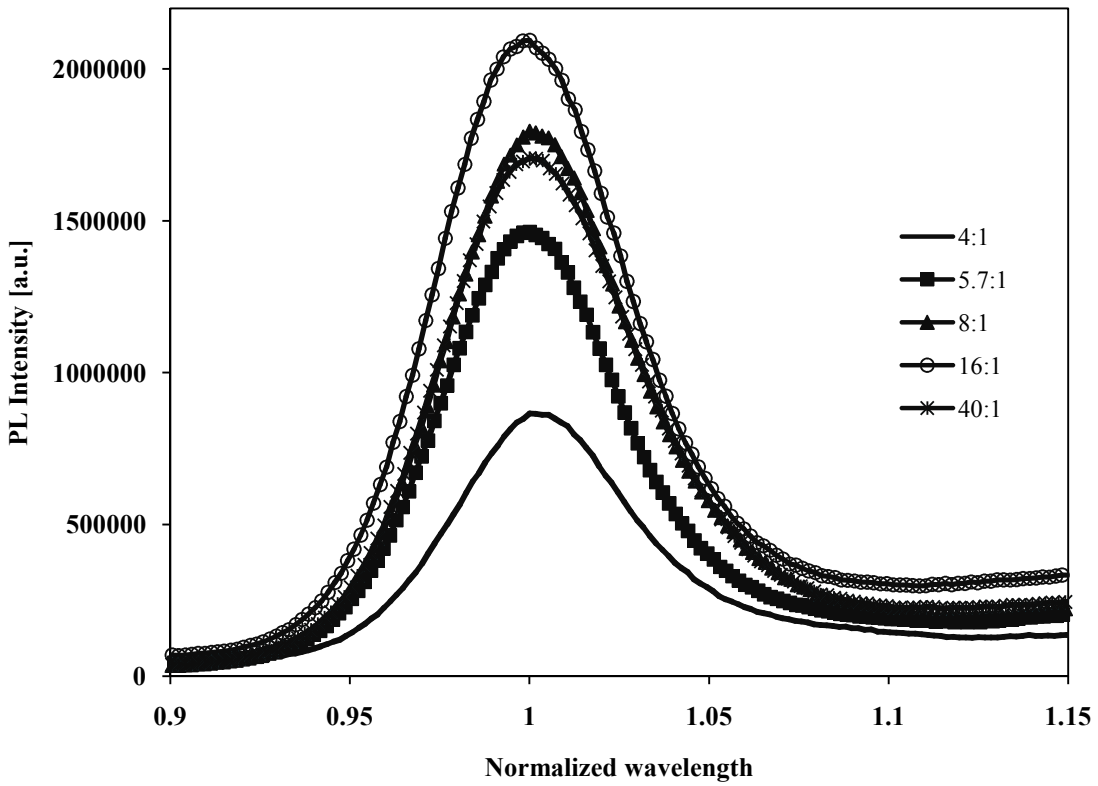

Figure 6.9. Profile of peak intensities for CdSe nanocrystals synthesized in high-temperature water at different Cd:Se molar ratios.

Cd:Se	λ_{max}, nm	fwhm, nm	QY, %
4:1	568	34	.05
5.7:1	566	34	2.2
8:1	563	35	.99
16:1	553	34	3.9
40:1	543	35	4.9

Table 6.3. A summary of the effect of the Cd:Se molar ratio on the PL emission peak (λ_{max}), size distribution (fwhm) and quantum yield (QY).

Numerous researchers have studied the characteristics of CdSe grown in excess selenium [6, 13, 15]. A selenium-rich environment promoted a faster nucleation process, higher quantum yields and narrower size distributions. Conversely, cadmium-rich systems resulted in fewer nuclei formed, slow nucleation, and low quantum yields [6]. We did not carry out experiments in excess of selenium because the selenium precursor reacted with oxygen from the air. In spite of this limitation, our results do show that the surface chemistry, as modified by the changing the Cd:Se molar ratio, is indeed a major influence of the nanoparticle's quality. These parameters had the most dynamic affect on the quantum efficiency.

6.3.5 Effect of pH

The results obtained from experiments using the cold-injection method showed that a higher basicity yielded smaller particles. We observed a similar trend for the rapid injection method (Figure 6.10). The emission peak from nanoparticles synthesized (200 °C) at a pH of 7 is much less defined in the rapid injection method, primarily due to the extremely weak intensity (Figure 6.11). Nanoparticles synthesized at higher pH values exhibit more intense emission and do generate well-defined peaks. The nanoparticle size decreases from the base case condition (pH = 9) as pH increases and yields more intense emission spectra. Additionally, the quantum efficiency increases with the increase in pH from the base case condition.

Our results imply that, in the presence of increased alkalinity, cadmium citrate complexes are more strongly bound, stabilizing growth (smaller nanocrystal) and electronically passivating the surface (stronger emission peak). Furthermore, cadmium adsorption to the nanocrystal may be stronger, since it is widely known that cadmium

ions tend to desorb at low pH values [16]. This increased affinity for the surface would aid in creating a more optimal surface structure, and with the cadmium's increased affinity to the citrate, reducing dangling bonds.

Gao et al. [17] observed enhanced fluorescence for CdTe nanoparticles prepared in low pH in an aqueous solution. They conclude that the particle surface coverage with thiol ligands is increased in acidic CdTe solutions. They suggest that a thick layer of cadmium thiol complexes is formed on the nanoparticle's surface and can be considered as a wide-band gap material, making it analogous to CdS or ZnS passivation shell around the CdTe core. Although our nanoparticles are prepared in the presence of a higher pH, this same type of pH-sensitive phenomenon could very well be occurring in our system.

For pH values above 9, we observed a reaction after the selenium precursor was injected into the cadmium and citrate solution. The color of the solution began to change while remaining optically clear, indicating the formation of CdSe. Thus, it seems that a chemically-induced nucleation event occurred. Subsequent injection of the solution into the hot reactor prompted a separate thermally-induced nucleation event. The initial CdSe nuclei may have been shrouded with cadmium citrate complexes, delaying any additional material to be adsorbed onto the particle during the thermal growth event. The thermally-induced nuclei may not have had much material addition due to fewer free cadmium and selenium ions available for appreciable growth.

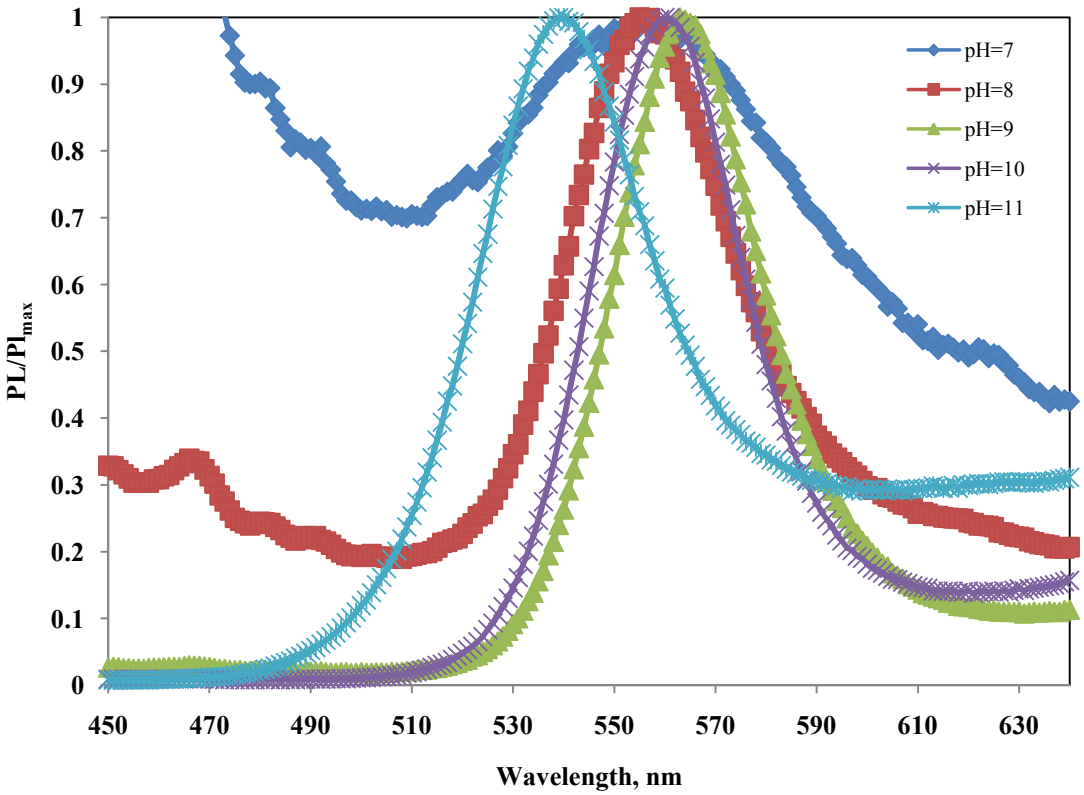

Figure 6.10. Normalized PL emission spectra for CdSe nanocrystals synthesized in high-temperature water at different pHs.

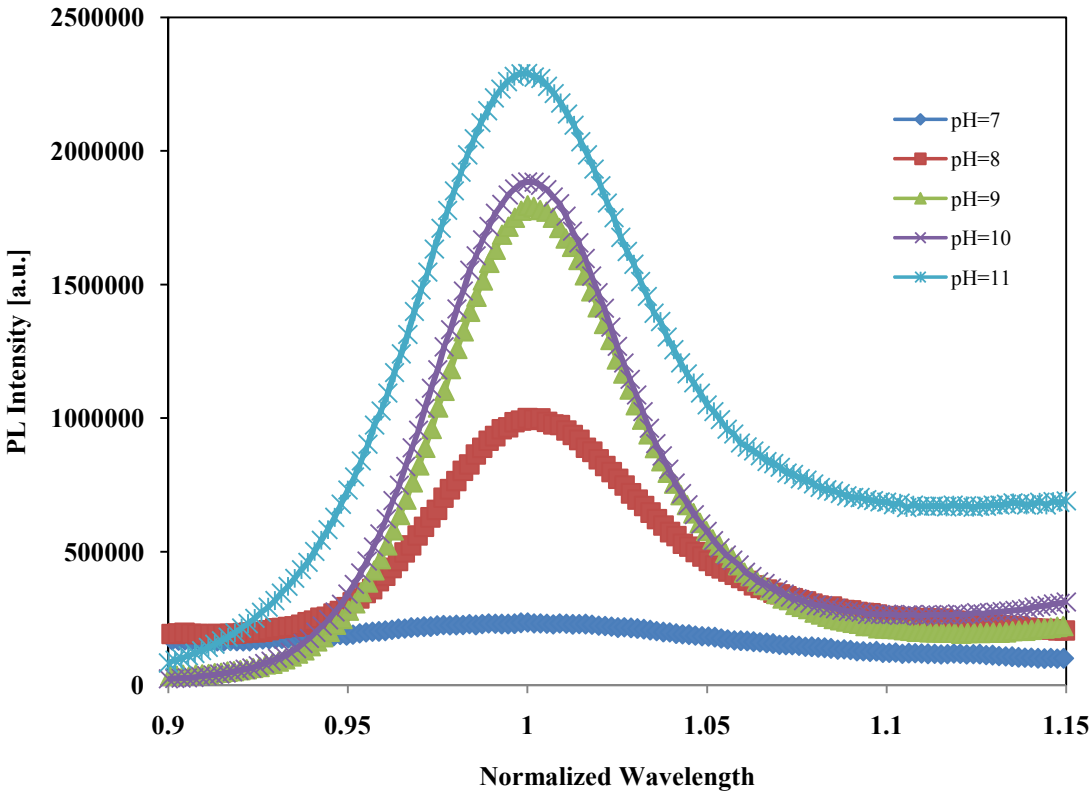

Figure 6.11. Profile of peak intensities for CdSe nanocrystals synthesized in high-temperature water at different pHs.

pH	λ_{max}, nm	fwhm, nm	QY, %
7	556	N/A	.56
8	555	36	3.3
9	563	35	.99
10	560	35	3.8
11	540	36	5.2

Table 6.4. A summary of the effect of pH on the PL emission peak (λ_{max}), size distribution (fwhm) and quantum yield (QY).

6.3.6 Effect of StabilizerLloading

We reported earlier that, under the cold injection method, larger amounts of stabilizer increased the particle size. We observed an identical trend with the rapid-injection method. As the stabilizer amounts decrease, the mean particle size decreases and the intensity increases dramatically (Figures 6.12 and 6.13). The data shows that dispersity increases initially, and then decreases as the nanoparticle size increases. There does not seem to be a consistent trend between the fwhm and the amount of stabilizer, although, at higher stabilizer amounts, the fwhm does trend downward. Reasons for this could be due to there being a small number of particles. The presence of too many citrate ions in the solution may be preventing the cadmium and selenium ions from attaching. The sheer number of citrate ions could overwhelm the cadmium, hindering the formation of many CdSe nuclei, but, at the same time, the citrate could rapidly complex to the cadmium ion as any nuclei form. Bullen et al. [4] observed this phenomenon while synthesizing CdSe nanoparticles in hot octadecene. They noticed that the number of nuclei linearly reduced as more oleic acid (capping agent) was added.

The decrease in the quantum yield with increasing amount of stabilizer may be a result of limited overgrowth to reconstruct the surface during the growth stage [13]. The excess citrate may provide a steric hindrance to the selenium monomer as it tries to move through the bulk to the nanocrystal's surface. This would increase the chance of there being dangling cadmium bonds, and would adversely affect the quantum efficiency.

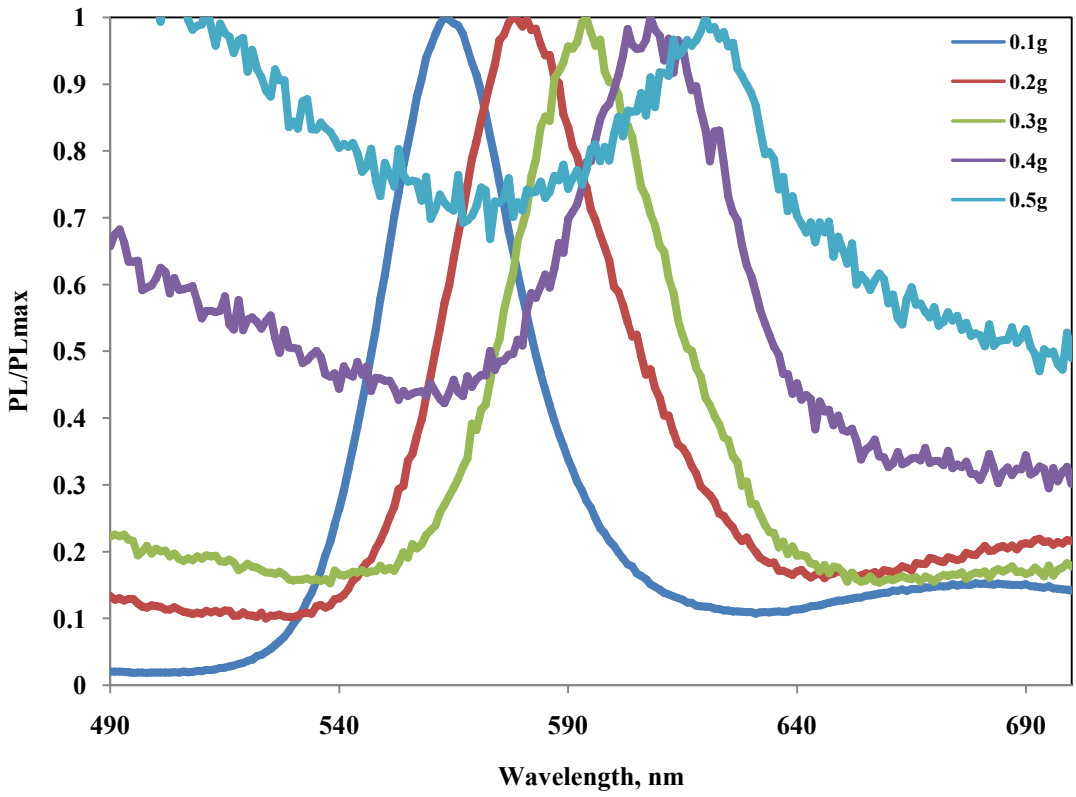

Figure 6.12. Normalized PL emission spectra for CdSe nanocrystals synthesized in high-temperature water at different stabilizer loadings.

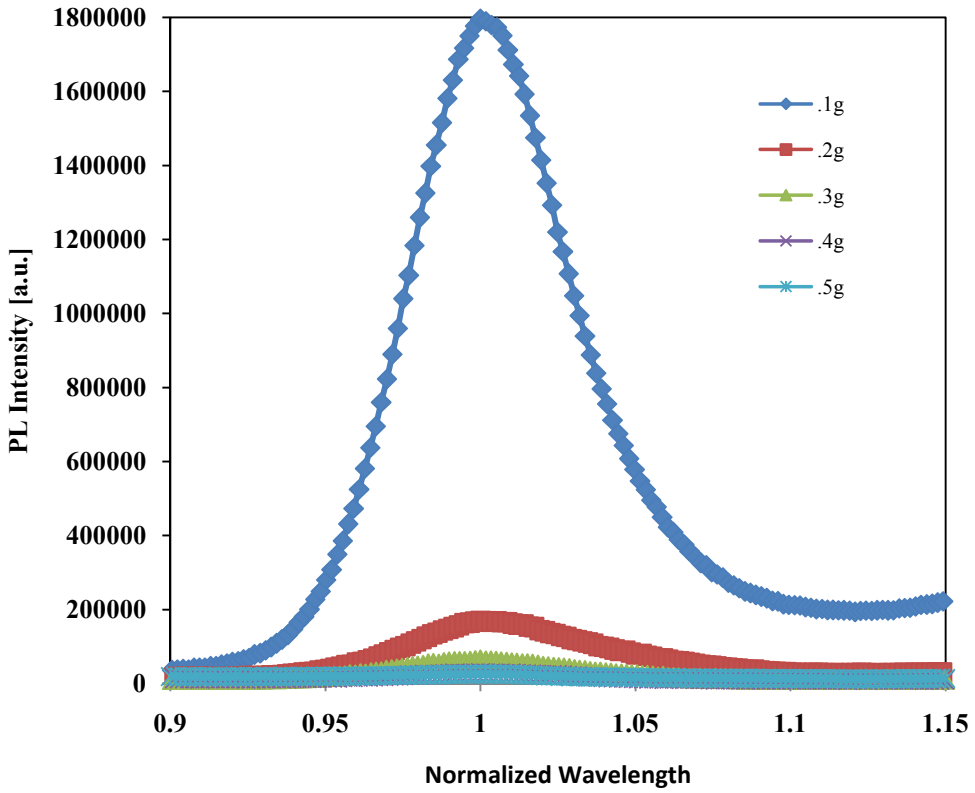

Figure 6.13. Profile of peak intensities for CdSe nanocrystals synthesized in high-temperature water at different stabilizer loadings.

Cd: stabilizer ratio	Stabilizer amount, g	λ_{max}, nm	fwhm, nm	QY, %
1.18	0.1	563	35	0.99
.59	0.2	578	40	0.64
.39	0.3	594	37	0.22
.27	0.4	608	32	0.08
.24	0.5	620	19	0.06

Table 6.5. A summary of the effect of the Cd:stabilizer ratio on the PL emission peak (λ_{max}), size distribution (fwhm) and quantum yield (QY).

6.4 Summary

This chapter highlights the results of using a rapid hot-injection method that is similar to that found in conventional methods. Our investigation revealed a smaller nanocrystal (λ_{max} = 563 nm) and a similar fwhm (35 nm) compared with Chapter 5's cold-injection method (λ_{max} = 613 nm; fwhm = 36 nm) under the same experimental conditions. The QY calculated for the rapid hot-injection method was 0.99%. This is not much different from the QY calculated for the cold-injection method of 1.5% under the same experimental conditions except for time, which differed by 30 seconds. We surveyed the effects of experimental parameters on the size (represented by λ_{max}, size-distribution (represented by fwhm) and QY.

size – an increase in reaction time increased the size, while an increase in Cd:Se molar ratio, pH and Cd:stabilizer ratio decreased the size. An increase in reaction temperature did not affect the nanocrystal size.

fwhm – an increase in the reaction temperature, Cd:Se molar ratio and pH did not affect the fwhm. There seemed to be no consistent trend with the stabilizer loading in general, but at higher stabilizer loadings, the fwhm tended to decrease.

QY – an increase in Cd:Se molar ratio, pH and Cd:stabilizer molar ratio increased the QY, but an increase in the reaction temperature and time had no effect on QY

The rapid hot-injection method offers advantages over the cold-injection method from the previous chapter in that a larger reaction temperature range can be explored. It is also an adaptation of the preferred injection method since it more readily separates nucleation from growth. These are reasons why we continued using this method for the kinetics study presented in the next chapter.

6.5 Bibliography

1. Qu, L. H.; Peng, Z. A.; Peng, X. G. Alternative Routes Toward High Quality CdSe Nanocrystals. *Nano Lett.* **2001***, 1*, 333-337.

2. Peng, X. G.; Manna, L.; Yang, W. D.; Wickham, J.; Scher, E.; Kadavanich, A.; Alivisatos, A. P. Shape Control of CdSe Nanocrystals. *Nature* **2000***, 404*, 59-61.

3. Peng, X. G.; Wickham, J.; Alivsatos, A. P. Kinetics of II-VI and III-V Colloidal Semiconductor Nanocrystal Growth: "Focusing" of Size Distributions. *J. Am. Chem. Soc.* **1998***, 120*, 5343-5344.

4. Bullen, C. R.; Mulvaey, P. Nucleation and Growth Kinetics of CdSe Nanocrystals in Octadecene. *Nano Lett.* **2004***, 4*, 2303-2307.

5. Qu, L. H.; Yu, W. W.; Peng, X. P. In Situ Observation of the Nucleation and Growth of CdSe Nanocrystals. *Nano Lett.* **2004***, 4*, 465-469.

6. Qu, L. H.; Peng, X. G. Control of Photoluminescence Properties of CdSe Nanocrystals in Growth. *J. Am. Chem. Soc.* **2002***, 124*, 2049-2055.

7. Talapin, D. V.; Rogach, A. L.; Kornowski, A.; Haase, M.; Weller, H. Highly Luminescent Monodisperse CdSe and CdSe/ZnS Nanocrystals Synthesized in a Hexadecylamine-Trioctylphosphine Oxide-Trioctylphospine Mixture. *Nano Lett.* **2001***, 1*, 207-211.

8. LaMer, V. K.; Dinegar, R. H. Theory, Production and Mechanism of Formation of Monodispersed Hydrosols. *J. Am. Chem. Soc.* **1950***, 72*, 4847-4854.

9. Murray, C. B.; Norris, D. J.; Bawendi, M. G. Synthesis and Characterization of nearly Monodisperse Cde (E = S, Se, Te) Semiconductor Nanocrystallites. *J. Am. Chem. Soc.* **1993***, 115*, 8706-8715.

10. Donega, C. D. M.; Liljeroth, P.; Vanmaekelbergh, D. Physicochemical Evaluation of the Hot-Injection Method, a Synthesis Rotue for Monodisperse Nanocrystals. *Small* **2005***, 1*, 1152-1162.

11. Nakamura, H.; Yamaguchi, Y.; Miyazaki, M.; Maeda, H.; Ueharab, M.; Mulvaney, P. Preparation of CdSe Nanocrystals in a Micro-Flow-Reactor. *Chem. Comm.* **2002**, 2844-2845.

12. Dushkin, C. D.; Saita, S.; Yoshie, K.; Yamaguchi, Y. The Kinetics of Growth of Semiconductor Nanocrystals in a Hot Amphiphile Matrix. *Adv. Coll. Inter. Sci.* **2000***, 88*, 37-78.

13. Donega, C. D.; Hickey, S. G.; Wuister, S. F.; Vanmaekelbergh, D.; Meijerink, A. Single-Step Synthesis to Control the Photoluminescence Quantum Yield and Size Dispersion of CdSe Nanocrystals. *J Phys Chem B* **2003***, 107*, 489-496.

14. Underwood, D. F.; Kippeny, T.; Rosenthal, S. J. Charge Carrier Dynamics in CdSe Nanocrystals: Implications for the use of Quantum Dots in Novel Photovoltaics. *Eur. Phys. J. D* **2001***, 16*, 241-244.

15. Peng, Z. A.; Peng, X. G. Nearly Monodisperse and Shape-Controlled CdSe Nanocrystals Via Alternative Routes: Nucleation and Growth. *J. Am. Chem. Soc.* **2002***, 124*, 3343-3353.

16. Lee, M. K.; Saunders, J. A. Effects of pH on Metals Precipitation and Sorption: Field Bioremediation and Geochemical Modeling Approaches. *Vadose Zone J.* **2003***, 2*, 177-185.

17. Gao, M.; Kirstein, S.; Mohwald, H.; Rogach, A. L.; Kornowski, A.; Eychmuller, A.; Weller, H. Strongly Photoluminescent CdTe Nanocrystals by Proper Surface Modification. *J. Phys. Chem.* **1998***, 102*, 8360.

Chapter 7

Kinetics Study

The feasibility study in Chapter 5 confirmed the presence of CdSe nanoparticles as a result of using high-temperature water as a reaction medium. The study provided insight into the effects of the process variables on the nanocrystal size and properties. Although this synthesis route yielded nanocrystals, we next explored (Chapter 6) a rapid-hot injection that better mimicked conventional routes. This new route yielded a smaller nanocrystal but behavior similar to that observed in the feasibility study. We decided that this route was the better one to use in follow-up studies on nanoparticle growth dynamics as it would better enable us to make comparisons with experiments conducted by others that used the rapid hot-injection route. The goal of this chapter is to explore and quantify the growth evolution of CdSe nanocrystals in an aqueous medium.

7.1 Introduction

A large amount of research has been dedicated to the preparation of nanocrystals with the aim of understanding the reaction conditions that favor high quality particles. The precise control of parameters such as pH, time, temperature, and reagent chemistries can determine the size, and hence the optical properties. The ability to control the size of

a nanocrystal and its size-dependent properties is what makes them desirable as materials with unique properties. It is therefore essential to understand the growth behavior so that a desired size, and ultimately, a targeted property can be realized.

A dearth of literature claims what mechanism actually controls the growth stage, or is even responsible for producing the best quality nanocrystal. The little research that does exist suggests that growth is consistent with diffusion-limited Ostwald ripening [1, 2, 3]. Peng et al. [3] further conclude that the greatest narrowing of size distributions occurs within the diffusion-limited regime, and suggests that this narrowing occurs just before the onset of Ostwald ripening.

Dushkin et al. [4] provided the first comprehensive study of the kinetics of CdSe nanocrystal growth by developing mathematical models that attempt to describe the entire growth process, using classical kinetics models. Their model contends that reaction and diffusion-limited growth both play a role in the growth of the nanocrystal. But, they suggest that the fast reaction-limited growth is important to obtain well-defined and uniform nanocrystals of high-quality, which is contrary to what Peng suggests. Talapin et al. [5] performed Monte Carlo simulations and concluded that growth could be limited by reaction, diffusion, or a combination of both processes, but agreed with Peng's assertion. A detailed look into the reaction conditions, however, could very well explain why, though general assumptions can be made, different conclusions can be drawn. When taking into consideration precursor chemistries, capping agents, and even analytical techniques, determining the actual kinetics of a system is quite complex. But, it seems that mathematical models of the growth process are needed to accurately describe the evolution of nanocrystal growth to determine which kinetic regime governs

growth. Those developed by [4, 5, 6] provide invaluable insight, but are for synthesis in organic solvent systems. As far as we know, there is no record of any quantitative kinetics modeling for aqueous systems. But because classic kinetic theory should be independent of the reaction medium, approaches developed for organics should apply, to some extent, to synthesis in aqueous systems.

The model herein only represents the influence of reaction time and temperature on the growth evolution. Chapter 6 does verify that other process variables, namely pH, Cd:Se molar concentration and Cd:stabilizer molar concentration also affect the growth of the nanocrystals. Including these parameters is essential for a more comprehensive kinetic model, but time and temperature data are the most readily treatable in well-established kinetic models.

7.2 Experimental Methods

We conducted experiments in stainless steel batch reactors fitted with a high-temperature rated bellows valve as described in Chapter 4. All analytical methods used for this study include spectroscopy and TEM, descriptions of which are in Chapter 4.

7.3 Model Development

One proposed route to exploring the kinetic behavior is by determining an activation energy, Q. For both reaction- and diffusion-controlled growth processes, the kinetic behavior should be characterized by Arrhenius behavior. The extraction of Q from an Arrhenius plot of ln rate vs. $1/T$could help reveal how much of the process is in fact controlled by diffusion.

Dickerson [7] provides a modeling framework for synthesis of CdSe in TOPO and stearic acid. We adapted his model to describe our synthesis as well. Dickerson's model assumes: 1) the growth of nanoparticles occurs after nucleation and before Ostwald ripening, 2) the number of nuclei remains constant, 3) the particles are spherical, 4) the diffusion of cadmium complexes is significantly slower than diffusion of selenium, 5) the concentration gradient is linear, and 6) the transport of the cadmium complex is by diffusion with Arrhenius temperature behavior.

Dickerson's model was built on the basis of Fick's first law of diffusion:

$$J = -D\frac{dC}{dx} \tag{7.1}$$

$$\frac{dC}{dx} \sim \frac{C_{bulk} - C_{inter}}{L_D} \sim \frac{C_{bulk}}{L_D} \tag{7.2}$$

$$D = D_o exp\left(-\frac{Q}{k_b T}\right) \tag{7.3}$$

where J is the flux of cadmium (moles/cm$^2 \cdot$ s), D is the diffusivity (cm^2/s), dC is the difference in concentration of cadmium complexes in the bulk solution and those at the nanocrystal's surface (moles/cm^3), C_{bulk} is the concentration of cadmium complexes (moles/cm^3) in the bulk solution, L_D is the diffusion length (cm), C_{inter} is the surface concentration of cadmium complexes (moles/cm^3) (it is assumed that it is orders of magnitude lower than in the bulk solution, so C_{inter}~0), dx is the radial distance (cm), D_o is the pre-exponential diffusivity coefficient (cm^2/s), Q is the activation energy (eV/molecule), k_b is the Boltzmann's constant (eV/molecule $\cdot$ K) and T is the absolute temperature (K). The governing equation for the growth rate is:

$$\nu_{(t)} = -4\pi R_{(t)}^2 \cdot J = 4\pi R_{(t)}^2 \frac{dC}{dx} D \tag{7.4}$$

$$v_{(t)} = 4\pi R_{(t)}^2 \frac{C_{bulk(t)}}{L_D} D_o exp\left(-\frac{Q}{k_b T}\right) \quad (7.5)$$

where $v_{(t)}$ = molar growth rate (moles/s) and $R_{(t)}$ is the average nanocrystal radius (cm) at time t.

Dickerson proposed using the temperature-dependence of the redshift rate of PL emission peak wavelengths ($d\lambda/dt$) as a way for estimating Q. The redshift rate is related to the rate of growth of the nanocrystal over time. Through application of the effective mass model, it can be shown that $d\lambda/dt \propto v_t$ at a fixed test wavlength [6]. A full model derivation is available in Section 7.6 "Appendix: Derivation of Redshift Rate Model ".

7.4 Results and Discussion

Since the peak emission wavelength, λ_{max}, is an indicator of nanoparticle size, a temporal profile of peak wavelengths will exhibit the particle growth behavior. Figure 7.1a shows such a profile for our system at various reaction temperatures. At higher temperatures, the profiles trend higher because the higher temperatures tend to yield larger nanoparticles, indicated by larger wavelengths. For each temperature it is apparent that the peak wavelength initially increases with increasing time, and then, in general, levels off at longer times.

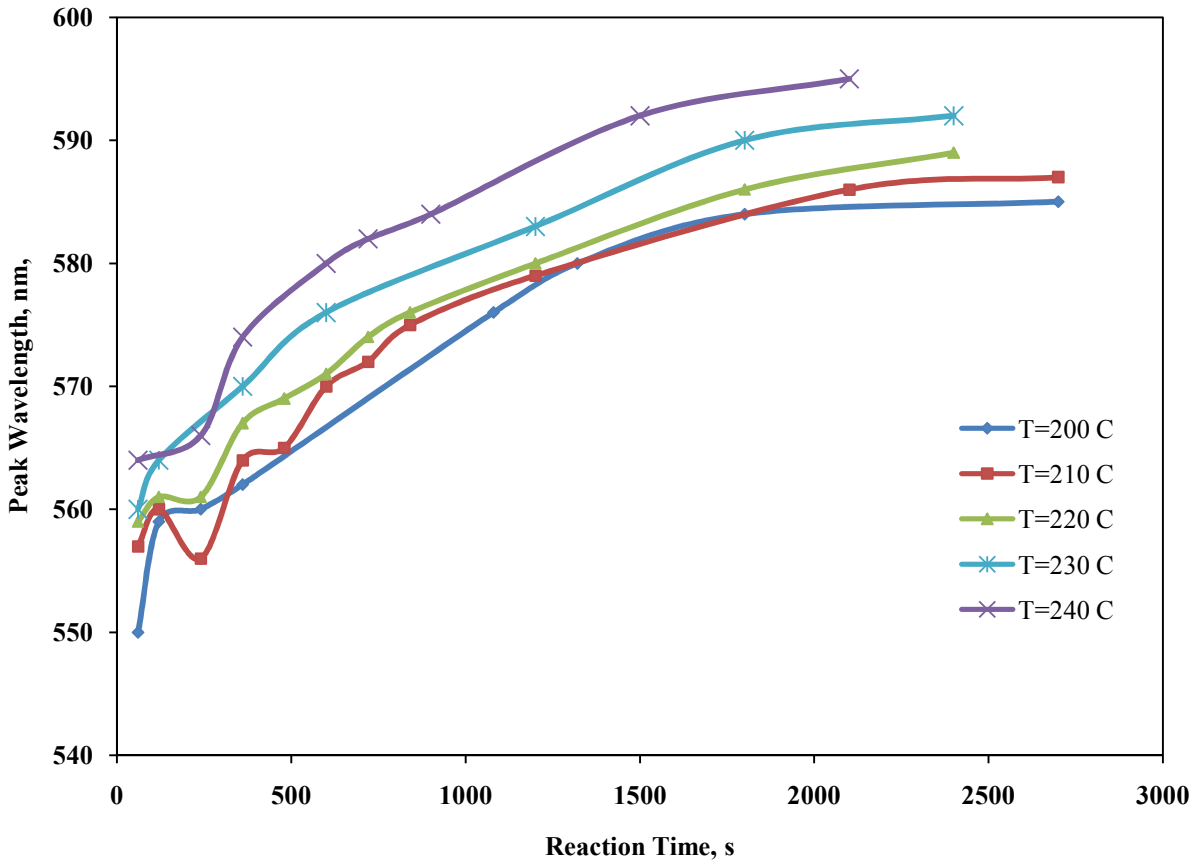

Figure 7.1a. Evolution of peak wavelength, λ_{max}, with reaction time at various reaction temperatures for CdSe nanocrystals synthesized in high-temperature water.

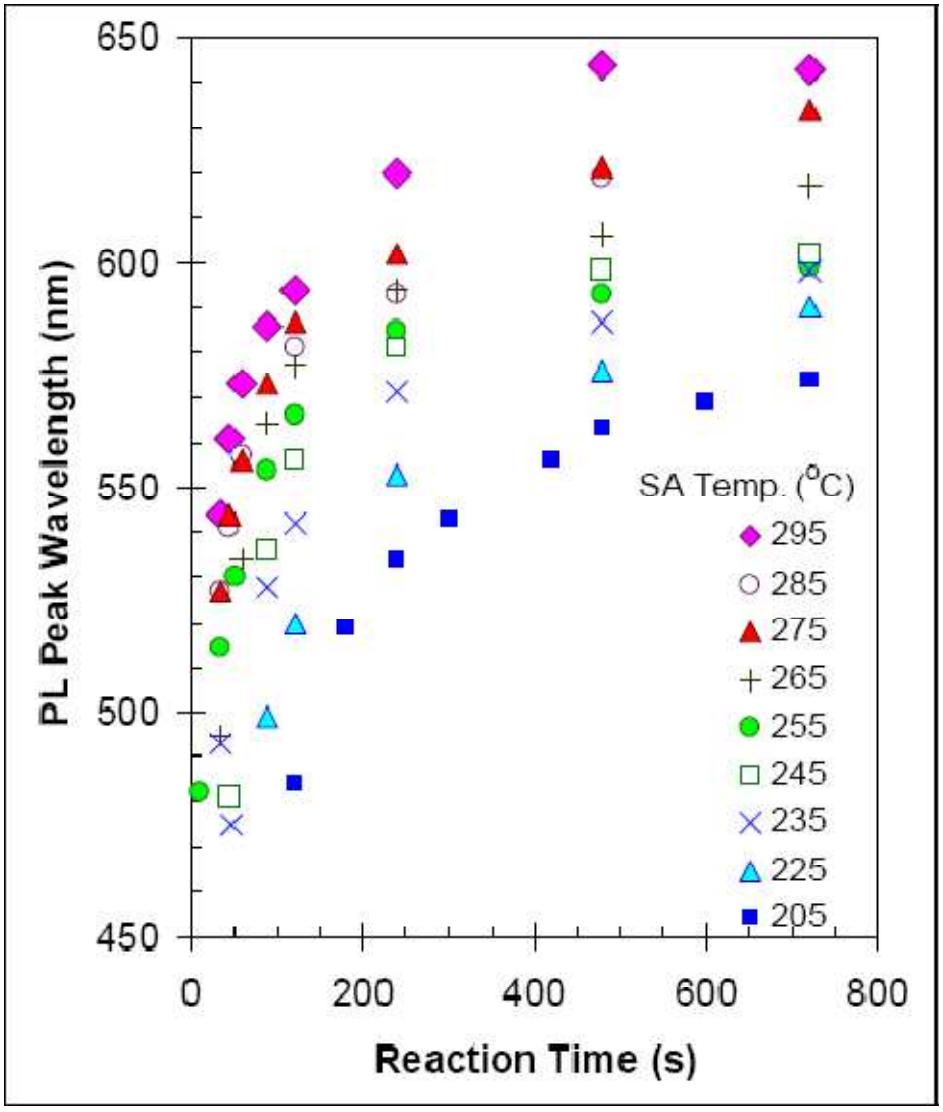

Figure 7.1b. Evolution of peak wavelength with reaction time at various reaction temperatures for CdSe nanocrystals synthesized in stearic acid [7].

Thus two distinct regimes, fast growth and slow growth, are apparent in Figure 7.1a. These profiles are similar to those observed for CdSe nanocrystals synthesized in stearic acid (Figure 7.1b) [7]. The rapid increase of the nanocrystal's size at the beginning of the growth curves could be due to a reaction-controlled process. Monomer from the particle's immediate vicinity adsorbs to the surface, and is subsequently exhausted. The longer time scale exhibits a slower growth process, which could be controlled by diffusion and then Ostwald ripening.

The redshift rate can be mathematically defined as the change in emission wavelength with reaction time. We fit a 3^{rd}-order polynomial function to the λ vs. time curves at each temperature (Figure 7.1c). Table 7.1 lists the best fit equation for each temperature. We then differentiated each function to obtain the redshift rate.

Figure 7.2a shows the profile of the red-shift rates. In general, at a fixed wavelength, the red-shift rates trend higher at higher temperatures. This is consistent with the growth profile shown in Figure 7.1a. Looking at a typical red-shift rate for a given synthesis temperature, we see that it decreases as the wavelength increases. The rate of growth of nanoparticles declines rapidly as the nanoparticle size increases. This trend is similar to that observed by Dickerson et al. for CdSe nanocrystals prepared in stearic acid (Figure 7.2b), as well as Dushkin's [4] observation for the preparation of CdSe nanocrystals in TOPO. Dushkin further suggested the existence of the two growth regimes based on this trend, which leads us to speculate that we have separated nucleation and growth, to a degree, using our rapid hot-injection method.

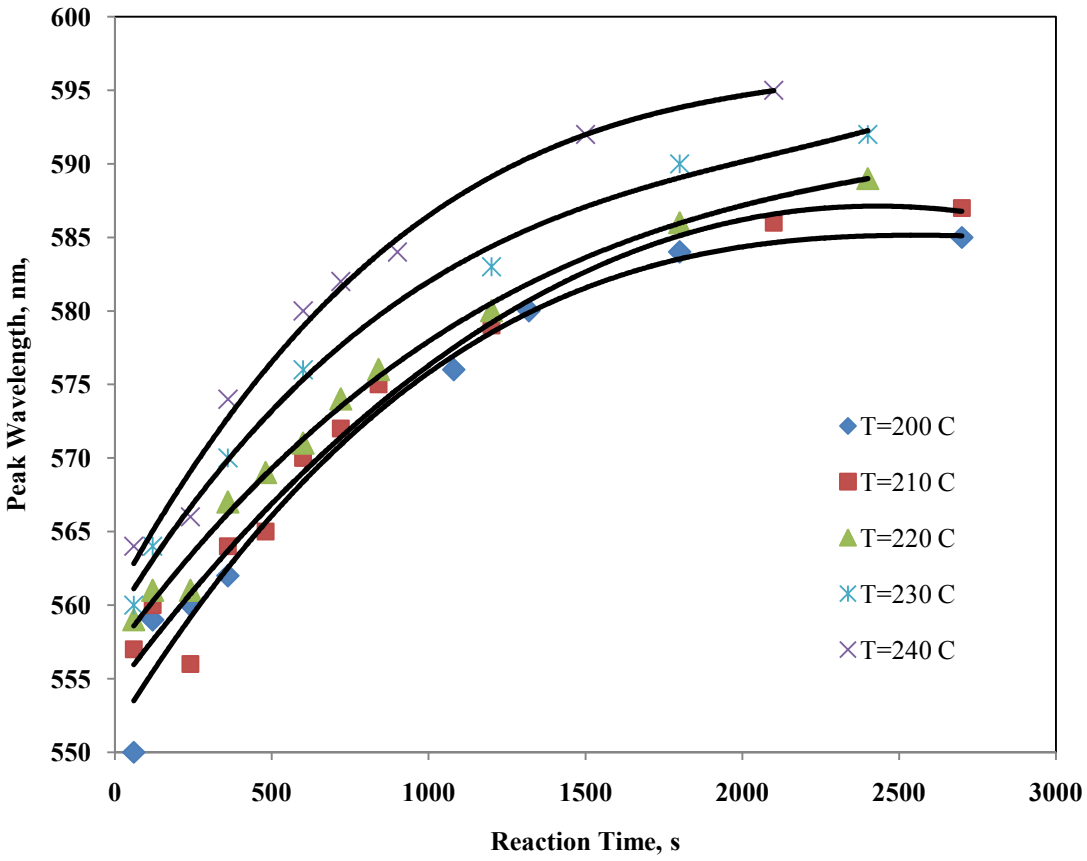

Figure 7.1c Evolution of peak wavelength, λ_{max}, with reaction time at various reaction temperatures for CdSe nanocrystals synthesized in high-temperature water, fitted with a 3rd order polynomial.

Temperature, °C	3rd-order Polynomial Function
200	$\lambda_{max} = 1.29\text{x}10^{-9}t^3 - 1.18\text{x}10^{-5}t^2 + 3.48\text{x}10^{-2}t + 551$
210	$\lambda_{max} = 2.63\text{x}10^{-10}t^3 - 6.85\text{x}10^{-6}t^2 + 2.86\text{x}10^{-2}t + 554$
220	$\lambda_{max} = 1.07\text{x}10^{-9}t^3 - 9.13\text{x}10^{-6}t^2 + 2.91\text{x}10^{-2}t + 557$
230	$\lambda_{max} = 2.22\text{x}10^{-9}t^3 - 1.40\text{x}10^{-5}t^2 + 3.47\text{x}10^{-2}t + 559$
240	$\lambda_{max} = 2.13\text{x}10^{-9}t^3 - 1.53\text{x}10^{-5}t^2 + 3.91\text{x}10^{-2}t + 561$

Table 7.1 Table showing the 3rd-order polynomial functions for each temperature.

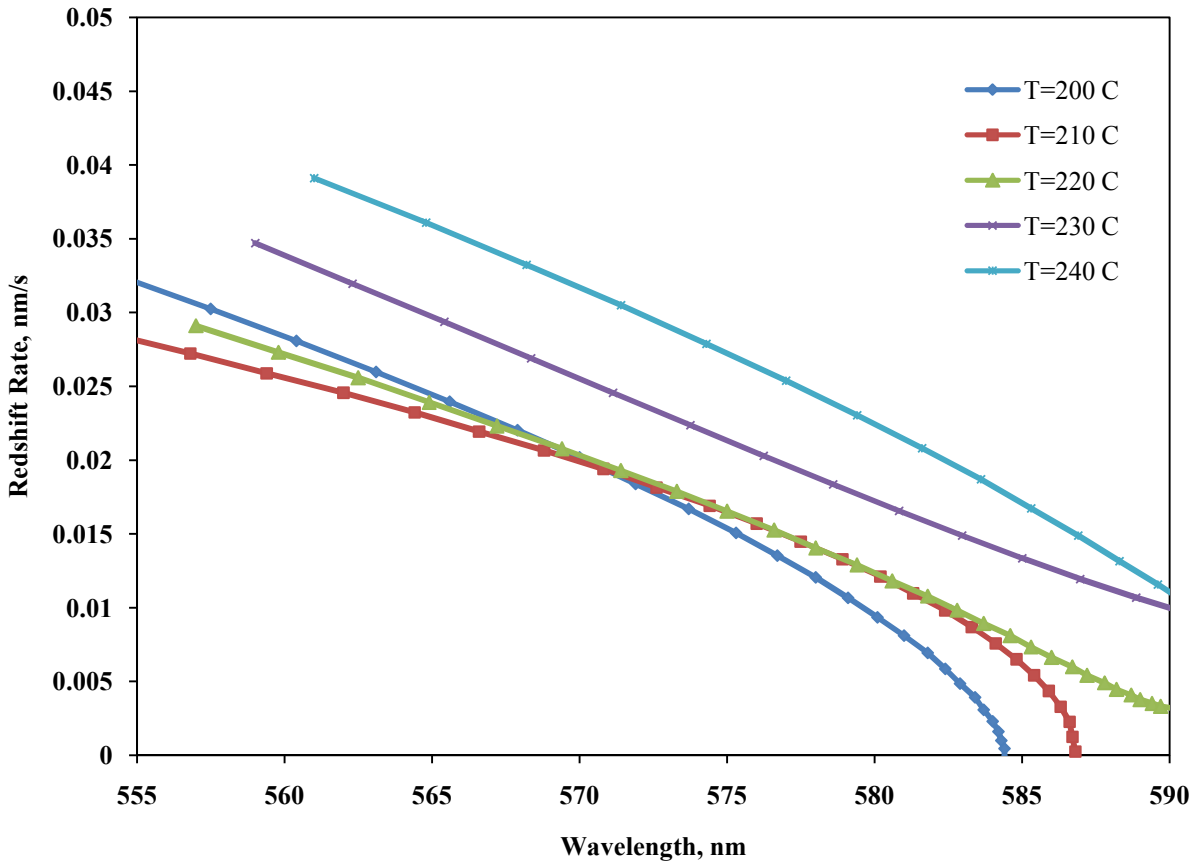

Figure 7.2a. Red-shift rates of peak wavelengths at various reaction temperatures for CdSe nanocrystals synthesized in high-temperature water. The completion wavelength, λ_c, is estimated to be about 573 nm.

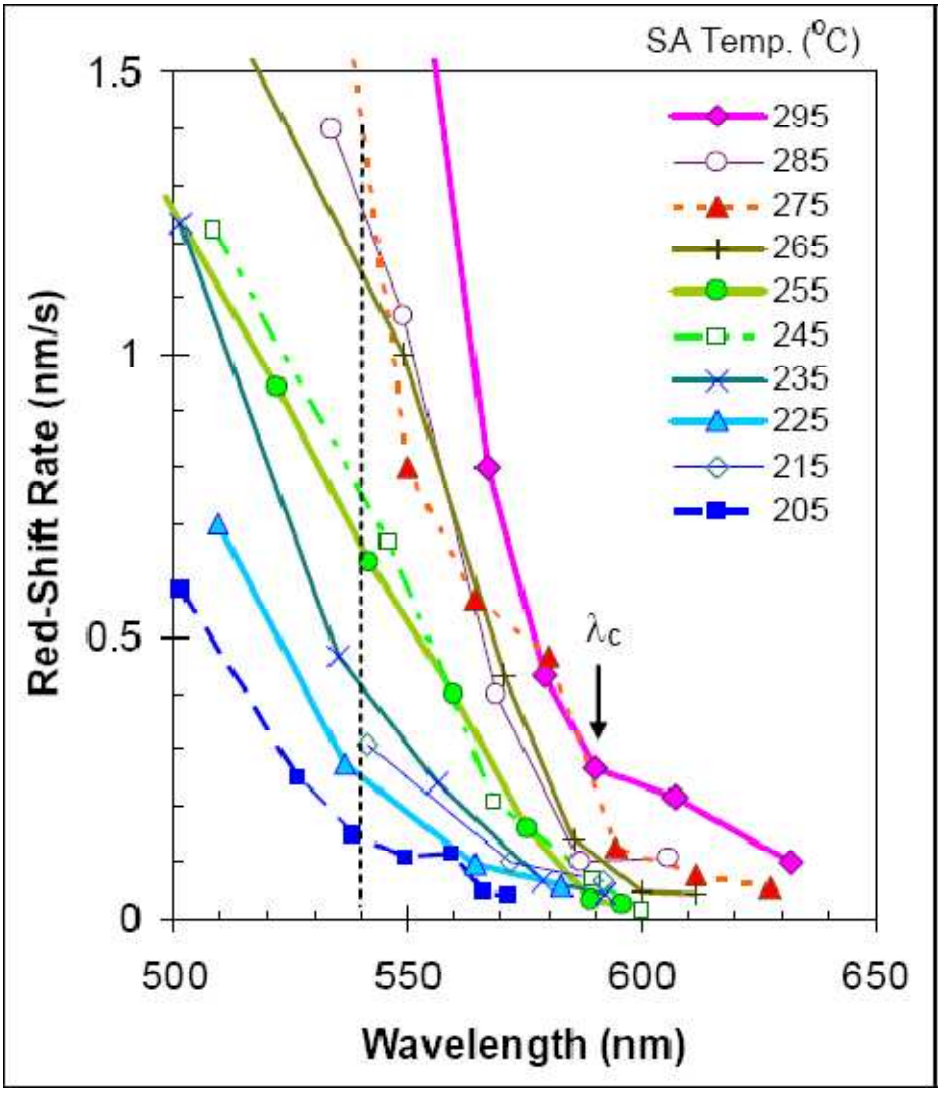

Figure 7.2b. Red-shift rates of peak wavelengths at various reaction temperatures for CdSe synthesized in stearic acid by Dickerson et al. The completion wavelength, λ_c, is shown to be 590 nm. [7]

According to Dickerson et al. [6], the redshift rate curves for the different temperatures tend to converge to a common wavelength, defined as a "completion wavelength", λ_c. It is at this wavelength that the limiting reactant can be assumed to be exhausted, and that further growth would be governed by Ostwald ripening. Our data begin to converge at roughly 573 nm for the temperature range 200 – 220 °C.

Activation energies were calculated from the red-shift rates by plotting the natural log of the red-shift rate against the reciprocal absolute temperature for a selected test wavelength. The activation energy, Q, for each test wavelength was extracted from the slope of the individual plots. An example plot is shown in Figure 7.2c for a test wavelength of 580 nm. Linear regression of these data lead to a Q = 0.40 ± 0.11 eV/molecule where the uncertainty represents the standard error from a regression analysis. The activation energies, at each test wavelength, were then plotted against the entire range of test wavelengths to generate the plot shown in Figure 7.3a. A similar plot for CdSe prepared in stearic acid and TOPO is shown in Figure 7.3b.

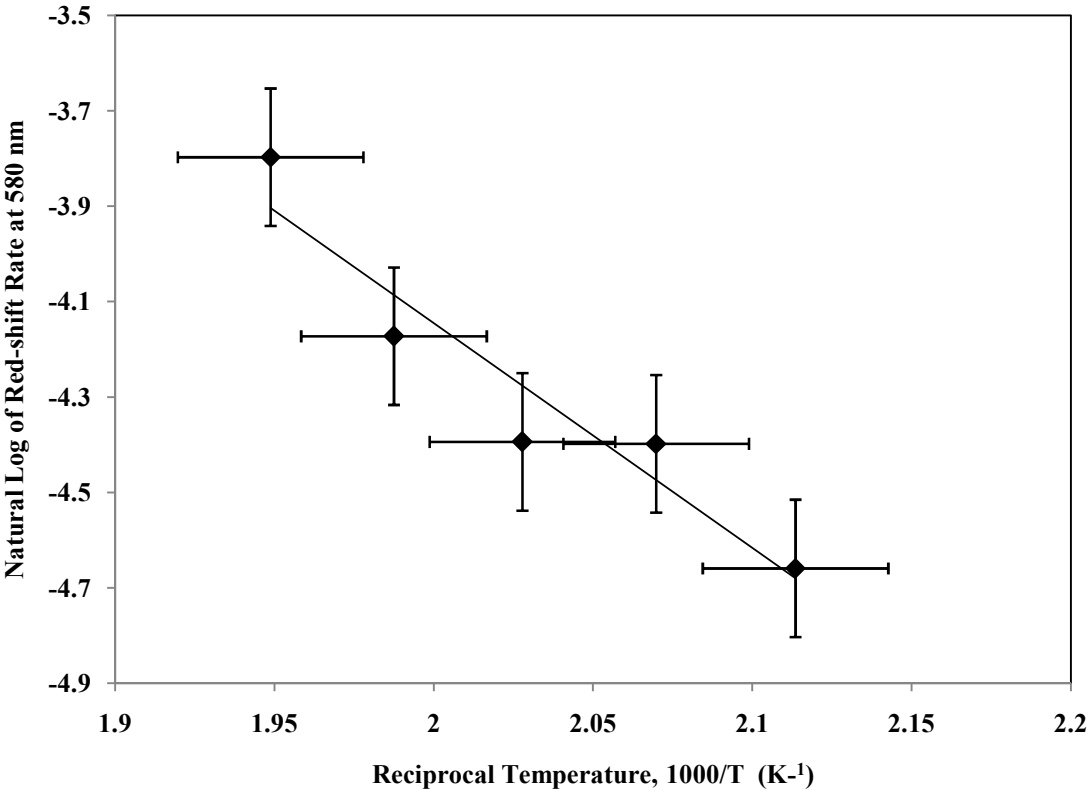

Figure 7.2c. Arrhenius plot of red-shift rates at a test wavelength of 580 nm for CdSe nanocrystals synthesized in high-temperature water. A value of Q was calculated, via linear regression, to be 0.40 eV/molecule with a standard error of 0.11 eV/molecule. The error bars represent the standard error.

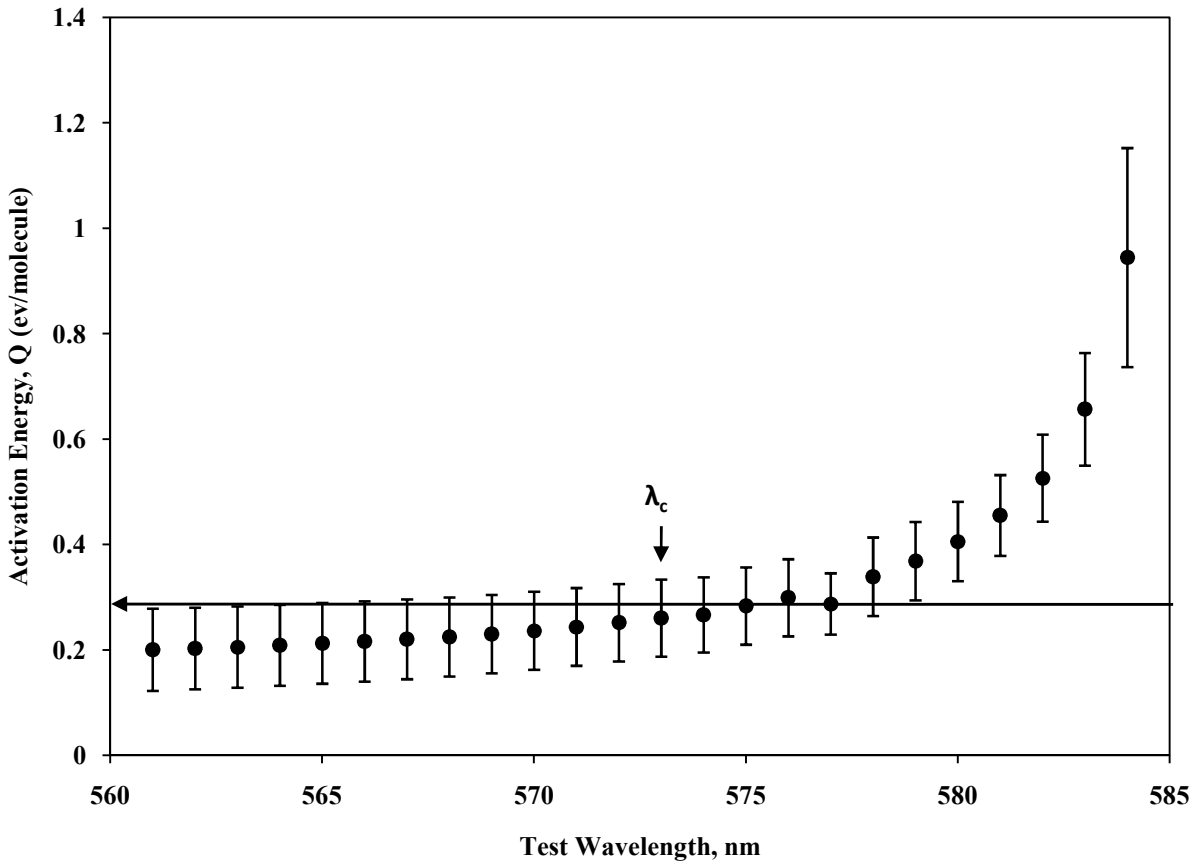

Figure 7.3a. Activation energies from redshift rates at various test wavelengths for CdSe nanocrystals synthesized in high-temperature water. The completion wavelength, λ_c, is marked at 573 nm. The average activation energy, Q, is 0.24 ± 0.04 eV/molecule. The error bars represent the standard error at each test wavelength.

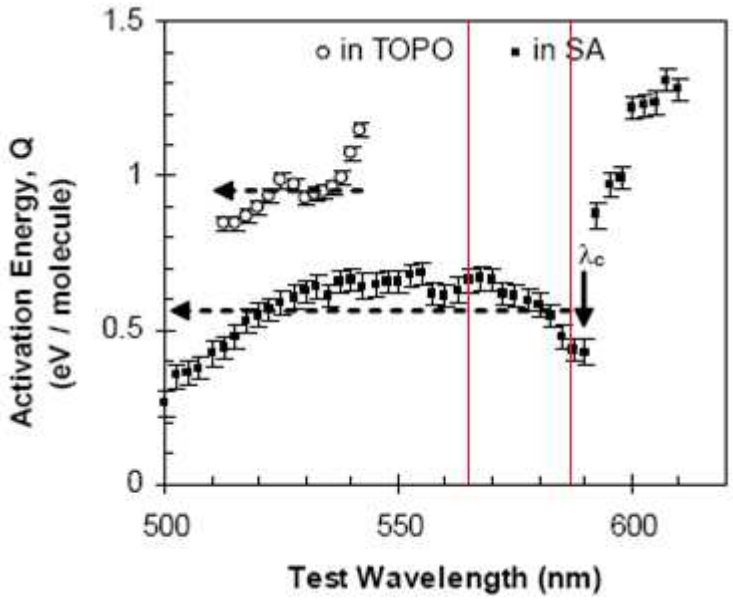

Figure 7.3b. Activation energies from red-shift rates at various test wavelengths for CdSe nanocrystals synthesized in stearic acid (SA) and TOPO by Dickerson et al. [6]. The average activation energy calculated for SA is 0.56 ± 0.12 eV/molecule and TOPO is 0.95 ± 0.27 eV/molecule. The two lines represent the experimental bounds of CdSe nanocrystals prepared in high-temperature water in this study.

As the size of the nanoparticle and test wavelength increase, the activation energy, according to the error bars, shows a slight increase. The plot seems to indicate that a more rapid increase occurs after 573 nm. This may be the occurrence of Ostwald ripening and the completion wavelength could be at about 573 nm. We calculated an average activation energy of Q = 0.24 ± 0.04 eV/molecule.

The error bars on Dickerson's plot are small enough to indicate that the variability of the activation energy with test wavelength is real along the entire range of wavelengths. Our the data likewise indicate that the activation energy is somehow a function of the test wavelength and, hence, the nanocrystal's size. It is possible that the

activation energy is a function of the evolving kinetic process, especially at the onset of Ostwald ripening which, as Figure 7.3a suggests, may occur at about 573 nm. Talapin et al. [5] assert, through their theoretical study of the evolution of a nanoparticle in colloidal solution, that activation energies of the growth and dissolution process are a function of nanoparticle radius. This is because the thermodynamic chemical potential of the nanoparticle depends on the nanoparticle's surface curvature. This may help explain the large increase in activation energy after the suggested completion wavelength, λ_c = 573 nm. At this point, the process of Ostwald ripening begins as smaller particles dissolve and larger ones grow.

The kinetics model provided by Dickerson et al. [7] may help us to begin to understand the growth dynamics for nanoparticles produced in aqueous media. In general, our data from aqueous-phase synthesis exhibits similar behavior to that obtained from synthesis in stearic acid. Our particle growth, as seen in Figure 7.1a, shows a two-step process, rapid initial growth, followed by a slower growth. Our redshift rate profile is different from that produced form the organic-based system. It is unknown at this time if this is a function of the experimental method, which may introduce more random error, or the type of reaction medium. The convergence of red-shift rates, known as the reaction completion wavelength, λ_c, was observed to be 590 nm for the organic-based system and 573 nm for the aqueous-based system. The lower completion wavelength may be a factor of the experimental method or the reaction medium. Further studies, with different reaction mediums and identical experimental methods, would have to verify this. The shape of the curve (Figure 7.3a) that shows the activation energies from the red-shift rates is different than what was obtained for stearic acid (Figure 7.3b).

When comparing the two profiles within the same test wavelength range, our curves seem to show a slight increase, then a more rapid increase in activation energies. It is interesting that our profile is more similar to that shown for TOPO (Figure 7.3b), although our profile is not within the same wavelength region. Dickerson et al. [6] do state that Q for TOPO could not be accurately estimated from test wavelengths near 560 nm due to a limited number of chosen synthesis temperatures. The plots showing the redshift rate and the activation energy profile indicate that the diffusion-controlled growth may have ceased at 573 nm.

Our activation energy value is lower than those obtained for synthesis in stearic acid and TOPO (Table 7.2). The difference may be due to the use of different stabilizer ligands. All three ligands differ in their carbon structure and length. Both stearic acid and sodium citrate contain carboxyl groups. Additionally, they possess linear carbon chains, but stearic acid is a longer chain acid (Scheme 7.1), and, therefore, bulkier with more mass. TOPO has a branched carbon chain structure (Scheme 7.1) and is more massive. The comparisons of the chemical structure of the different stabilizer ligands may help explain the higher activation energy for that system as it would take more energy to move the stearic acid and TOPO molecules, as they complex with cadmium, from the bulk solution to the nanoparticle's surface.

	High-temperature Water	Stearic Acid [6]	TOPO [6]
Q (eV/molecule)	0.24 ± 0.04	0.56 ± 0.12	0.95 ± 0.27

Table 7.2. Summary of average activation energies obtained by analysis of redshift rates

Stearic Acid

TOPO

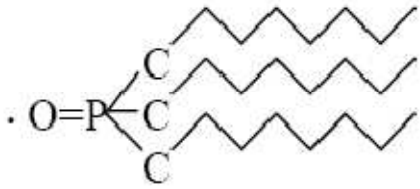

Sodium Citrate

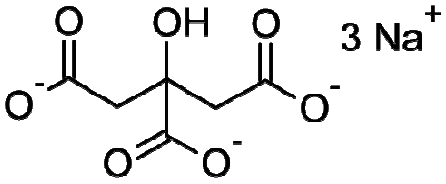

Scheme 7.1. Comparison of stearic acid, TOPO and sodium citrate ligands.

The activation energy for the self-diffusion of water is approximately 0.14 eV/molecule [8] for our experimental temperature range (200 – 240 °C). The calculated activation energy is higher than this value, which is not surprising since the value takes into account the diffusion of cadmium citrate complexes and selenium monomer, entities that will diffuse more slowly than the much smaller water molecules. From comparison

with the self-diffusion number alone, we do not know if growth is entirely diffusion-limited.

The error bars on our activation energy profile are larger than those on Dickerson's profile. Careful inspection of Figure 7.1a reveals wide variability of the raw peak wavelength vs. time data, especially at smaller times. This is most likely an artifact of the way the experiments were run as we were not able to continuously draw samples from a large batch. Each wavelength represents one distinct experiment, likely introducing more random error.

The presence of a self-focusing size distribution can provide evidence for diffusion-controlled growth, according to Dickerson [7]. The fwhm value should decrease with an increase in wavelength, with the minimum value occurring at λ_c (Figure 7.6b). Figure 7.4a shows the profile of the fwhm for the base case conditions. The observed minimum occurs at λ = 576 nm, but the characteristic rapid decrease in the fwhm, observed in stearic acid, does not exist in our data. It is possible that nucleation does not completely separate from growth, and that nuclei continue to form during the synthesis process. The nuclei that do form may experience the reaction-limited growth kinetics at the same time that the mature particles experience diffusion-limited growth kinetics. The plot seems to indicate that growth is not necessarily governed by one kinetic regime, but, may in fact be controlled by both reaction and diffusion.

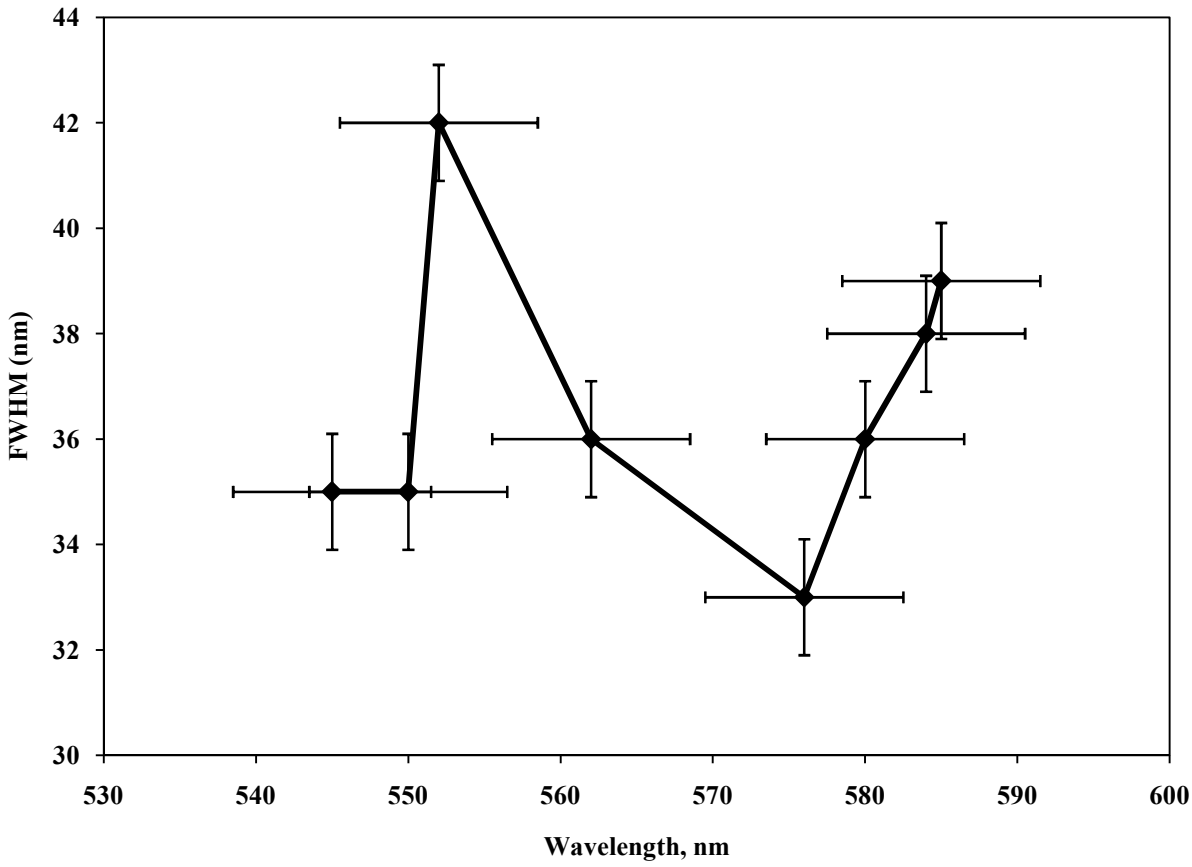

Figure 7.4a. Profile of fwhm for CdSe nanocrystals prepared in high-temperature water under base case conditions (T = 200 °C) at varying times. The error bars correspond to the standard deviation for repeat base case experiments.

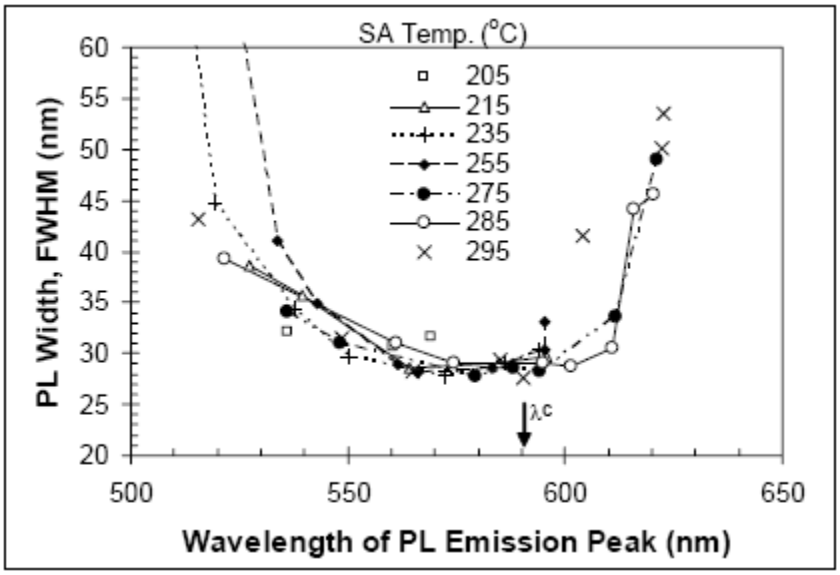

Figure 7.4b. Profile of fwhm for CdSe nanocrystals prepared in stearic acid by Dickerson et al. [7]

7.5 Summary

This chapter reports the first quantitative analysis of the growth kinetics for CdSe nanoparticles prepared in high-temperature water. We adapted a model originally developed for organic-based systems. Two growth regimes are apparent: a rapid increase in nanoparticle size followed by a slower growth. An activation energy, Q, was determined by using a red-shift rate (Q = 0.24 ± 0.04 eV/molecule). The red-shift rate method yielded activation energies that seemed to vary with the particle size. Our activation energy is lower than those obtained from synthesis of CdSe in stearic acid and TOPO possibly due to the stearic and TOPO ligands being bulkier and more massive than the citrate ligand. We cannot, at this point, determine if the synthesis in high-temperature water is reaction- or diffusion-controlled, but we do provide an analytical framework to build on this research.

7.6 Appendix: Derivation of Redshift Rate Model

The full derivation of the Dickerson's redshift rate model, used to calculate activation energy, is shown in this section.

The model is based on Fick's first law of diffusion:

$$J = -D\frac{dC}{dx} \tag{A-1}$$

where J is the flux of cadmium into the nanocrystal (moles/cm^2·s, D is the diffusivity (cm^2/s), and dC/dx is the radial concentration gradient from $x = R$ to $x = L_D$:

$$\frac{dC}{dx_{x=R}} \sim \frac{C_{bulk} - C_{inter}}{L_D} \sim \frac{C_{bulk}}{L_D} \tag{A-2}$$

where C_{bulk} is the concentration of cadmium complexes (moles/cm^3) in the bulk solution, L_D is the diffusion length (cm), C_{inter} is the surface concentration of cadmium complexes (moles/cm^3) and it is assumed to be orders of magnitude lower than in the bulk solution ($C_{inter} \sim 0$).

The diffusion process can be described in terms of Arrhenius behavior:

$$D = D_o \exp\left(-\frac{Q}{k_b T}\right) \tag{A-3}$$

where D_o is the pre-exponential term for the diffusion coefficient, Q is the activation energy, k_b is the Boltzman's constant and T is the absolute temperature.

The molar growth rate, v, can then be described as:

$$v = -A \cdot J \tag{A-4}$$

$$v = A \cdot D \frac{dC}{dx} \tag{A-5}$$

$$A = 4\pi R^2 \tag{A-6}$$

Since we are interested in the Arrhenius behavior of the nanocrystal's growth, we can combine equations A-2, A-3, A-5 and A-6 to obtain the relationship between the molar growth rate and an activation energy, Q:

$$v_{(t)} = 4\pi R^2 \frac{C_{bulk}}{L_D} D_o \exp\left(-\frac{Q}{k_b T}\right) \tag{A-7}$$

Taking the natural log of both sides of equation A-7 yields:

$$\ln v_{(t)} = \ln\left(4\pi R^2 \frac{C_{bulk}}{L_D} D_o\right) + -\frac{Q}{k_b T} \tag{A-8}$$

A plot of $\ln v_{(t)}$ vs.$1/T$ should yield a straight line with a slope = $-Q/k_b$.

Dickerson suggests that the molar growth rate is proportional to $d\lambda/dt$ as derived from the effective mass approximation. We can express the effective mass approximation as:

$$\frac{hc}{\lambda} = E_g + \frac{X}{R^2} \tag{A-9}$$

where E is represented by hc/λ and X represents the constants $h^2/2m^*$ (see Equation 1.5). Solving for R^2:

$$R^2 = \frac{X}{hc/\lambda - E_g} \tag{A-10}$$

$$\frac{1}{R^2} = \frac{hc}{\lambda X} - \frac{E_g}{X} \tag{A-11}$$

We can express the decrease in cadmium concentration by:

$$C_{bulk(t)} = C_o - \frac{4}{3}\frac{N_{eff}}{V_{mat}}\frac{\pi}{V_m}R_{(t)}^3 \tag{A-12}$$

Where C_o is the original molar concentration of cadmium in the reactor (moles/cm^3), V_{mat} is the total volume of material in the reactor, V_m is the molar volume of CdSe (cm^3/moles) and N_{eff} is the effective number of spherical nanocrystals. The molar growth rate can be expressed in terms of cadmium depletion:

$$v_{(t)} = -\frac{V_{mat}}{N_{eff}}\frac{dC_{bulk}}{dt} \tag{A-13}$$

Differentiation of Equation A-12 and substituting the result into A-13 yields:

$$dC_{bulk} = -\left(\frac{4}{3}\frac{N_{eff}}{V_{mat}}\frac{\pi}{V_m}\cdot 3R^2 dR_{(t)}\right) \tag{A-14}$$

From Equation A-9:

$$dR_{(t)} = \frac{R^3 hc}{2\lambda^2 X}d\lambda \tag{A-15}$$

So the growth rate can be written as:

$$v_{(t)} = 2\frac{\pi}{V_m}R^5\frac{hc}{\lambda^2 X}\frac{d\lambda}{dt} \tag{A-16}$$

Equation A-16 shows that it is convenient to monitor the red-shift rate as a way to track the growth rate of the nanocrystals. Thus, substituting $d\lambda/dt$ at a fixed test wavelength for $v_{(t)}$ in Equation A-8 should still exhibit Arrhenius behavior.

7.7 Bibliography

1. Murray, C. B.; Norris, D. J.; Bawendi, M. G. Synthesis and Characterization of nearly Monodisperse Cde (E = S, Se, Te) Semiconductor Nanocrystallites. *J. Am. Chem. Soc.* **1993***, 115*, 8706-8715.

2. Peng, Z. A.; Peng, X. G. Nearly Monodisperse and Shape-Controlled CdSe Nanocrystals Via Alternative Routes: Nucleation and Growth. *J. Am. Chem. Soc.* **2002***, 124*, 3343-3353.

3. Peng, X. G.; Wickham, J.; Alivsatos, A. P. Kinetics of II-VI and III-V Colloidal Semiconductor Nanocrystal Growth: "Focusing" of Size Distributions. *J. Am. Chem. Soc.* **1998***, 120*, 5343-5344.

4. Dushkin, C. D.; Saita, S.; Yoshie, K.; Yamaguchi, Y. The Kinetics of Growth of Semiconductor Nanocrystals in a Hot Amphiphile Matrix. *Adv. Coll. Inter. Sci.* **2000***, 88*, 37-78.

5. Talapin, D. V.; Rogach, A. L.; Haase, M.; Weller, H. Evolution of an Ensemble of Nanoparticles in a Colloidal Solution: Theoretical Study. *J. Phys. Chem. B* **2001***, 105*, 12278-12285.

6. Dickerson, B. D.; Irving, D. M.; Herz, E.; Claus, R. O.; Spillman, W. B.; Meissner, K. E. Synthesis Kinetics of CdSe Quantum Dots in Trioctylphosphine Oxide and in Stearic Acid. *Applied Physics Letters* **2005***, 86*, 171915-1-171915-3.

7. Dickerson, B. D. Organometallic Synthesis Kinetics of CdSe Quantum Dots, Virginia Polytechnic Institute and State University, 2005.

8. Kyrnicki, K.; Green, C. D.; Sawyer, D. W. Pressure and Temperature Dependence of Self-Diffusion in Water. *Faraday Discuss. Chem. Soc.* **1978***, 66*, 199-208.

Chapter 8

Summary and Conclusions

8.1 Summary

This thesis is a culmination of a series of studies of the potential for high-temperature water to serve as a viable reaction solvent in the preparation of CdSe nanocrystals. We tested a hypothesis that CdSe nanocrystals could be produced in high-temperature water through a feasibility study (non-isothermal conditions). Additionally, we examined the effects of various process parameters on the as-prepared nanocrystals. We then adapted a rapid hot-injection method (isothermal conditions) similar to convention to examine how the influence of the process parameters was affected by the synthesis method. Finally, we assessed the kinetics of the growth evolution of the nanocrystals in high-temperature water, and compared our results with those from organic-based synthesis. The following is a summation of key results from our investigative studies:

- CdSe nanocrystals that exhibit quantum behavior can be synthesized in liquid water at temperatures > 200 °C;
- Under non-isothermal conditions, the reaction temperature greatly affected the nanocrystal's growth, possibly due to Ostwald ripening. Under isothermal conditions, and at short times growth was about the same at all temperatures, being an

effect of either a short reaction time or the nucleation kinetics. An increase in the temperature had negligible effect on the quantum yield or on the fwhm;

- An increase in reaction time increased the size of the nanocrystals but had negligible effect on quantum yield. Under non-isothermal conditions, reaction time had negligible effect on the fwhm, while, under isothermal conditions, we did not observe a consistent trend.
- An increase in the Cd:Se molar ratio resulted in an increase in the nanocrystal size under non-isothermal conditions. This trend was observed to be just the opposite under isothermal conditions, where, additionally, higher Cd:Se molar ratios had a negligible effect on fwhm but significantly increased quantum yield;
- The pH of the solution greatly affected the nanocrystal size. An increase in pH caused a decrease in the size under non-isothermal and isothermal conditions. An increase in pH produced nanocrystals with higher quantum yields;
- An increase in the amount of stabilizer increased the nanocrystal size. It caused negligible effect on fwhm under non-isothermal conditions, but no consistent general trend was observed under isothermal conditions (there did seem to be a dramatic decrease in the fwhm at higher stabilizer amounts). The increase in stabilizer decreased the quantum yield;
- Under non-isothermal conditions, the addition of a CdS shell increased the quantum yield from 1.5% to ~7%;

- A kinetic model developed for CdSe nanocrystals synthesized in stearic acid and TOPO was adapted for our hydrothermal synthesis. A redshift rate method for obtaining an activation energy was used. This method yielded a value of Q equal to 0.24 ± 0.04 eV/molecule. ;
- It is very possible that the nanocrystal growth in our studies is governed by both reaction- and diffusion-controlled processes.

8.2 Conclusions and Future Work

It is apparent that traditional experimental parameters can and do affect growth dynamics but, not surprisingly, the variability of surface atoms had a greater influence on the optical properties. An increase in the Cd:Se molar ratio and Cd:stabilizer molar ratio had a profound effect on the nanocrystal's quantum yield. Quantum dots have a higher surface area-to-volume ratio than their bulk analogues. Surface reconstruction and composition are expected to have a large influence on the optical properties of semiconductor nanocrystals [1]. Literature recognizes the role of the surface in determining the quantum yields of semiconductor nanocrystals [1, 2, 3, 4, 5]. To better understand how growth conditions determine the surface structure of CdSe nanocrystals prepared in high-temperature water, more comprehensive studies of each contribution of individual parameters, and the effect of their combination, will need to be assessed.

Our kinetics study provided the first quantitative analysis for CdSe prepared hydrothermally. Even though our experimental data agreed well with a model developed for organic-based systems [6], the model is probably not a complete representation of the growth dynamics of the nanocrystals. The analytical expression uses only two process

variables, time and temperature. Our feasibility and rapid hot-injection studies, however, confirm the influence of additional parameters such as pH and surface chemistries on nanoparticle size and even quantum yield. Such parameters would need to be included in a kinetics model to make it more complete and more broadly applicable.

Another interesting observation about our hydrothermal study is that some of the growth behavior is similar to that seen in studies conducted in octadecene [7], an organic non-coordinating solvent. Growth was hardly affected as the temperature increased at a reaction time of two minutes, a phenomenon also observed in octadecene after five minutes of growth. But our kinetics study confirmed that growth was appreciable after longer time periods (Figure 7.1a), especially at higher temperatures (T > 220 °C). It could simply be that a two minute reaction time was not long enough to survey the growth in high-temperature water. Moreover, a five minute reaction time may not be adequate time to observe appreciable growth in octadecene. Another observation, made in both the hydrothermal and organic non-coordinating systems, was the increase in nanocrystal size as the amount of stabilizer increased. To our knowledge, this effect has not been reported by researchers using coordinating organic solvents (e.g. TOPO, stearic acid). It is likely that the non-coordinating property of the medium plays an integral role in the nucleation and growth dynamics of semiconductor nanocrystals.

We have shown, in this work, that the hydrothermal synthesis of CdSe nanocrystals is feasible and controllable. This route could be a new strategy for semiconductor nanocrystals. Much additional work is required if this ultimate goal is to be achieved. The following paragraphs suggest some future research directions.

8.2.1 Autoclave Batch and Flow Reactor Studies

An autoclave reactor can allow isothermal studies of large batches to be conducted. This capability is important when a full suite of analyses needs to be performed and volume of product is essential. It can also allow for samples to be withdrawn at various time intervals and possibly enable online analysis to be conducted so that trends can be assessed in real-time without disturbing the reaction [8]. Finally, studies conducted in an autoclave would represent a scale-up of about 100X from the 1.5 mL reactors used in this work.

A continuous flow reactor would allow for small scale studies that could simulate high-volume production. It can enable the experimenter to operate at high temperatures at very short times, possibly improving quantum yield.

8.2.2 Kinetics Modeling

A comprehensive study on the kinetics of CdSe nanocrystals grown hydrothermally needs to be performed to truly determine the mechanism behind the growth at all time scales. Data need to be obtained by conducting additional experiments in an autoclave batch and continuous flow reactor mentioned above. Samples taken at time intervals that cover the entire growth process can result in optical spectra that better represents more complete growth kinetics [9]. An in situ method, akin to that developed by Qu et al. [8] may uncover aspects of the growth stages that cannot be observed using conventional analyses. A thorough and reliable kinetics model would be useful for designing and optimizing large-scale processes for hydrothermal synthesis of CdSe nanocrystals.

8.2.3 X-ray Analysis

X-ray studies should be implemented to complement TEM in order to obtain a description of the nanocrystal structure. X-ray studies can further determine the crystal phases (wurtzite vs. zinc blende) and indicate the presence of stacking faults. This information is important in understanding the influence of structure on the electronic properties.

8.2.4 Design of Experiments

A design of experiments (DOE) is a systematic approach to maximizing information gained while reducing time and resources. A DOE can identify the most influential sources of variation of the process parameters. It can also quantify the effects of the important factors including their interactions and can identify the optimal conditions.

8.2.5 Life-cycle Assessment

To verify the environmental benefits provided by the hydrothermal route, a life-cycle assessment should be performed. The assessment would involve quantifying the amount of energy and raw materials used and the amount of waste generated. The assessment would entail choosing alternative reaction mediums (e.g. TOPO, heat transfer fluids), defining system boundaries and environmental parameters, and performing preliminary screens. This work would ensure a direct and objective comparison of synthesis in the different reaction mediums and their impact on the environment.

8.2.6 Emission Spectra Fitting

Many of the emission spectra collected in these studies were not true Gaussian curves as they possessed tails. A fit of the measured data to, for example, either Gaussian or Lorentzian functions could reduce the error in determining the fwhm of the spectra. This effort may also reveal some additional information about the effect of a process parameter on the nanocrystal's growth and size distribution.

8.3 Bibliography

1. Alivisatos, A. P. Perspectives on the Physical Chemistry of Semiconductor Nanocrystals. *J. Phys. Chem.* **1996***, 100*, 13226-13239.

2. Donega, C. D.; Hickey, S. G.; Wuister, S. F.; Vanmaekelbergh, D.; Meijerink, A. Single-Step Synthesis to Control the Photoluminescence Quantum Yield and Size Dispersion of CdSe Nanocrystals. *J Phys Chem B* **2003***, 107*, 489-496.

3. Hines, M. A.; Guyot-Sionnest, P. Synthesis and Characterization of Strongly Luminescing ZnS-Capped CdSe Nanocrystals. *J. Phys. Chem.* **1996***, 100*, 468-471.

4. Dabbousi, B. O.; RodriguezViejo, J.; Mikulec, F. V.; Heine, J. R.; Mattoussi, H.; Ober, R.; Jensen, K. F.; Bawendi, M. G. (CdSe)ZnS Core-Shell Quantum Dots: Synthesis and Characterization of a Size Series of Highly Luminescent Nanocrystallites. *J. Phys. Chem. B* **1997***, 101*, 9463-9475.

5. Qu, L. H.; Peng, X. G. Control of Photoluminescence Properties of CdSe Nanocrystals in Growth. *J. Am. Chem. Soc.* **2002***, 124*, 2049-2055.

6. Dickerson, B. D.; Irving, D. M.; Herz, E.; Claus, R. O.; Spillman, W. B.; Meissner, K. E. Synthesis Kinetics of CdSe Quantum Dots in Trioctylphosphine Oxide and in Stearic Acid. *Applied Physics Letters* **2005***, 86*, 171915-1-171915-3.

7. Bullen, C. R.; Mulvaey, P. Nucleation and Growth Kinetics of CdSe Nanocrystals in Octadecene. *Nano Lett.* **2004***, 4*, 2303-2307.

8. Qu, L. H.; Yu, W. W.; Peng, X. P. In Situ Observation of the Nucleation and Growth of CdSe Nanocrystals. *Nano Lett.* **2004***, 4*, 465-469.

9. Dushkin, C. D.; Saita, S.; Yoshie, K.; Yamaguchi, Y. The Kinetics of Growth of Semiconductor Nanocrystals in a Hot Amphiphile Matrix. *Adv. Coll. Inter. Sci.* **2000***, 88*, 37-78.